Materials Science & Engineering R 160 (2024) 100829

Contents lists available at ScienceDirect

Materials Science & Engineering R

journal homepage: www.elsevier.com/locate/mser

Coupled electrocatalytic hydrogen production

Donglian Li [a], Xuerong Xu [a], Junzheng Jiang [a], Hao Dong [a], Hao Li [c], Xiang Peng [a,*], Paul K. Chu [b,*]

[a] Hubei Key Laboratory of Plasma Chemistry and Advanced Materials, Engineering Research Center of Phosphorus Resources Development and Utilization of Ministry of Education, School of Materials Science and Engineering, Wuhan Institute of Technology, Wuhan 430205, China
[b] Department of Physics, Department of Materials Science and Engineering, and Department of Biomedical Engineering, City University of Hong Kong, Hong Kong, China
[c] School of Chemistry and Materials Engineering, Guangdong Provincial Key Laboratory for Electronic Functional Materials and Devices, Huizhou University, Huizhou, Guangdong 516007, China

ARTICLE INFO

Keywords:
Energy-efficient hydrogen production
Water splitting
Electrocatalysts
Small molecule oxidation
Electrosynthesis

ABSTRACT

Hydrogen has emerged as a clean and renewable energy source with the potential to mitigate global energy and environmental crises. Electrolytic water splitting, a highly efficient and sustainable technology, has garnered significant attention for hydrogen production. However, the slow kinetics of the oxygen evolution reaction on the anode and the high energy consumption limit the practicality of industrial-scale electrocatalytic water splitting. To address the challenge, the development of advanced electrolytic systems and the exploration of alternative oxidation reactions are crucial. This review highlights the recent advancements in coupled electrocatalytic hydrogen production strategies, including urea and hydrazine oxidation, value-adding electrosynthesis using small molecules, and waste upcycling and degradation. Various catalysts, the pertinent catalytic mechanisms for anodic oxidation reactions, and methods to decrease the energy barriers are discussed. Furthermore, the potential challenges and prospects for energy-saving electrolysis and promotion of hydrogen production are examined. A comprehensive understanding of these strategies and their implications is important to the development of efficient and sustainable hydrogen production.

1. Introduction

Hydrogen is a clean and renewable energy source with the potential to replace fossil fuels and address the global energy and environmental crisis [1,2]. Electrocatalytic water splitting ($2H_2O\,(l) \rightarrow 2H_2\,(g) + O_2\,(g)$, $\Delta G = 237.2$ kJ mol^{-1}), a highly efficient and sustainable strategy, has emerged as a promising platform for hydrogen production [3]. This technology has garnered significant attention due to its ability to facilitate water splitting and reduce energy consumption through the use of electrocatalysts. Electrocatalytic water splitting involves the oxygen evolution reaction (OER) at the anode and the hydrogen evolution reaction (HER) at the cathode. Various electrocatalysts, including precious metal-based materials [4–7], non-precious metal-based oxides [8–11], carbides [12–14], nitrides [15–17], selenides [18–22], phosphides [23, 24], sulfides [25,26], and alloys [27,28], have been developed for the HER and OER processes.

OER occurring at the anode is a four-electron transfer process with slow kinetics, resulting in high energy consumption and limiting the commercial practicality of electrocatalytic water splitting [29]. To address the issue, advanced electrolytic systems are crucial. One approach adopts thermodynamically favorable small molecule oxidation reactions using ethanol [30], benzyl alcohol [31], 5-hydroxymethyl furfural [32], and urea [33], to replace the sluggish OER and couple it with HER to achieve energy-efficient hydrogen production. This approach is currently a hot research topic as illustrated in Fig. 1. For example, Jiang et al. [34] have demonstrated that the potential required for the urea oxidation reaction (UOR) is 340 mV lower than that for conventional OER. However, UOR produces carbon emissions in the form of CO_2, and the industrial value of the products is relatively low.

Hence, it is of utmost importance to enhance the practical and industrial value of the anodic products. Electrosynthesis utilizing small molecules holds great promise in the production of high-value chemicals. For instance, Ma et al. [35] have prepared the Pt-NP/NiO-NS catalyst with excellent properties in both the methanol oxidation reaction (MOR) and HER for the co-production of hydrogen and value-adding formate based on a two-electrode electrolytic cell. The

* Corresponding authors.
E-mail addresses: xpeng@wit.edu.cn (X. Peng), paul.chu@cityu.edu.hk (P.K. Chu).

https://doi.org/10.1016/j.mser.2024.100829
Received 1 April 2024; Received in revised form 7 June 2024; Accepted 8 July 2024
Available online 26 July 2024

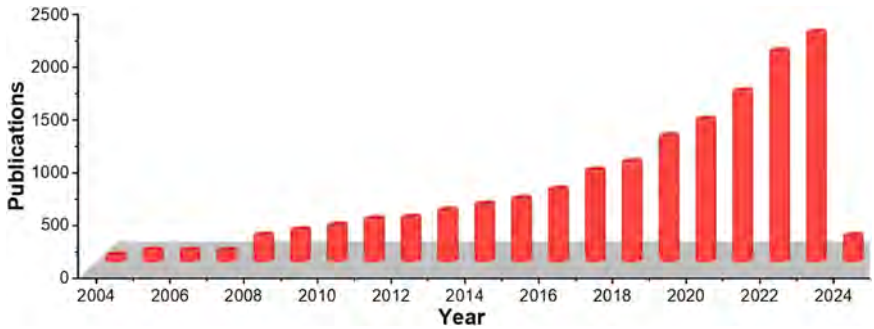

Fig. 1. Number of papers on the topic of coupled electrocatalytic hydrogen production from 2004 to 2024 (Data collected from the Web of Science all databases using "coupled hydrogen production" as keywords).

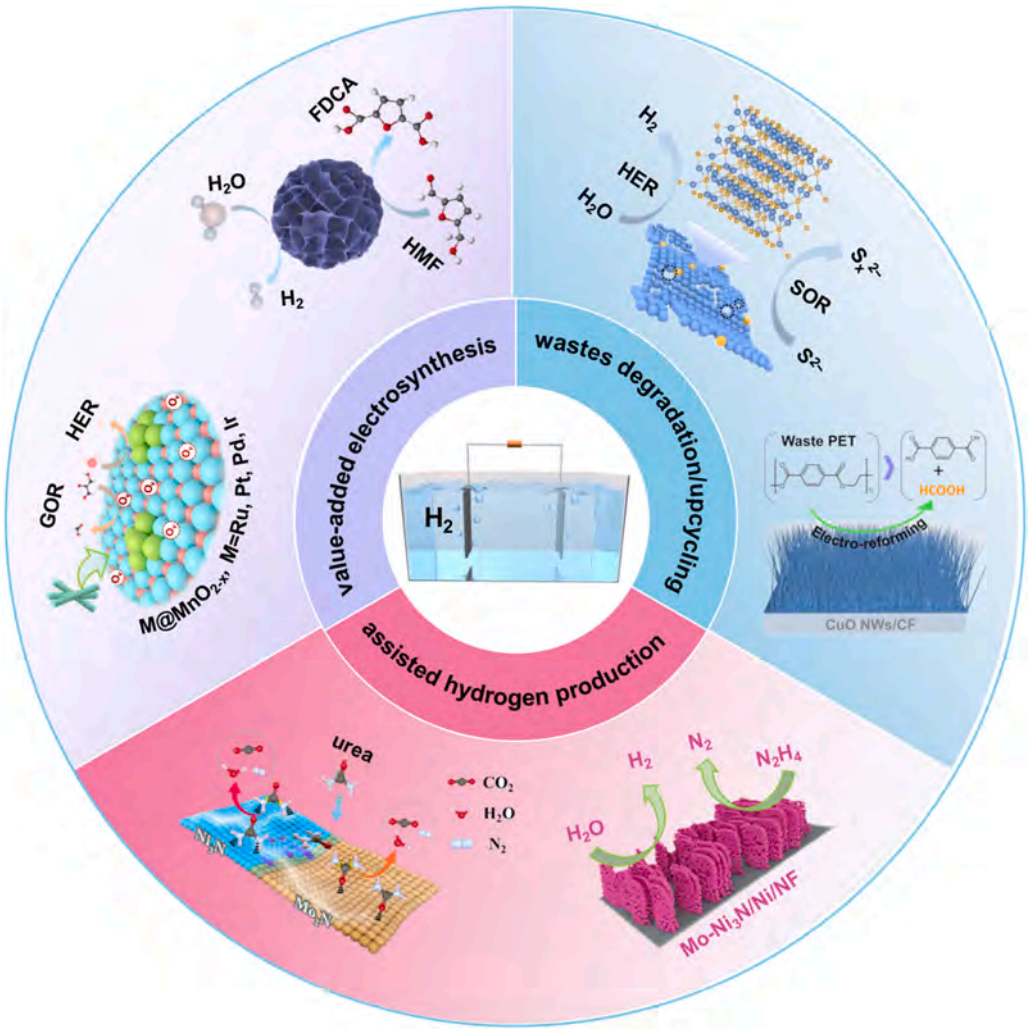

Fig. 2. Schematic of coupled electrocatalytic hydrogen production systems. Copyright permission has been received for all the images.

catalyst requires a voltage of 1.39 V to achieve a current density of 10 mA cm^{-2}, which is significantly lower than that of the typical HER/OER couple. We have proposed a two-electrode MOR/HER configuration catalyzed by the Ni-Mo-Se bifunctional electrocatalyst, which boasts a lower voltage than the OER/HER couple [21]. This configuration enables the oxidation of methanol into high-value formate, resulting in both energy-efficient hydrogen production and value-adding products simultaneously. In addition to generating value-adding by-products at the anode, waste upcycling and degradation can be coupled with HER to accomplish energy-efficient hydrogen production. Zhou et al. [36] have utilized Fe^{3+}/Fe^{2+} as a redox medium to construct a system for hydrogen production and electrolysis of H_2S. This coupled system significantly reduces the energy consumption for hydrogen production while recovering useful sulfur resources. Although how to decrease the energy barrier of the anodic oxidation reaction for energy-saving hydrogen production is a hot research area, there have been few comprehensive reviews on this important topic. It is noted that some of the catalytic properties including selectivity and yield for value-adding and assisted hydrogen production have been reviewed [37–41]. However, the mechanisms of various oxidation reactions and

Table 1
Typical assisted hydrogen production systems.

Catalyst	Electrolyte	Cell voltage at 10 mA cm^{-2}	ΔE[a]	ref
Cu_1Co_2-Ni_2P/NF	1.0 M KOH + 0.1 M N_2H_4	0.16 V	1.44 V	[45]
Ru-(Ni/Fe)C_2O_4	1.0 M KOH + 0.1 M N_2H_4	0.01 V	1.472 V	[46]
Cu_1Ni_2-N	1.0 M KOH + 0.5 M N_2H_4	0.24 V	1.39 V	[47]
Rh_2P uNSs	0.5 M H_2SO_4 + 0.05 M N_2H_4	0.377 V	1.373 V	[48]
Ni-C HNSA	1.0 M KOH + 0.1 M N_2H_4	0.14 V @ 50 mA cm^{-2}	1.5 V @ 200 mA cm^{-2}	[49]
Ru-Cu_2O/CF	1.0 M KOH + 0.5 M N_2H_4	0.0174 V	1.3646 V	[50]
RuFe-Ni_2P@NF	1.0 M KOH + 0.5 M N_2H_4	0.14 V	1.4 V @ 1000 mA cm^{-2}	[51]
RhIr MNs	1.0 M KOH + 0.5 M N_2H_4	0.13 V	1.456 V	[52]
Ni_3N-Co_3N PNAs/NF	1.0 M KOH + 0.1 M N_2H_4	0.668 V @ 100 mA cm^{-2}	–	[53]
Mo-Ni_3N/Ni/NF	1.0 M KOH + 0.1 M N_2H_4	0.055 V	1.485 V	[54]
CC@WS_2/Ru-450	1.0 M KOH + 0.5 M N_2H_4	0.0154 V	1.7046 V	[55]
Ru-Ni$(OH)_2$ NW_2/NF	1.0 M KOH + 0.1 M N_2H_4	0.152 V @ 100 mA cm^{-2}	1.58 V @ 100 mA cm^{-2}	[56]
6W-O-CoP/NF	1.0 M KOH + 0.1 M N_2H_4	0.00873 V	1.611 V	[57]
Ni_2P/NF	1.0 M KOH + 0.5 M N_2H_4	1.0 V @ 500 mA cm^{-2}	–	[58]
N-Ni_5P_4@CoP/CFP	1.0 M KOH + 0.1 M N_2H_4	0.037 V	1.515 V	[59]
$RhRu_{0.5}$	1.0 M KOH + 1 M N_2H_4	0.054 V @ 100 mA cm^{-2}	–	[60]
Ru_1-NiCoP	1.0 M KOH + 0.3 M N_2H_4	0.09 V @ 50 mA cm^{-2}	1.57 V @ 50 mA cm^{-2}	[61]
$CoSe_2$	1.0 M KOH + 0.5 M N_2H_4	0.017 V	1.483 V	[42]
CoS_2/TiM	1.0 M KOH + 0.1 M N_2H_4	0.81 V @ 100 mA cm^{-2}	1.08 V @ 100 mA cm^{-2}	[62]
Ni_3S_2/NF-2	1.0 M KOH + 0.2 M N_2H_4	0.867 V @ 100 mA cm^{-2}	1.143 V @ 100 mA cm^{-2}	[63]
Rh/RhO_x	1.0 M PBS + 0.3 M N_2H_4	0.598 V	0.422 V	[64]
RP-CPM	1.0 M KOH + 0.3 M N_2H_4	0.023 V	2.416 V	[65]
Ni-Co-P/NF	1.0 M KOH + 0.1 M N_2H_4	0.88 V @ 200 mA cm^{-2}	1.04 V @ 200 mA cm^{-2}	[66]
CoFeNiCrMnP/NF	1.0 M KOH + 0.4 M N_2H_4	0.14 V @ 200 mA cm^{-2}	1.54 V @ 200 mA cm^{-2}	[67]
(P-Co/$Ni_3P)_{A3}$/NF	1.0 M KOH + 0.4 M N_2H_4	0.017 V @ 100 mA cm^{-2}	1.77 V @ 300 mA cm^{-2}	[68]
CC@CoNC-600	1.0 M KOH + 0.5 M N_2H_4	0.353 V @ 100 mA cm^{-2}	–	[69]
PW-Co_3N NWA/NF	1.0 M KOH + 0.1 M N_2H_4	0.028 V	1.222 V	[70]
NiMo/Ni_2P	1.0 M KOH + 0.5 M N_2H_4	0.181 V @ 100 mA cm^{-2}	–	[71]
CoP/Co-20	1.0 M KOH + 0.5 M N_2H_4	0.26 V	1.64 V	[72]
RuPd/C	1.0 M KOH + 0.5 M N_2H_4	0.0177 V	1.8923 V	[73]
CoNi@CN-CoNiMoO	1.0 M KOH + 0.5 M urea	1.58 V @ 500 mA cm^{-2}	0.3 V@ 500 mA cm^{-2}	[74]
1 %Cu:α-Ni$(OH)_2$/NF	1.0 M KOH + 0.33 M urea	1.49 V	–	[75]
NF/NiMoO	1.0 M KOH + 0.5 M urea	1.38 V	0.17 V	[33]
NiCoP/CC	1.0 M KOH + 0.5 M urea	1.42 V	0.16 V	[76]
Ni_3N/$Ni_{0.2}Mo_{0.8}N$/NF	1.0 M KOH + 0.5 M urea	1.348 V	0.139 V	[77]
Co_2P/Co_4N	1.0 M KOH + 0.5 M urea	1.37 V	0.329 V	[78]
CoP/C-3	1.0 M KOH + 0.1 M urea	1.40 V	0.22 V	[79]
Ni/C-1	1.0 M KOH + 0.33 M urea	1.60 V	–	[80]
Mo-NiS	1.0 M KOH + 0.5 M urea	1.64 V @ 100 mA cm^{-2}	0.138 V @ 100 mA cm^{-2}	[81]
Fe-$Co_{0.85}Se$/FeCo	1.0 M KOH + 0.5 M urea	1.32 V	–	[82]
Ni-NiO-$Mo_{0.84}Ni_{0.16}$/NF	1.0 M KOH + 0.5 M urea	1.37 V	0.15 V	[83]
Ni-S-Se/NF	1.0 M KOH + 0.5 M urea	1.47 V	0.1 V	[84]
(Ni-WO_2)@C/NF	1.0 M KOH + 0.5 M urea	1.38 V	0.18 V	[85]
$NiSe_2$/$MoSe_2$	1.0 M KOH + 0.5 M urea	1.44 V	0.279 V @ 100 mA cm^{-2}	[86]
NiF_3/Ni_2P@CC-2	1.0 M KOH + 0.33 M urea	1.54 V	0.04 V	[87]
CoFeCr LDH/NF	1.0 M KOH + 0.33 M urea	1.467 V	0.138 V	[88]
NiCoMoCuO_xH_y	1.0 M KOH + 0.33 M urea	1.5 V @ 100 mA cm^{-2}	–	[89]
Ni/MoC/$Ti_3C_2T_x$@C	1.0 M KOH + 0.3 M urea	1.56 V	0.08 V	[90]
NiCoP	1.0 M KOH + 0.5 M urea	1.36 V	0.17 V	[91]
F-NiO/Ni@C	1.0 M KOH + 0.33 M urea	1.37 V	0.29 V @ 200 mA cm^{-2}	[92]

[a] The voltage decrease of the coupled reactions compared to the HER/OER couple at 10 mA cm^{-2}.

coupling with waste degradation and upgrading have not been thoroughly discussed. Therefore, a comprehensive review of the latest research advances and challenges in assisted hydrogen production, value-adding hydrogen production, and waste degradation/upgrading will help guide future research in this important area.

In this review, we comprehensively discuss various strategies of coupled electrocatalytic hydrogen production, including the adoption of urea and hydrazine oxidation, value-adding electrosynthesis using small molecules such as alcohol, aldehyde, glucose, and amine, as well as waste upcycling and degradation, as described in Fig. 2. We also delve into the latest research progress on the design and synthesis of efficient electrocatalysts and explore the catalytic mechanisms of various anodic oxidation reactions. Finally, we discuss the potential challenges of coupled electrocatalytic hydrogen production and the prospects of hydrogen production by energy-saving electrolysis.

2. Assisted hydrogen production

Electrochemical oxidation of some small molecules normally requires low potentials. For example, hydrazine and urea can be electrochemically oxidized into N_2 and CO_2 at very low potentials (−0.33 V and 0.37 V *vs.* the reversible hydrogen electrode (RHE), respectively) [42]. Moreover, the products of these reactions are safer than those of OER, which is vulnerable to the mixing of hydrogen and oxygen [43,44]. Therefore, coupling-assisted oxidation reactions such as hydrazine oxidation reaction (HzOR) and UOR with HER can improve the efficiency and safety of electrocatalytic hydrogen production, as listed in Table 1.

2.1. Hydrazine oxidation reaction

HzOR exhibits a lower energy barrier ($N_2H_4 + 4OH^- \rightarrow N_2 + 4H_2O + 4e^-$, −0.33 V *vs.* RHE) and emits no polluting gas [54,93,94]. By

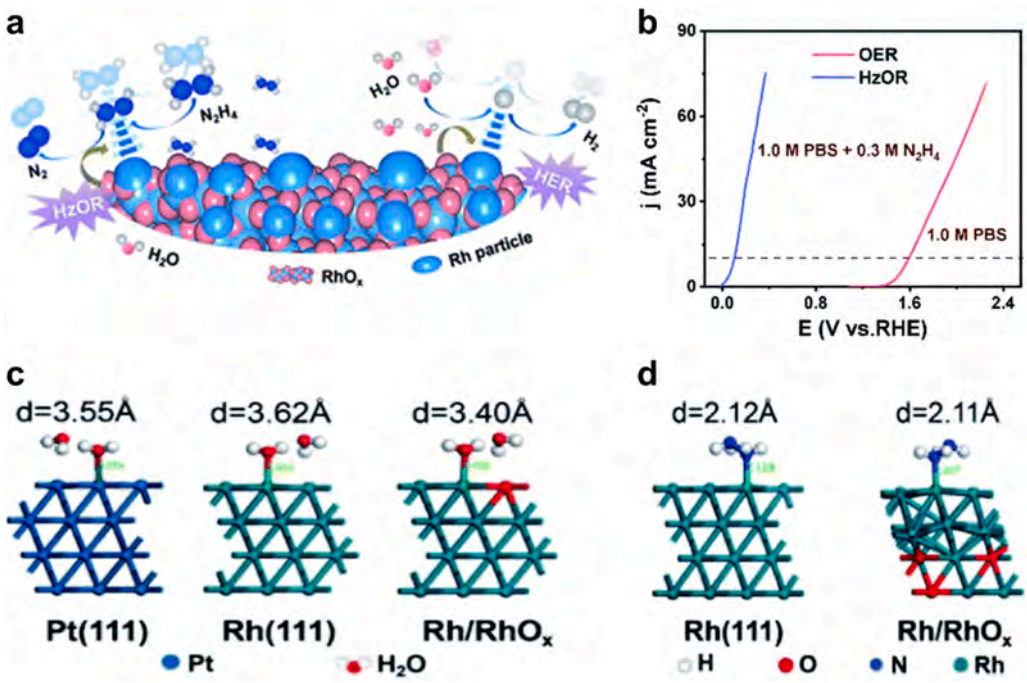

Fig. 3. (a) Schematic diagram of the reaction mechanism of HER and HzOR of the Rh/RhO_x catalyst. (b) LSV curves for HzOR in 1.0 M PBS/0.3 M N_2H_4 and for OER in 1.0 M PBS. (c) Distance between O (H_2O) and Rh or Pt (active site) in Pt(111), Rh(111), and Rh/RhO_x systems for HER. (d) Distance between N (NH_2NH_2) and Rh (active site) in Rh(111) and Rh/RhO_x systems for HzOR. Reproduced with permission from reference [64]. Copyright 2022, the Royal Society of Chemistry.

replacing the slow OER with HzOR in water electrolysis, it is possible to reduce the voltage required and energy consumption to produce green hydrogen gas [60,95].

In the past few decades, many transition metal-based electrocatalysts such as alloys [73,96], oxides [97], hydroxides [98,99], chalcogenides/phosphides [63,100], nitrides/carbides, and their derivatives [99,101] have been proposed for HzOR-coupled HER. For instance, Liu et al. [63] have reported an ultra-thin nanosheet array of Ni_3S_2 with 9–14 nm thick grown directly on a commercial nickel foam substrate (Ni_3S_2/NF). Owing to the smaller Gibbs free energy of N_2H_4 (−1.41 eV) adsorption on the Ni_3S_2 surface compared to the H_2O molecule (−0.82 eV), an applied voltage of only 86.7 mV is required for the Ni_3S_2/NF electrocatalyst to achieve a high current density of 100 mA cm^{-2} for HzOR, which is 1.143 V lower than that of OER. Senthil et al. [102] have modified the ratios of single palladium nanoparticles on $NiCo_2O_4$ nanoplates by pulsed laser irradiation (PLI) to form $Pd/NiCo_2O_4$ composites. $Pd/NiCo_2O_4||Pd/NiCo_2O_4$ is used in an overall hydrazine splitting (OHzS) electrolysis cell at low cell voltages of 0.35 V and 0.94 V to drive current densities of 10 and 100 mA cm^{-2}, respectively. *In situ*/operando Raman spectroscopy confirms the formation of α-Co $(OH)_2$ and γ-NiOOH during HER and HzOR. Yang et al. [64] have introduced the Rh-O-Rh interface to Rh/RhO_x nanosheets to form a bifunctional electrocatalyst for HzOR and HER, as illustrated in Fig. 3a. Linear sweep voltammetry (LSV) shows that HzOR electrolysis has many advantages over OER (Fig. 3b). The O atoms shorten the distance between H_2O and active centers (Fig. 3c), thus weakening the H-O bond and lowering the energy barrier for water decomposition. Moreover, the O atoms weaken the N-H bond (Fig. 3d), promote the dehydrogenation of $*NH_2NH_2$ adsorbed onto the Rh site, and improve the catalytic activity of Rh(111). Optimal adjustment of the Rh/RhO_x interface improves the catalytic activity and reduces energy consumption boding well for hydrogen production.

Ru-based nanomaterials not only promote the dehydrogenation kinetics of HzOR but also are promising catalysts for HER [103,104]. However, the high cost of precious metals is the key obstacle to practical applications. Therefore, the design of atomically dispersed precious metal catalysts is beneficial. Furthermore, the catalytic activity can be enhanced by fine-tuning the interface interactions between the single atom and carrier. Li et al. [105] have prepared Ru-SACs anchored to the sulfur-deficient tungsten disulfide (WS_2/Ru-SACs) by sulfidation and galvanostatic deposition. The two-electrode cell with WS_2/Ru-SACs as bifunctional catalysts assembled for the HzOR/HER overall reaction is depicted in Fig. 4a. To produce a current density of 10 mA cm^{-2}, the cell voltage is only 15.4 mV, which is much lower than that of the commercial Pt/C catalyst, as shown in Fig. 4b. Fig. 4c shows that the Ru sites in WS_2/Ru-SACs are the active centers for HzOR multistep dehydrogenation, and the energy barrier of the rate-determining step (RDS) decreases by 0.5 eV compared to the pristine WS_2 catalyst. Because of the bifunctional activity of Ru atoms, the RDS of both Volmer reactions in alkaline HER and dehydrogenation reactions in HzOR are accelerated, consequently improving the HER and HzOR properties.

A twisted NiCoP nanowire array immobilized with Ru-SACs (Ru_1-NiCoP) has been reported by Hu et al. [106]. At a current density of 10 mA cm^{-2}, an ultralow potential of HzOR was −60 mV in addition to an overpotential of 32 mV achieved for HER. The two-electrode electrolyzer for OHzS with Ru_1-NiCoP as both the anode and cathode produces a current density of 522 mA cm^{-2} at a voltage of 0.3 V, which is a significant energy-saving process compared to typical overall water splitting (OWS), as shown in Fig. 4d. The Ru atoms optimize the adsorption of H* in NiCoP and decrease the vacant *d*-band centers (Fig. 4e), resulting in an enhanced adsorption capacity for $*N_2H_2$ and HzOR capability. In particular, an innovative self-powered hydrogen production system is used to achieve a potential hydrogen generation rate of 24.0 mol h^{-1} m^{-2} without an external power supply.

Non-precious metal-based materials have outstanding electrocatalytic oxidation capability, which can be further enhanced by heteroatom doping [107–109]. For instance, Sun et al. [110] have deposited NiFeP on the nickel mesh (NiFeP/NM), followed by potentiostatic depositing and dealloying with a nanotube Ni(Cu) coating (Ni(Cu)@NiFeP/NM). The open and hollow nanostructures provide a large electrochemically active surface area and expose a large number of active sites for catalysis. The strong synergistic effect between crystalline Ni(Cu) and amorphous NiFeP layers produces enhanced catalytic activity at the active centers. As a result, the bifunctional Ni(Cu)

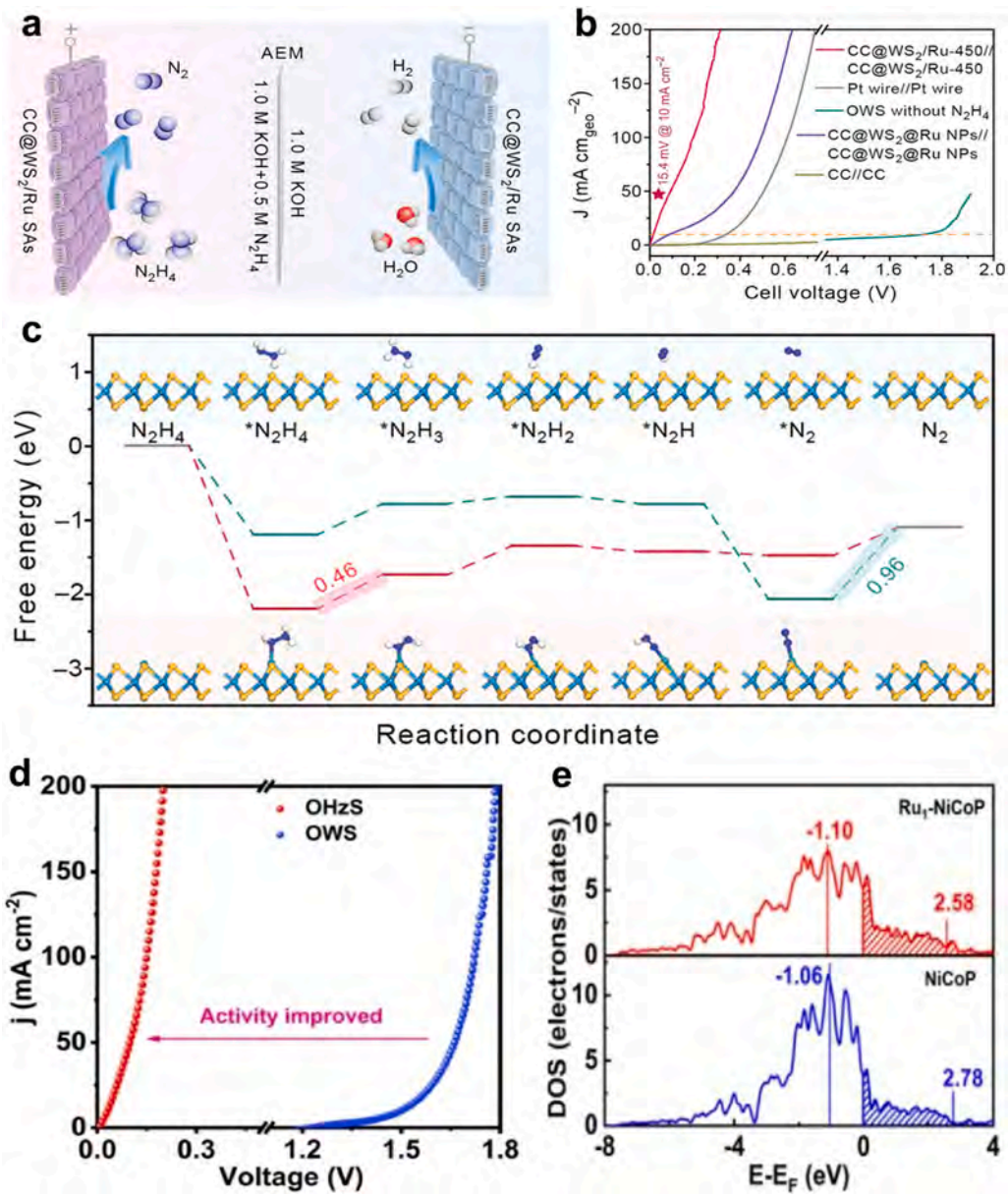

Fig. 4. (a) Schematic illustration of the OHzS in a two-electrode electrolyze using WS_2/Ru-SACs as both anode and cathode. (b) LSV curves of two-electrode configuration for CC@WS_2/Ru-450||CC@WS_2/Ru-450 with or without N_2H_4, Pt wire||Pt wire, CC@WS_2@Ru NPs||CC@WS_2@Ru NPs, and CC||CC. (c) Gibbs free energy profiles and reaction pathways for HzOR. Reproduced with permission from reference [105]. Copyright 2022, Wiley-VCH. (d) LSV curves of Ru_1-NiCoP||Ru_1-NiCoP couples for OWS and OHzS. (e) The DOS plots and *d*-band center of NiCoP and Ru_1-NiCoP. Reproduced with permission from reference [106]. Copyright 2023, Wiley-VCH.

@NiFeP/NM catalyst needs a voltage of only 0.491 V to achieve a current density of 100 mA cm^{-2} in 1.0 M KOH and 0.5 M N_2H_4 electrolyte, which is obviously superior to the OWS.

It is worth noting that the HzOR-assisted hydrogen production system can be directly driven by a direct hydrazine fuel cell (DHzFC) with a fairly high H_2 yield, which is promising for practical application. For example, Li et al. [65] have designed partially exposed RuP_2 nanoparticles on N, P co-doped carbon porous microsheets (CPMs). Due to the strong coupling between RuP_2 nanoparticles and N, P co-doped CPMs, electron transfer and durability during electrocatalysis are promoted. The OHzS needs a mere 23 mV to deliver a current density of 10 mA cm^{-2} under alkaline conditions. Furthermore, the overall reaction can be powered by DHzFC with hydrazide as the only liquid fuel, where H_2 is generated at a rate of 0.68 mmol h^{-1} with a high power density of 64.77 mW cm^{-2}.

Liu et al. [70] have reported P, W co-doped Co_3N nanowires (PW-Co_3N NWs) with superior catalytic activity for both HzOR (−55 mV @ 10 mA cm^{-2}) and HER (−41 mV @ 10 mA cm^{-2}). P and W doping reduces the dehydrogenation-free energy of adsorbed N_2H_4, resulting in more thermally neutral Gibbs free energy (ΔG_{H^*}) than pristine Co_3N. The PW-Co_3N NWs-assembled overall reaction configuration shows a current density of 10 mA cm^{-2} at a voltage of only 28 mV. The system is powered by DHzFC and shows a hydrogen production rate of 1.25 mmol h^{-1} at room temperature.

Previous studies have shown that the construction of a heterogeneous interface can modulate the electronic structure of the catalyst to enhance the electrochemical activity [33,111]. Qian et al. [111] have proposed *in situ* growth of layered porous nanosheet arrays of Ni_3N-Co_3N on nickel foam (Ni_3N-Co_3N PNAs/NF) as bifunctional electrocatalysts for HzOR and HER in the overall reaction. The voltages required to achieve current densities of 10 and 400 mA cm^{-2} are only 0.071 and 0.76 V, respectively, which are significantly superior to OWS. The

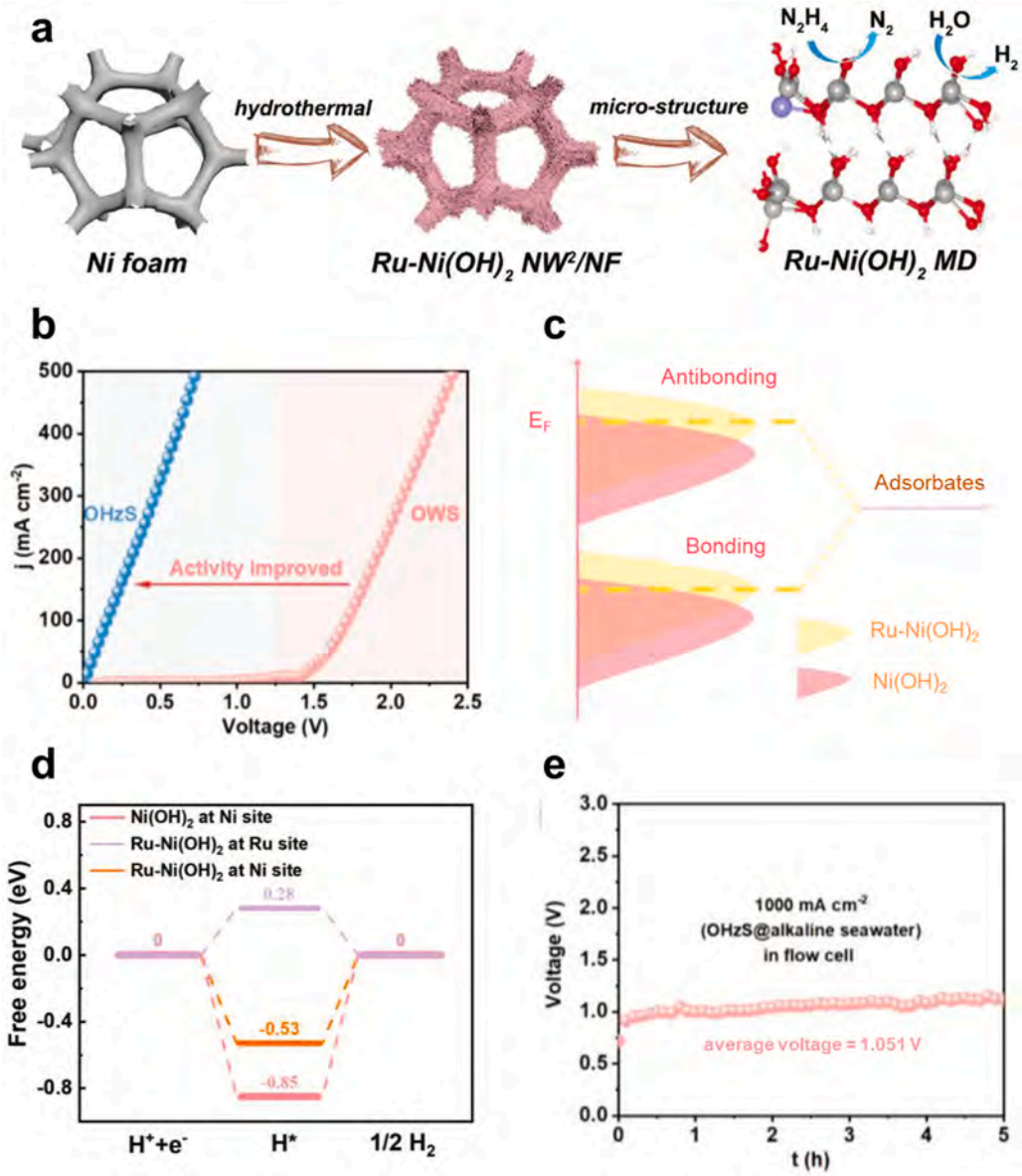

Fig. 5. (a) Schematic illustration of the synthesis of Ru-Ni(OH)$_2$ NW^2/NF and bifunctional application in OHzS. (b) LSV curves for OHzS in 1.0 M KOH/0.1 M N_2H_4 and OWS in 1.0 M KOH using Ru-Ni(OH)$_2$ NW^2/NF as both the anode and cathode. (c) Schematic illustration of bond formation of Ni(OH)$_2$ and Ru-Ni(OH)$_2$. (d) Free energy profiles of HER. (e) Stability test of the flow cell electrolyzer. Reproduced with permission from reference [56]. Copyright 2023, Wiley-VCH.

heterointerface optimizes the electronic structure of the catalyst surface to modulate the free energy of reactants/intermediates adsorption and promote the kinetics of hydrazine dehydrogenation.

Recently, Zhu et al. [66] have prepared three-dimensional (3D) nickel foam-supported nickel-cobalt phosphide heterostructures (Ni-Co-P/NF) by interface engineering. The heterogeneous interface improves the bifunctional activity of Ni-Co-P/NF catalysts in both HER and HzOR. In particular, HzOR requires a voltage of only 176 mV to achieve a high current density of 1000 mA cm^{-2}. The HzOR/HER electrolyzer assembled with the Ni-Co-P/NF catalyst shows a voltage input as low as 0.88 V for a current density of 200 mA cm^{-2}, which is 1.04 V lower than that of OWS (1.92 V). The results reveal that the HzOR/HER system greatly reduces energy consumption for hydrogen production. Moreover, the electrolyzer can be powered by a self-assembled DHzFC with Ni-Co-P/NF as the anode catalyst and shows a self-powered hydrogen production rate of up to 19.6 mol m^{-2} h^{-1} without an external power supply.

Wang et al. [47] have prepared porous nanofilms of copper-nickel nitrite (Cu_1Ni_2-N) supported by carbon fiber cloth by thermal ammoniation using Cu-Ni layered double hydroxide (CuNi-LDH) as the precursor. Due to the high conductivity and porous nanostructure of the catalyst and exploiting the synergistic effect of nickel nitride and copper nitride, the Cu_1Ni_2-N catalyst has excellent catalytic properties and stability in HER and HzOR. The two-electrode electrolytic system with Cu_1Ni_2-N as both the cathode and anode shows a small cell voltage of 0.24 V to obtain a current density of 10 mA cm^{-2} in the 1.0 M KOH/0.5 M N_2H_4 electrolyte.

Recently, the use of inexhaustible seawater as a hydrogen source has shown great potential in H_2 production by water electrolysis [112,113]. The coupling of HzOR with HER in seawater electrolysis and hydrogen production systems has attracted much attention [114–117]. Zhai et al. [51] have developed Ru, Fe co-doped Ni_2P nanofilms (RuFe-Ni_2P@NF) as a bifunctional catalyst for the production of chlorine-free hydrogen by coupling HER with HzOR in seawater. In the two-electrode electrolyzer, a current density of 1 A cm^{-2} is achieved at an ultra-low voltage of 0.69 V, which is 1.39 V lower than that of the overall seawater splitting.

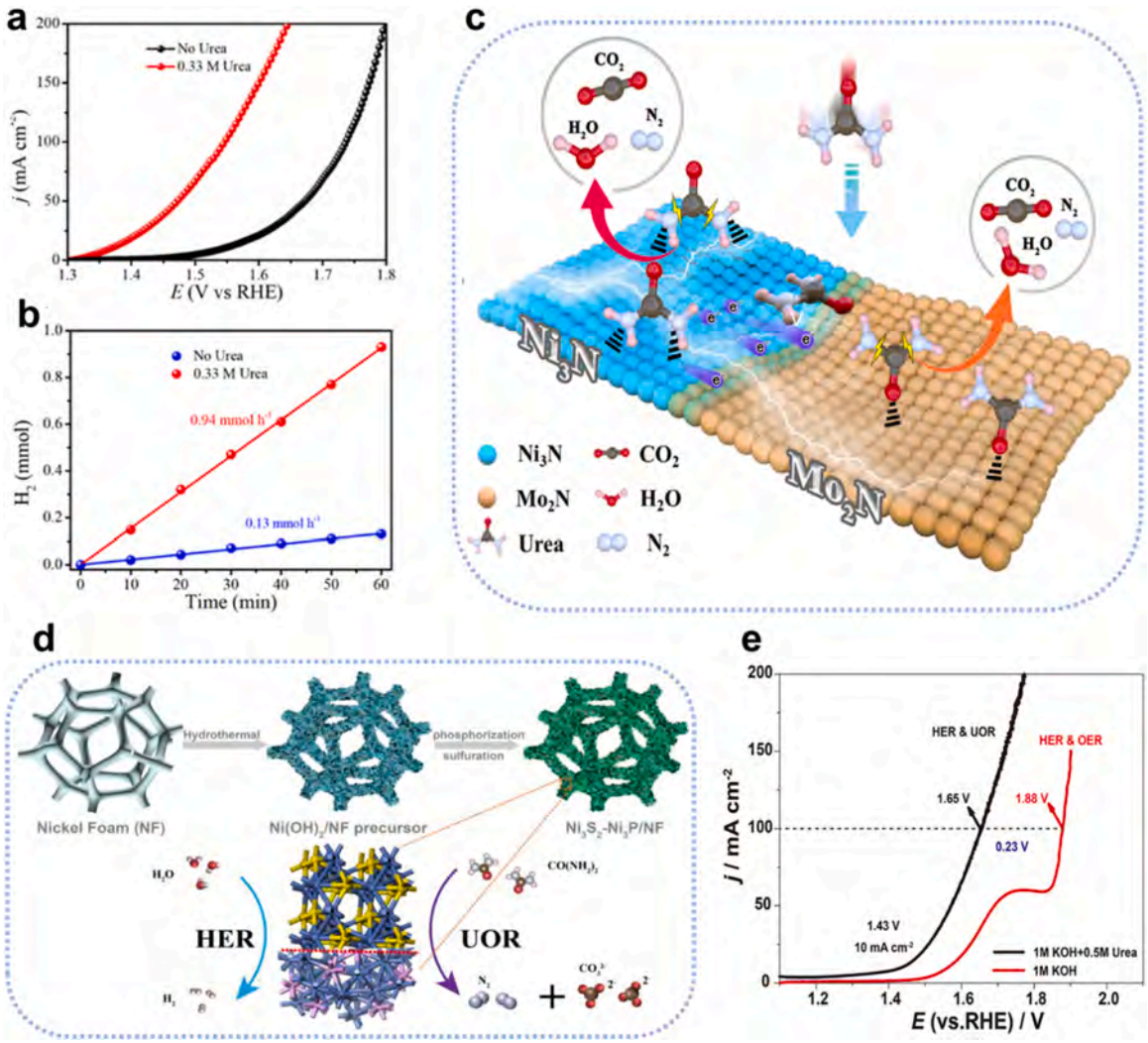

Fig. 6. (a) LSV curves for UOR and OER of Ni_3N/Mo_2N. (b) Amount of H_2 evolution and production rate at 1.50 V in 1.0 M KOH with or without 0.33 M urea. (c) Schematic illustration of the UOR mechanism using Ni_3N/Mo_2N catalyst. Reproduced with permission from reference [126]. Copyright 2023, American Chemical Society. (d) Schematic diagram of the preparation process and reaction mechanism of Ni_3S_2-Ni_3P/NF. (e) LSV curves of Ni_3S_2-Ni_3P/NF in 1.0 M KOH with and without 0.5 M urea. Reproduced with permission from reference [133]. Copyright 2021, American Chemical Society.

Intuitive power consumption calculations show that the production of 1.0 L of hydrogen gas by the OHzS system saves 4.70 kWh compared to the OWS system, thereby realizing energy-efficient hydrogen production.

Li et al. [56] have proposed a unique active-site injection strategy by constructing a Ru-doped $Ni(OH)_2$ nanowire network on nickel foam (Ru-$Ni(OH)_2$ NW^2/NF), as illustrated in Fig. 5a. The LSV curves in Fig. 5b show that OHzS requires a smaller voltages than OWS, demonstrating that OHzS has many low-energy applications. The two-electrode configuration comprising HzOR and HER in seawater can drive a high current density of 500 mA cm^{-2} at the voltage of 0.736 V and works stably for more than 200 h. The up-shift of the *d*-band center of Ru-Ni $(OH)_2$ in Fig. 5c indicates an increase in the back bonding energy, leading to enhanced interactions between the adsorbent materials and catalyst. The ΔG_{H^*} values of Ru and Ni sites in Ru-$Ni(OH)_2$ are 0.28 and −0.58 eV, respectively, as shown in Fig. 5d, indicating that the Ru sites are the active center for the accelerated HER. A domestic flow electrolyzer is constructed for continuous hydrogen production at an industrial current density of 1 A cm^{-2}, driven by a record low cell voltage of 1.051 V (Fig. 5e). The electrolyzer shows superior energy consumption of 2.25 kWh m^{-3} (H_2), which helps market penetration of electrolytic seawater for hydrogen production.

2.2. Urea oxidation reaction

The urea oxidation reaction (UOR, $CO(NH_2)_2 + 6OH^- \rightarrow N_2 + 5H_2O + CO_2 + 6e^-$, $E^\theta = -0.46$ V *vs.* RHE) coupled with HER ($6H_2O + 6e^- \rightarrow 3H_2 + 6OH^-$, $E^\theta = -0.83$ V *vs.* RHE) in alkaline media has a theoretical equilibrium voltage of 0.37 V [118–120], which reduces the energy consumption of electrocatalytic hydrogen production intrinsically. In addition, urea in wastewater can produce corrosive ammonia and nitrate, leading to environmental pollution and eutrophication of water [119,121]. Therefore, the use of UOR reduces not only the cost of hydrogen production but also the pollution of urine-rich wastewater, thus achieving the dual purpose of producing clean energy and solving environmental problems [122].

The 6 electron-transfer mechanism of UOR results in slow reaction kinetics and therefore, efficient and stable electrocatalysts are essential in order to achieve energy-efficient hydrogen production [123]. Generally, noble metal-based catalysts (Pt, IrO_2, RuO_2, etc.) have high catalytic activity for UOR, but the high cost and scarcity are challenging. Therefore, much effort has been devoted to developing non-precious metal-based materials for efficient UOR. Ni-based materials, such as Ni-based alloys, oxides, hydroxides, phosphides, nitrides, and sulfides are candidates for UOR [83,122,124–129]. In particular, NiO has

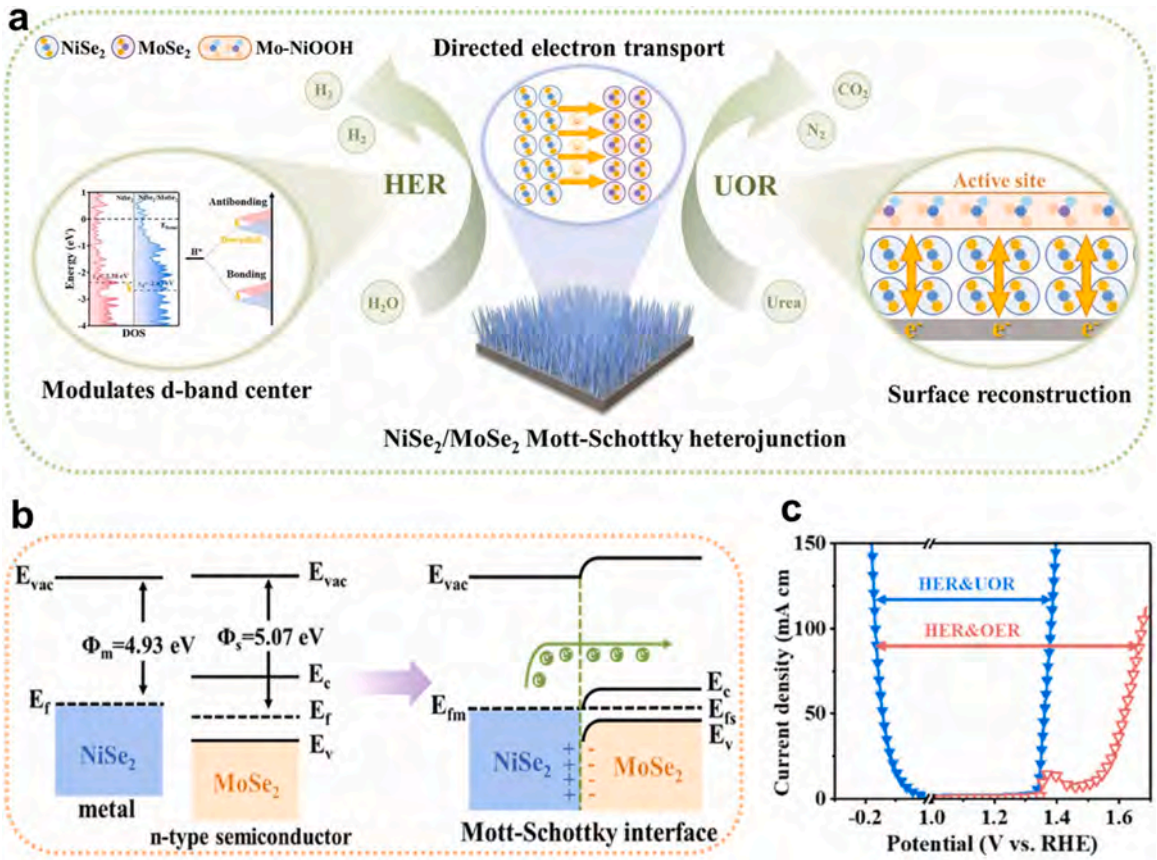

Fig. 7. (a) Schematic diagram illustrating direct electron transfer regulation of the *d*-band center and promotion of surface reconstruction in the $NiSe_2/MoSe_2$ Mott-Schottky heterojunction catalyst. (b) The energy band diagrams of $NiSe_2$ and $MoSe_2$ before and after the formation of the Mott-Schottky heterojunction. (c) LSV curves of HER, OER, and UOR of $NiSe_2/MoSe_2$. Reproduced with permission from reference [86]. Copyright 2024, Elsevier.

attracted much attention due to its environmental friendliness, cost-effectiveness, and high corrosion resistance. However, Ni^{2+} ($t_{2g}^6e_g^2$) of pristine NiO has a high e_g occupancy, leading to strong binding with reaction intermediates and unfavorable desorption of gaseous products. In order to optimize the adsorption and desorption of the reaction intermediates, an interfacial engineering strategy has been developed [130–132]. It has been reported that the transition metal/transition metal oxide heterojunction can weaken the absorption of intermediates and promote the reaction kinetics.

Xu et al. [92] have developed an effective organic-inorganic hybridization strategy for the simultaneous formation of multiple heterostructures and F doping of F-NiO/Ni@C. F doping enhances electron delocalization, facilitates electron transport from Ni to NiO, and lowers the *d*-band center of the NiO/Ni@C catalyst. The optimized electronic state endows F-NiO/Ni@C with excellent HER kinetics and a smaller energy barrier in urea dehydrogenation. As a result, F-NiO/Ni@C requires an overpotential of only 46 mV in HER and a potential of 1.31 V *vs*. RHE in UOR to achieve a current density of 10 mA cm^{-2} in alkaline media. The voltage required to obtain a current density of 10 mA cm^{-2} by the F-NiO/Ni@C||F-NiO/Ni@C cells is 80 mV lower than that of the state-of-the-art Pt/C||RuO_2 cells, indicating the high promise of noble metal-free catalysts for UOR-assisted high-energy-efficiency hydrogen production.

Wang et al. [126] have prepared Ni_3N/Mo_2N heterostructured nanosheets by hydrothermal and nitriding methods, which require an ultra-low overpotential of only 20 mV in HER and a low operating potential of 1.32 V *vs*. RHE in UOR to reach a current density of 10 mA cm^{-2} (Fig. 6a). In the two-electrode configuration, the UOR-assisted HER overall reaction requires a voltage of 1.36 V to drive a current density of 10 mA $cm^{-2,}$ showing a seven-time larger rate of hydrogen production than conventional OWS, as shown in Fig. 6b. Meanwhile, both temperature-programmed desorption and theoretical calculations demonstrate that the Ni_3N/Mo_2N heterostructure combines the advantages of both Ni_3N and Mo_2N phases, leading to the optimal urea adsorption and enhanced UOR reactivity, as schematically illustrated in Fig. 6c. Liu et al. [133] have reported a heterogeneous Ni_3S_2-Ni_3P catalyst with a lot of highly active interfaces for bifunctional UOR and HER, as illustrated in Fig. 6d. Electrons are transferred from Ni_3S_2 to Ni_3P at the heterointerface and as a result, Ni_3S_2-Ni_3P delivers superior performance in the UOR-coupled HER system showing current densities of 10 and 100 mA cm^{-2} at cell voltages of only 1.43 and 1.65 V, respectively, as shown in Fig. 6e.

Mott-Schottky heterojunctions, such as CoS_2/MoS_2 [134], NiS/MoS_2 [135], Co_2P/Co_4N [78], and $CoMn/CoMn_2O_4$ [127], have received particular attention because the built-in electric field permits directional transition of electrons to form electron-rich and electron-poor regions [136,137]. On the one hand, this promotes OH^- adsorption in the electron-poor regions to facilitate the generation of oxide/hydroxide active species in OER/UOR. On the other hand, it tunes the electronic structure to optimize the adsorption energy of hydrogen in HER [138, 139]. Xu et al. [86] have constructed a $NiSe_2/MoSe_2$ Mott-Schottky heterojunction catalyst for UOR-assisted water splitting, as shown in Fig. 7a. The work functions of metallic $NiSe_2$ and semiconductor $MoSe_2$ are 4.93 and 5.07 eV, respectively, thus forming the Mott-Schottky heterojunction that facilitates electron directional transport, promotes surface reconstruction, and endows $NiSe_2/MoSe_2$ with excellent HER and UOR characteristics. The Mott-Schottky heterojunction is conducive to the adsorption of OH^-, thereby promoting surface reconstruction. Density functional theory (DFT) calculations indicate that Mo-NiOOH has optimized adsorption energy for intermediates compared to

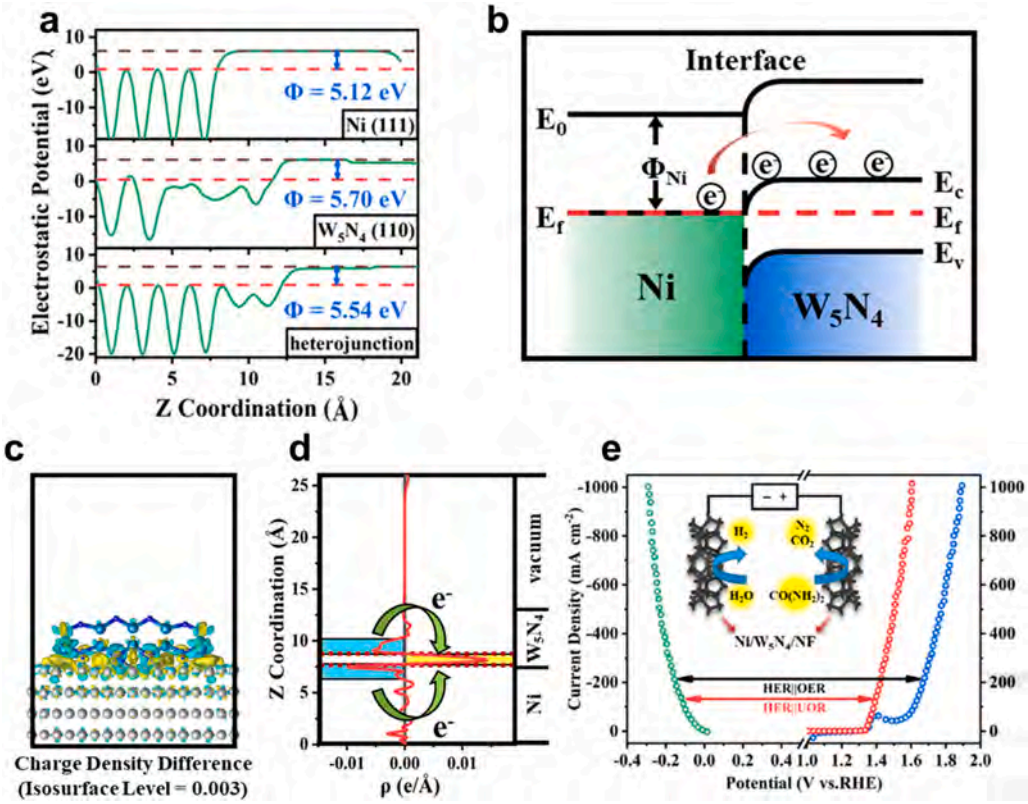

Fig. 8. (a) Electrostatic potentials of the corresponding geometries. (b) Energy band diagram of metallic Ni and W_5N_4 at the Mott-Schottky interface. (c) CDD of the Mott-Schottky heterojunction between Ni (111) and W_5N_4 (100) (cyan stands for holes and yellow for electrons). (d) Planar average of CDD along the *Z* direction of the Mott-Schottky heterojunction. (e) LSV curves of the Ni/W_5N_4 catalyst for HER, UOR, and OER, with the insert showing an illustrative scheme of the UOR-assisted water electrolysis system. Reproduced with permission from reference [140]. Copyright 2023, Elsevier.

NiOOH during UOR, thus promoting UOR. Additionally, there is significant electron transfer at the interface of $NiSe_2$ and $MoSe_2$ (Fig. 7b) to modulate the electronic structure of the catalyst to optimize H adsorption. Hence, the $NiSe_2/MoSe_2$ catalyst has excellent HER and UOR properties such as a current density of 10 mA cm^{-2} at a voltage of 1.44 V in the UOR/HER overall reaction (Fig. 7c).

Zhou et al. [140] have synthesized the Ni/W_5N_4-based Mott-Schott heterojunction loaded on NF by hydrothermal and nitriding methods to form highly active catalysts for UOR and HER. Since the work function of Ni is smaller than that of W_5N_4 (Fig. 8a), a Mott Schottky heterojunction is formed [141,142]. Theoretical calculations show that after the formation of the Schottky contact, the difference in the work function spontaneously drives electron transfer from Ni to W until the establishment of the built-in electric field and equilibrium of the work function, as shown in Fig. 8b. The redistribution of electrons can be further demonstrated by the charge density difference (CDD) and corresponding plane-averaged CDD along the *Z* direction, as illustrated in Fig. 8c-d [143,144]. The Ni/W_5N_4 catalyst has high electrocatalytic activity such as a potential of only 1.34 V *vs*. RHE to achieve a current density of 10 mA cm^{-2}. Due to the charge redistribution, the catalyst requires a mere overpotential of 25 mV for a current density of 10 mA cm^{-2} in HER. In particular, the Ni/W_5N_4 catalyst-based UOR/HER overall reaction requires only 1.77 V to afford a high current density of 1000 mA cm^{-2} (Fig. 8e). The results indicate that the established built-in electric field accelerates electron transfer, improves the electrical conductivity, and ultimately enhances the HER and UOR activity.

Xu et al. [145] have synthesized a bimetallic metal-organic framework (MOF), NiMn-BDC, based on Ni/Mn sites and terephthalic acid (BDC) ligands by a one-pot solvothermal method. As shown in Fig. 9a, in $NiMn_{0.14}$-BDC, the π-symmetric (t_{2g}) *d*-orbital of Ni^{2+} is fully occupied, which results in a strong e^--e^- repulsive force between the bridging O^{2-} and Ni^{2+}. Fewer electrons are occupied in the t_{2g} orbitals of Mn^{4+} compared to Ni^{2+}, thus allowing electrons to be accommodated in the t_{2g} orbitals of Mn^{4+}. This feature facilitates the transfer of electrons from Ni to adjacent Mn *via* O^{2-} bridging. In addition, the electron density of NiMn-BDC increases at the Fermi level, and the *d*-band center is closer to the Fermi level compared to Ni-BDC, as shown in Fig. 9b. The results indicate higher electrical conductivity and stronger adsorption of the reaction intermediates of the NiMn-BDC, which is conducive to promoting the catalytic reaction. The Gibbs free energy profile in Fig. 9c indicates that the Ni site in NiMn-MOF is the active center for CO $(NH_2)_2$* adsorption, while the Mn site is the adsorption center for NH* and CO*, which effectively reduces the reaction barrier of the rate-determine step and jointly promotes the UOR. As a result, NiMn-BDC exhibits a low voltage of 1.317 V to provide a current density of 10 mA cm^{-2} as well as a high turnover frequency (TOF) of 0.15 s^{-1} achieved at a voltage of 1.4 V, giving rise to a urea degradation rate of 81.87 % in the 0.33 M urea solution. The outstanding properties stem from the MOF platform to tailor the binary active centers.

Under alkaline conditions, UOR requires OH^- to participate in a series of proto-coupled electron transfer processes and break C-N bonds in urea molecules. However, excessive adsorption of OH^- at the active site hinders the adsorption of urea reactants and accelerates the competitive OER [146,147]. Although nickel-based catalysts are suitable for UOR, their performance is hampered by the oxidation of the Ni^{3+}, which initially occurs at the potential of 1.37 V *vs*. RHE [148–150]. Oxidation of NiOOH into high-valence Ni species reduces the UOR activity and stability [151]. The competition between UOR and OER is even more evident in practical applications, especially at high current densities. Therefore, catalysts that can eliminate OER from UOR at high potentials to obtain large apparent current densities and

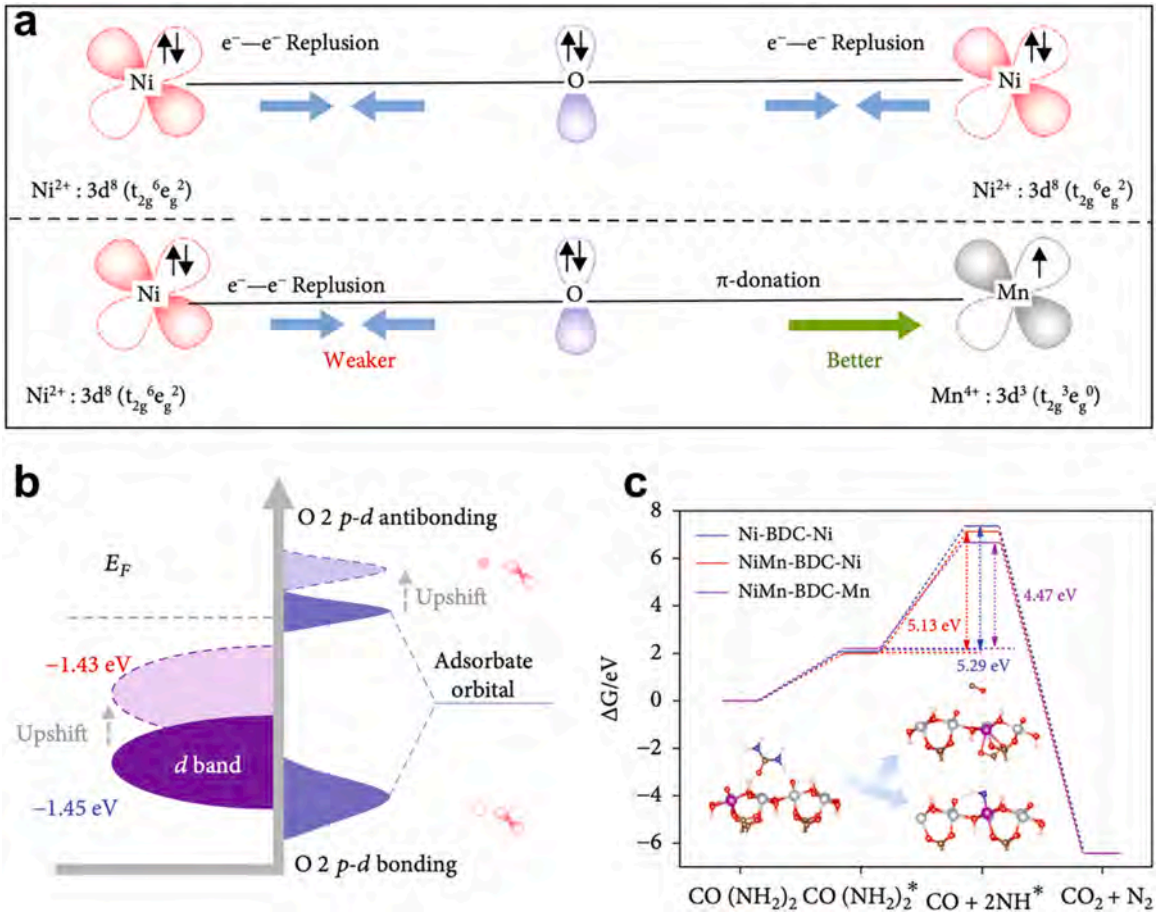

Fig. 9. (a) Schematic illustration of the electronic coupling among Ni, O, and Mn in Ni-BDC and NiMn-BDC. (b) The schematic diagram for the band structures of Ni-BDC and NiMn-BDC. (c) Free energy profiles of the UOR on Ni-BDC and NiMn-BDC with inset showing the structural evolution of the intermediates. Reproduced with permission from reference [145]. Copyright 2022, AAAS.

excellent electrode stability are critical for the development of the UOR-assisted hydrogen production industry [147,152,153].

Zhu et al. [154] have prepared ultra-thin amorphous nickel hydroxide (ANH) flocculent catalysts. At a potential of 2 V *vs*. RHE, the catalyst achieves a current density of 650 mA cm^{-2}, which is higher than the $Ni(OH)_2$ catalyst of 290 mA cm^{-2}. In addition, the mass activity and TOF of the ANH catalyst are 30-fold and 27-fold higher than the Ni $(OH)_2$ catalyst, respectively. Li et al. [89] have proposed the NiCoMoCuO_xH_y electrocatalyst with derived polymetallic co-doped hydroxides showing fairly high UOR activity in an alkaline medium such as potentials of 1.32 and 1.52 V *vs*. RHE to produce current densities of 10 and 500 mA cm^{-2}, respectively. NiCoMoCuO_xH_y with dendritic nanostructures produces a strong electric field distribution to enrich OH^- in the electron double layer and directly strengthen the dehydrogenation oxidation for outstanding UOR performance. Moreover, the NiCoMoCuO_xH_y-based UOR/HER overall reaction greatly accelerates the hydrogen production rate.

Li et al. [155] have proposed the sea urchin-like $Ni_xCo_{3-x}O_4$ (x = 0, 0.75, 0.86, 1, and 1.20) spinel and explored the effect of octahedral nickel atoms in the spinel structure on the UOR properties. The UOR activity is promoted by embedding more Ni ions into the octahedral sites to allow the accumulation of a large number of nickel redox equivalents and increase the low-spin state of Ni^{3+}, as illustrated in Fig. 10a-b. The near-unity occupancy of the e_g orbital of Ni ions enhances the intrinsic UOR activity of spinel catalysts. With increasing Ni content, the TOF of UOR positively correlates with the accumulation capacity of the Ni oxidation equivalent (Fig. 10c). Therefore, $Ni_{1.20}Co_{1.80}O_4$ delivers the highest UOR performance (Fig. 10d) with NiOOH as the active center in UOR.

Carbon coatings are effective in optimizing the adsorption behavior of the active sites to the intermediates, providing high electrical conductivity, preventing serious corrosion of the active material, and improving the UOR performance [156,157]. For example, Wang et al. [158] have prepared Ni/NiO heterostructure nanoparticles coated by graphene for hydrogen production *via* the UOR-coupled HER system. Due to the synergistic effect of Ni nanoparticles, Ni/NiO heterostructure, and oxygen-doped graphene coating layer, the UOR/HER overall reaction configuration requires a voltage of only 1.46 V to drive a current density of 10 mA cm^{-2} in the alkaline electrolyte.

Qian et al. [74] have prepared a carbon-encapsulated (CN) nickel-cobalt alloy coupled with nickel-cobalt molybdenum oxide heterojunction (CoNi@CN-CoNiMoO) for UOR-assisted hydrogen production. Experimental and theoretical studies reveal that electron redistribution occurs between CoNi and CN, leading to the down-shift of the *d*-band center of Co and Ni. This electronic interaction optimizes the adsorption/desorption behavior of the catalyst surface to the reaction intermediates, thereby strengthening the intrinsic activity of UOR and HER. At the same time, the carbon-encapsulated structure enhances the corrosion resistance of the catalyst. The micro-nanoarray structure not only facilitates the exposure of more active sites but also accelerates gas-liquid transport. As a result, the voltages at current densities of 10, 500, and 1000 mA cm^{-2} are 1.34, 1.58, and 1.67 V, respectively, for the UOR/HER overall reaction system. In addition, the catalyst is stable for 120 h at a high current density of 500 mA cm^{-2}.

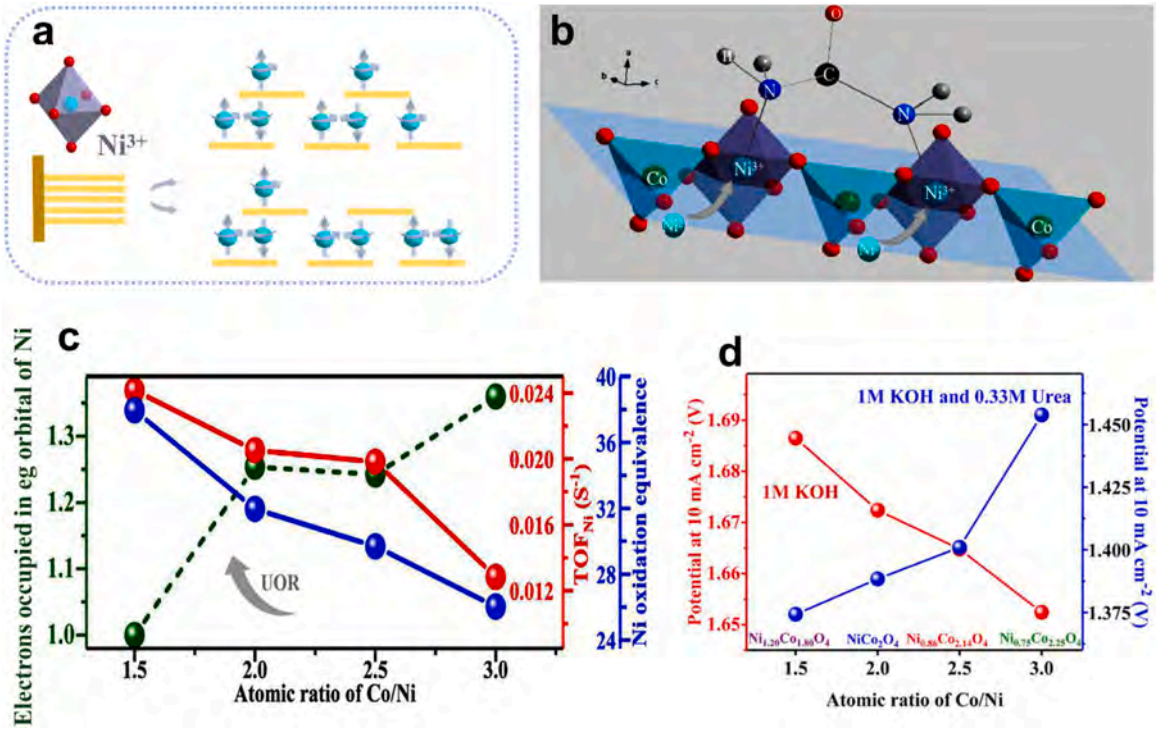

Fig. 10. (a) Spin states of Ni^{3+} at octahedral sites. (b) Combination of urea molecules with the nickel active site on the (311) crystal surface of $Ni_xCo_{3-x}O_4$ spinel. (c) Variation of oxidation equivalence, TOF, and e_g orbital as a function of x in $Ni_xCo_{3-x}O_4$ catalysts. (d) Potentials of OER and UOR at different metal atomic ratios. Reproduced with permission from reference [155]. Copyright 2021, American Chemical Society.

3. Value-adding electrosynthesis coupled with hydrogen production

Coupling the small molecules (hydrazine, urea, etc.) oxidation reaction with HER to produce the hydrogen exhibits superior characteristics in reducing the voltage and energy consumption of the overall reaction system. However, the anodic products are N_2 and CO_2, which are useless and even cause carbon emissions and making full use of the anodic products would enhance the energy conversion efficiency further. In this realm, the meticulous selection of suitable organic and inorganic precursors, which can be used as raw materials to synthesize value-added products, becomes paramount. Potential candidate raw materials, such as low-carbon alcohols, aromatic alcohols, primary amines, benzylamines, and biomass-derived platform molecules, play crucial roles in this respect, as listed in Table 2.

3.1. Alcohol oxidation reaction

Methanol is a typical and commonly used C_1 feedstock for chemicals such as formic acid (HCOOH) or formate. The partial methanol oxidation reactions (MOR, $CH_3OH_{solution} + H_2O\ (l) \rightarrow 4H^+ + HCOOH_{solution}$, $\Delta G^0_{reaction} = 40.1\ kJ\ mol^{-1}$, $E^0_{cell} = 0.103\ V$) requires lower potential than that of OER [196]. Additionally, the price of HCOOH (approximately $1300) is higher than that of methanol (approximately $350) [197, 198]. Therefore, coupling the MOR with HER to produce hydrogen not only reduces energy consumption but also produces high-value products [199,200]. For instance, Zhao et al. [201] have prepared carbon nanofibers@NiSe (CNFs@NiSe) core/sheath nanostructures by one-pot method. DFT calculations show that the high electrocatalytic selectivity is attributable to the unique exposure of the NiSe(102) surface, which promotes the conversion of methanol to formic acid by inhibiting further oxidation to CO_2. Therefore, the catalyst has been applied to convert the methanol into value-adding formate at a high current density (approximately 345 mA cm^{-2}) with a Faraday efficiency of more than 95 %. The results indicate that hydrogen is produced simultaneously with the value-added formate at high selectivity with less energy consumption.

Modification of surface structures can alter the electronic configuration and the band structure of the surface-active sites to ensure fast charge transfer and optimal adsorption to the intermediates during electrocatalysis. Hao et al. [69] have synthesized highly dispersed FeNi oxide heterojunction (Fe_2O_3/NiO) anchored on NF by ultrafast solution combustion strategy. To understand the effect of the strong electronic interaction between NiO and Fe_2O_3 on the catalytic performance, the detailed MOR mechanism is investigated. As shown in Fig. 11a, the reaction occurs on the surface of the NiOOH. The MOR/HER overall reaction configuration (Fig. 11b) composed of Fe_2O_3/NiO shows a high current density of 500 mA cm^{-2} at the voltage of 1.654 V with a high Faraday efficiency of more than 98 %. The highly dispersed Ni-O-Fe structure is considered to be the main active site for the conversion of methanol to formate. The Fe_2O_3/NiO heterojunction provides a unique synergistic active site and lowers the potential barriers of the dehydrogenation steps (Fig. 11c), resulting in the favorable dynamic conversion of methanol to formate.

Peng et al. [21] have proposed an integrated MOR and HER system driven by solar cells to realize energy-efficient hydrogen production, as shown in Fig. 12a. The bifunctional electrocatalyst containing NiSe/-$MoSe_2$ heterointerfaces (NMS/CC) is prepared on a carbon cloth, and the interactions between the atoms at the heterointerfaces balance the adsorption energies of the reactants/intermediates/products and promote the kinetics of the HER and MOR reactions. The NMS/CC electrocatalyst has a higher efficiency in MOR with a potential of 15 % smaller than that of OER at a current density of 100 mA cm^{-2}, as shown in Fig. 12b. ^1H NMR performed on the electrolyte after MOR reveals CHOO- (Fig. 12c), which is an industrial value-adding by-product that can be extracted and converted to formic acid. Therefore, using MOR instead of OER is beneficial to energy-saving hydrogen production.

The glycerol oxidation reaction (GOR), a typical nucleophilic oxidation reaction, is a promising alternative anodic reaction to couple with cathodic HER for hydrogen production [202]. Electrocatalytic GOR

Table 2
Typical value-adding electrosynthesis coupled hydrogen production systems.

Catalyst	Raw material	By-product	Cell voltage at 10 mA cm^{-2}	$FE^{[a]}$ of H_2 [%]	$\Delta E^{[b]}$	ref
NiIr-MOF/NF	methanol	formate	1.39 V	100	170 mV	[159]
$Co(OH)_2$@HOS/CP	methanol	formate	1.497 V	100	134 mV	[160]
Fe_2O_3/NiO	methanol	formate	1.654 V @ 500 mA cm^{-2}	98	135 mV	[69]
Pd@RhPd NDs	methanol	formate	0.813 V	–	859 mV	[161]
$CoPt_3$@Co_2P/Co@NCNT	methanol	formate	1.43 V	–	–	[162]
Pt-NP/NiO-NS	methanol	formate	1.39 V	–	300 mV	[35]
NiS/NF	methanol	formate	1.5 V	–	140 mV	[163]
NMS/CC	methanol	formate	1.5 V @ 50 mA cm^{-2}	–	150 mV @ 50 mA cm^{-2}	[21]
Ru/$Ni(OH)_2$	ethanol	acetaldehyde	1.49 V	–	110 mV	[164]
C@Ni-Pd	ethanol	acetic acid	0.95 V @ 100 mA cm^{-2}	–	859 mV @ 100 mA cm^{-2}	[165]
SA In-Pt NWs/C	ethanol	acetic acid	0.62 V	100	190 mV	[166]
MoO_x/Pt	glycerol	glycerate	0.70 V	100	900 mV	[167]
Ni-Mo-N/CFC	glycerol	formate	1.36 V	99.7	260 mV	[168]
Ru@Ni-B/NF	glycerol	–	1.24 V	–	180 mV	[169]
Ru-Ni_xP_y/N-C	glycerol	formate	1.36 V	99.5	–	[170]
$NiCrO_x$/Ni	glycerol	formate	1.675 V @ 20 mA cm^{-2}	100	226 mV @ 20 mA cm^{-2}	[171]
Ni_3N/Co_3N-NWs	glycerol	formate	1.79 V @ 400 mA cm^{-2}	96.7	220 mV @ 400 mA cm^{-2}	[172]
Cu-Cu_2O/CC	glycerol	formate	0.59 V	100	320 mV	[173]
Au/CoOOH	Benzyl Alcohol	Benzoic acid	1.50 V @ 540 mA cm^{-2}	99	–	[174]
NC@$CuCo_2N_x$/CF	Benzyl Alcohol	Benzoic acid	1.55 V	80	70 mV	[31]
Co_3O_4/CF	HMF[c]	FDCA[d]	1.385 V	99.8	121 mV	[175]
Ni_3N@C	HMF	FDCA	1.55 V @ 50 mA cm^{-2}	–	240 @ 50 mA cm^{-2}	[176]
Co-P/CF	HMF	FDCA	1.44 V @ 20 mA cm^{-2}	–	150 @ 20 mA cm^{-2}	[177]
MoO_2-FeP@C	HMF	FDCA	1.486 V	97.8	106 mV	[178]
Cu_xS $Ni_{0.75}Co_{0.25}O_mH_n$	HMF	FDCA	1.58 V @ 100 mA cm^{-2}	–	270 mV @ 100 mA cm^{-2}	[179]
NF/Co_4N@CeO_2	HMF	FDCA	1.33 V	86.5	200 mV	[180]
$NiCo_2$@MoO_2/NF	HMF	FDCA	1.25 V	99.1	264 mV @ 50 mA cm^{-2}	[181]
Co@NiMoO-Ni/NF	HMF	FDCA	1.21 V	98.9	400 mV	[182]
Cu/Ni_3S_2-R	HMF	FDCA	1.57 V @ 50 mA cm^{-2}	–	230 mV @ 50 mA cm^{-2}	[183]
NiVP/Pi-VC	glucose	gluconic acid	1.3 V	99.1	280 mV	[184]
Ni-MoS_2 NPs	glucose	gluconic acid	1.67 V	–	270 mV	[185]
Cu(I)/Cu(II)	glucose	gluconic acid	0.92 V @ 100 mA cm^{-2}	–	980 mV @ 100 mA cm^{-2}	[186]
CNTs@Co/CoP	glucose	gluconic acid	1.42 V	–	320 mV	[187]
Cr, S-NiFe	glucose	formate	1.337 V @ 20 mA cm^{-2}	–	227 mV @ 20 mA cm^{-2}	[188]
$NiCoSe_x$	glucose	formate	1.5 V @ 200 mA cm^{-2}	–	390 mV @ 20 mA cm^{-2}	[189]
$Co_2P_4O_{12}$	benzylamine	benzonitrile	1.44 V @ 50 mA cm^{-2}	100	201 mV @ 50 mA cm^{-2}	[190]
NiSe	benzylamine	benzonitrile	1.49 V @ 20 mA cm^{-2}	100	210 mV @ 20 mA cm^{-2}	[191]
t-Ni/Co MOF	benzylamine	benzonitrile	1.48 V	90	275 mV	[192]
$CoSe_2$/NiSVs	benzylamine	benzonitrile	1.37 V	98.9	320 mV	[193]
$Mo_{0.8}Ni_{0.2}N$-Ni_3N/NF	benzylamine	benzonitrile	1.39 V @ 50 mA cm^{-2}	100	230 mV @ 50 mA cm^{-2}	[194]
$Ni(OH)_2$-UNMs/NF	benzylamine	benzonitrile	1.41 V	100	–	[195]

[a] FE: Faraday efficiency
[b] ΔE: The voltage decrease of the coupled reactions compared to the HER/OER couple at 10 mA cm^{-2}.
[c] HMF: 5-hydroxymethylfurfural.
[d] FDCA: 2,5-furandicarboxylic acid.

is able to convert biomass by-products into high-value chemicals, which are environmentally friendly, sustainable, and highly efficient [203]. Moreover, GOR (E^{θ} = 0.69 V *vs.* RHE) is more thermodynamically favorable than the OER (E^{θ} = 1.23 V *vs.* RHE). Therefore, replacing the OER with GOR to couple with HER not only significantly reduces the energy consumption for hydrogen production, but also utilizes biomass-derived resources for the synthesis of value-added chemicals in an environmentally sustainable manner [168,204]. For instance, Zhu et al. [172] have synthesized Ni_3N/Co_3N heterostructure nanowires (Ni_3N/Co_3N-NWs). The heterointerface modulates the electron distribution and accelerates glycerol dehydrogenation kinetics. Additionally, it is more favorable for *H adsorption/desorption in HER, giving rise to enhanced bifunctional electrocatalytic performance. In GOR, the Ni_3N/Co_3N-NWs achieve current densities of 50 and 200 mA cm^{-2} at low potentials of 1.26 and 1.34 V *vs.* RHE, respectively, with a Faraday efficiency of 94.6 % from glycerol to formate. Moreover, a flow cell assembled with Ni_3N/Co_3N-NWs (Fig. 13a) requires only 2.01 V to achieve an industrial-level current density of 1 A cm^{-2}, with formate and H_2 yields reaching 11 and 21.4 mmol cm^{-2} h^{-1} (Fig. 13b-c), respectively. This highlights the exceptional electrocatalytic properties of Ni_3N/Co_3N-NWs and the potential for efficient energy conversion and electrosynthesis of valuable chemicals.

Yu et al. [205] have reported an environmentally controllable γ-ray irradiation reduction method to synthesize a series of noble metal nanoparticles anchored on defect-rich manganese oxide (M@MnO_{2-x}, where M=Ru, Pt, Pd, Ir), as schematically illustrated in Fig. 14a. The Ru nanoparticles are firmly immobilized within the defective MnO_2 to exhibit strong interface synergistic effects. Due to electron repulsion in the symmetric structure, electrons around the Ru site of Ru-O-Mn-O in Ru@MnO_2 are difficult to transfer to the adjacent Mn site. On the contrary, because of the oxygen vacancies in Ru@MnO_{2-x}, an asymmetric Ru-O-Mn-O_v configuration is formed to accelerate electron transport from the Mn site to the Ru-bound O, as shown in Fig. 14b. This synergy, facilitated by the penetrating power of γ-rays, allows the simultaneous formation of nanoparticles and defect carriers. The metal-oxygen bonds bridging these entities ensure structural stability and ample exposure to active sites [206]. An anion exchange membrane (AEM) flow electrolysis cell is assembled with Ru@MnO_{2-x} as a bifunctional electrocatalyst. The flow cell achieves an industrial-level current density of 0.5 A cm^{-2} at a low voltage of 1.68 V (Fig. 14c). Furthermore, the system demonstrates stable operation for over 100 hours at 0.5 A cm^{-2}, as shown in Fig. 14d. *In situ* spectroscopic analysis during the electrocatalysis indicates that Ru@MnO_{2-x} effectively balances the competitive adsorption of glycerol and OH* on the catalyst surface. This work underscores the potential application of this environmentally controllable γ-ray irradiation reduction method in the preparation of efficient bifunctional

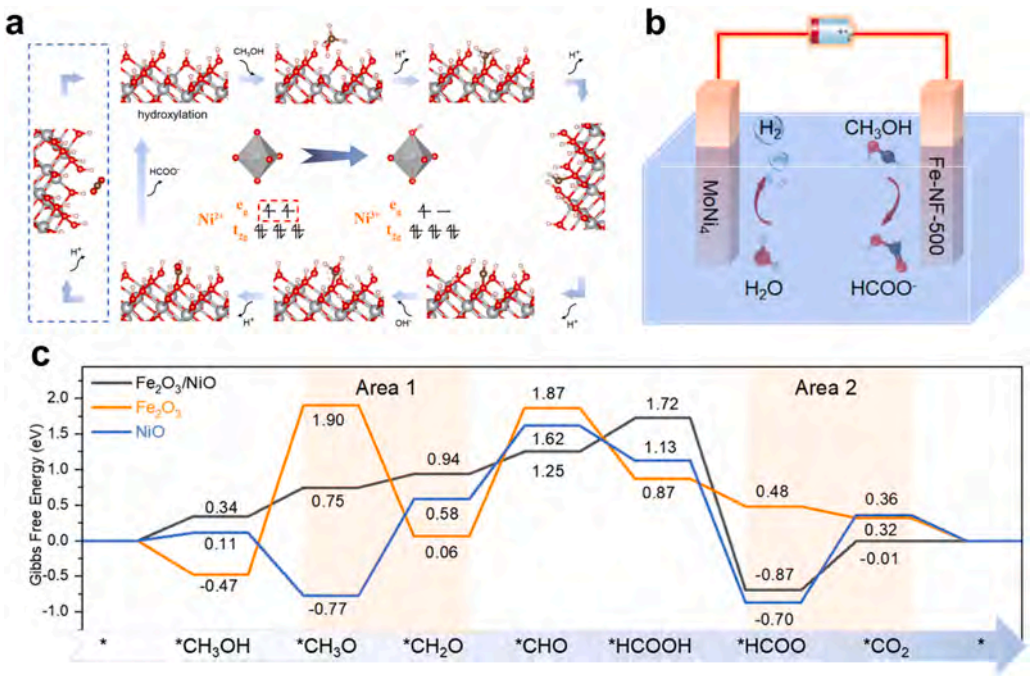

Fig. 11. (a) Schematic of the MOR mechanism for Fe_2O_3/NiO. (b) The two-electrode electrolyzer of MOR/HER overall reaction. (c) Gibbs free energy diagrams for MOR. Reproduced with permission from reference [69]. Copyright 2023, the Royal Society of Chemistry.

electrocatalysts and provides strong support for practical electrolysis energy conversion applications.

Electrocatalytic oxidation of ethanol [166], 1,3-propanediol [207], ethylene glycol [208], and benzyl alcohol [31,209] can also serve as alternatives to anodic OER to reduce the energy input for the anodic oxidation reaction. This is attributed to the easier oxidation property of the active hydroxyl groups compared to water molecules. Furthermore, the alcohols not only have abundant resources but also hold the potential for conversion into value-added products. For example, Li et al. [210] have synthesized an Au/CoOOH nanoparticle catalyst. The benzyl alcohol enriches at the Au/CoOOH interface, leading to the generation of electrophilic oxygen species (OH*) on CoOOH and higher activity than pure Au. In benzyl alcohol oxidation, a current density of 340 mA cm^{-2} is observed at the potential of 1.3 V *vs.* RHE from the Au/CoOOH catalyst. The benzyl alcohol oxidation rate and H_2 yield reach 3.19 mmol cm^{-2} h^{-1} and 117.9 mL cm^{-2} h^{-1}, respectively. In a membrane-free flow electrolysis cell with two electrodes, the current reaches 4.8 A at a voltage of 2.0 V.

3.2. Aldehyde oxidation reaction

The combination of thermodynamically advantageous electro-oxidation of biomass derivatives and HER not only upgrades the biomass to high-value-added chemicals, but also achieves energy-efficient hydrogen production [211]. 5-Hydroxymethylfurfural (HMF) is an important biomass-platform molecule, which is an acid-catalyzed dehydration product of biomass-derived hexose and pentose. Its oxidation to value-adding chemicals is one of the most prominent reactions studied in the field [212]. The oxidation reaction of HMF (HMFOR) to 2, 5-furandicarboxylic acid (FDCA) is considered a "green" chemical platform, which replaces terephthalic acid as a list of synthetic polymer materials [179]. The potential of HMFOR (0.113 V *vs.* RHE) is much lower than that of OER. It possesses two distinct active functional groups, aldehyde and hydroxyl, which can undergo oxidation reactions to yield various high-value products [213]. The production of FDCA by highly selective electrooxidation of HMF is a more convenient, gentle, and economical method than the traditional production route of high-value-added chemicals [214]. Therefore, coupling the HMFOR with HER is proposed to produce additional products with high value and improve the energy efficiency of hydrogen production [215].

There are several methods for the selective oxidation of HMF to FDCA by organic chemical reactions, which typically require a harsh reaction environment. For example, high temperature (> 100 °C) and high oxygen pressures (0.3–2.4 MPa) are essential, which pose serious problems in terms of safety and cost [216,217]. The electrocatalytic reaction has the advantages of accurate process control, mild reaction conditions, wide substrate tolerance, high energy utilization, and safe operation. In addition, the electrocatalytic oxidation driven by the directional flow of electrons is promising in the selective oxidation of alcohols and aldehydes [175]. Up to now, various non-noble metal materials, such as Ni-based, Co-based, and Fe-based catalysts, have been applied as electrocatalysts for these reactions [178,218–220]. Although Ni_xB [215], NiCoFe-LDHs [221], and $NiCo_2O_4$ [222] have been proposed as potential electrocatalysts for HMFOR, they are inferior in HER. Hence, bifunctional electrocatalysts for both HER and HMFOR are essential to achieving highly efficient coupled hydrogen production [172,223–225].

The heterojunction formed by interface engineering promotes electron transfer, modifies the adsorption/desorption behavior of the active species in the electrocatalytic reaction, and optimizes the catalytic capability [226,227]. The heterojunction-based materials, such as Ni_3S_2-MoS_2 and Cu_xS@NiCo-LDH [179,223], have been reported as the bifunctional electrocatalysts for HMFOR coupled HER. Yang et al. [178] have designed and fabricated porous nanoparticles consisting of carbon-encapsulated MoO_2-FeP heterojunction (MoO_2-FeP@C) with an abundant active interface as bifunctional electrocatalysts for HER and HMFOR. The electrons accumulated at FeP optimize H_2O and H* absorption, while holes accumulated at MoO_2 improve the HMFOR activity. The electrolytic cell comprising MoO_2-FeP@C for the production of H_2 at the cathode and FDCA at the anode can be operated at a low voltage of only 1.486 V for a current density of 10 mA cm^{-2}. Thapa et al. [228] have synthesized a ternary heterostructure based on Ni_xS_y, MoS_2, and MoC on onion-like carbon for anodic additive oxidation of HMF. The heterostructured electrocatalyst selectively catalyzes the oxidation of HMF to produce FDCA with Faraday efficiency and yield of 100 %.

Wu et al. [181] have controllably grown a MoO_2 layer with a

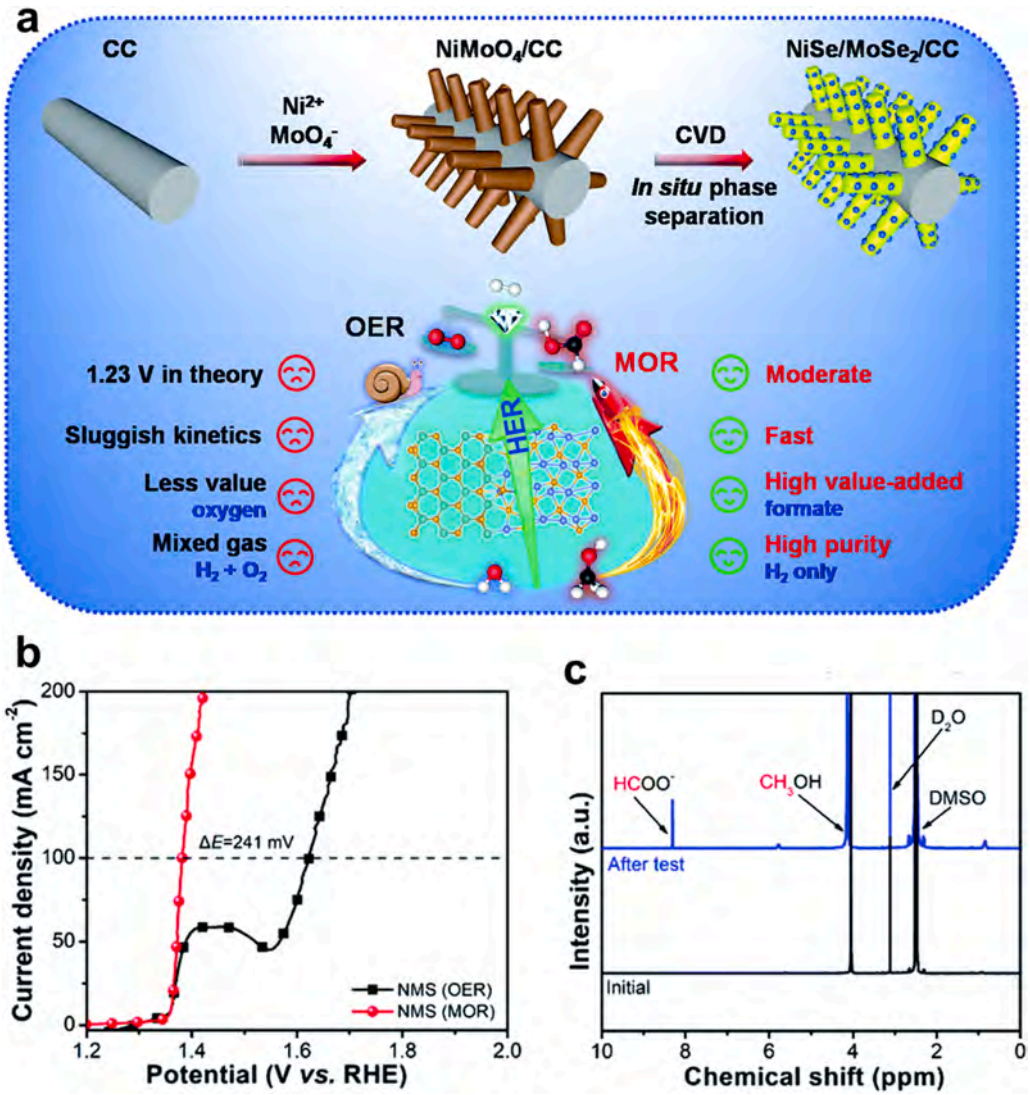

Fig. 12. (a) Schematic illustration of the preparation of the bifunctional NMS/CC electrocatalyst and application for MOR-coupled energy-saving hydrogen production. (b) Polarization curves. (c) ^{1}H NMR spectra of the electrolyte before and after the test. Reproduced with permission from reference [21]. Copyright 2022, the Royal Society of Chemistry.

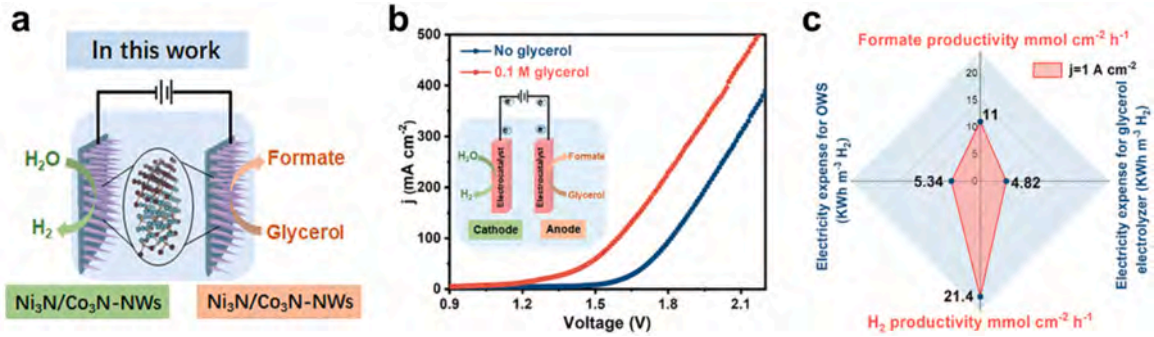

Fig. 13. (a) GOR/HER configuration composed of Ni_3N/Co_3N-NWs catalyst. (b) LSV curves with or without 0.1 M glycerol in 1.0 M KOH. (c) Yields and electricity expense for the electrolyzers. Reproduced with permission from reference [172]. Copyright 2023, Wiley-VCH.

thickness of 2–4 nm on a $NiCo_2$ nanowire skeleton ($NiCo_2$@MoO_2/NF). The precise control modulates the electronic structure of $NiCo_2$@MoO_2/NF, thereby accelerating electron/proton transfer and optimizing the adsorption behavior of intermediates in both HMFOR and HER. Consequently, efficient coupling of biomass upgrading and hydrogen production is achieved. Additionally, they have prepared a three-dimensional hierarchical micro-nanoarray catalyst by leveraging synergistic interactions between components to achieve bifunctionality in catalyzing HMFOR coupled with HER, as illustrated in Fig. 15a [182]. The resulting Co@NiMoO-Ni/NF delivers excellent electrocatalytic

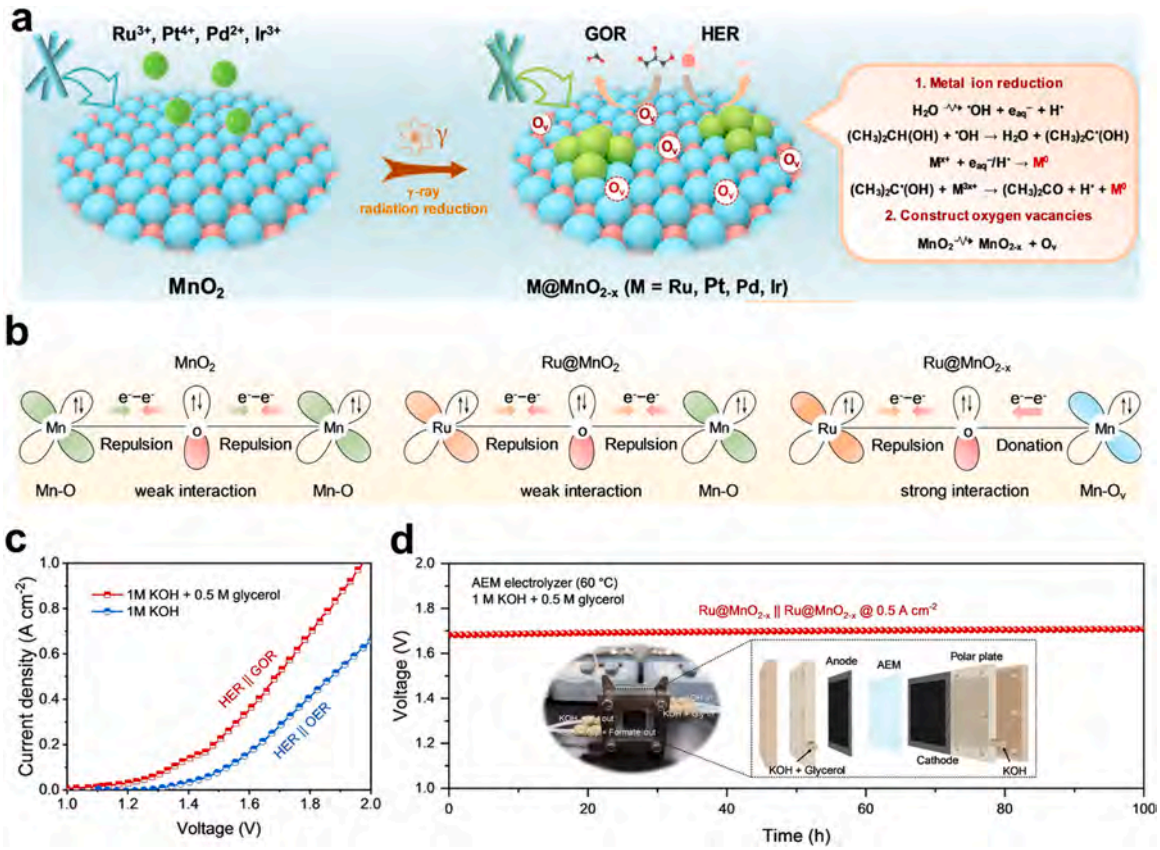

Fig. 14. (a) Schematic illustration of the synthesis of M@MnO_{2-x} (M=Ru, Pt, Pd, and Ir) and application as bifunctional catalysts for GOR and HER. (b) Electronic coupling on adjacent Ru/Mn-O-Mn in MnO_2, Ru@MnO_2, and Ru@MnO_{2-x}. (c) LSV curves of HER||GOR and HER||OER couples. (d) Stability test of the GOR/HER couple in the flow cell with an inset showing the AEM flow electrolyzer. Reproduced with permission from reference [205]. Copyright 2023, Wiley-VCH.

performance for biomass upgrading and hydrogen production. In the two-electrode system, a remarkable current density of 10 mA cm^{-2} for HMFOR/HER is achieved at a low voltage of only 1.21 V (Fig. 15b), highlighting the significant potential for biomass upgrading and hydrogen production. When HMFOR/HER is carried out at a voltage of 1.40 V, HMF can be completely transformed within 120 min. The FDCA yield is high (~98.6 %), and the Faraday efficiency can reach ~ 99.1 %, as shown in Fig. 15c. The superior catalytic performance is attributed to the strong interaction between the template (Co) and nanosheet-modified nanoarray (NiMoO-Ni), effectively tuning the catalyst's electronic structure, optimizing the adsorption behavior of intermediates in HMFOR/HER, and promoting the bond cleavage of crucial intermediates during the HMFOR process (Fig. 15d).

Rare-earth oxides possess abundant oxygen vacancies and excellent affinity to oxygen-containing species and significant potential in superior electrocatalysis [229,230]. Xie et al. [231] have prepared a Co $(OH)_2$-CeO_2 composite *via* electrodeposition as the catalyst in the selective electrocatalytic conversion of HMF into value-adding chemicals. Through the double-electron oxidation of aldehyde groups, HMF is selectively converted to 2-furancarboxylic acid (HMFCA) with a high selectivity of 89.4 % and a yield of 8.5 mmol cm^{-2} at 1.4 V *vs.* RHE under neutral conditions. The coupled hydrogen production at the cathode is 4.1 times higher than that of the OWS system at the voltage of 1.4 V, indicating that HMFOR can replace OER to achieve highly efficient hydrogen production.

Zhou et al. [180] have constructed the Co_4N@CeO_2 heterostructure, in which CeO_2 serves as an "electron pump" to facilitate the electron transfer from Co_4N to CeO_2. The optimized electronic structure at the interface endows Co_4N@CeO_2 with outstanding HER and HMFOR properties. Specifically, to achieve a current density of 10 mA cm^{-2}, HMFOR only requires an ultra-low potential of 1.22 V *vs.* RHE in the electrolyte of 1.0 M KOH and 300 mM HMF, which is 273 mV lower than the potential required in 1.0 M KOH electrolyte. Theoretical calculations indicate that CeO_2 reduces the potential barriers of the rate-determining steps to facilitate the HMFOR process. The multifunctional electrocatalyst has remarkable HER and HMFOR activities and promises to achieve "carbon neutrality".

3.3. Glucose oxidation reaction

Glucose is the most abundant monosaccharide with the characteristics of non-toxicity, low cost, easy-to-obtain and sustainable resources from biomass. The glucose oxidation reactions (GOR) can be applied to produce a variety of commercial chemicals such as HMF, sorbitol, D-gluconic acid (GNA), and gluconic acid (GRA) [232,233]. GRA is considered to be the "highest value-adding compound" produced from biomass. Oxidation of glucose produces GRA and hydrogen gas as a product stream, which also has a lower reaction potential (0.05 V *vs.* RHE) than OER [232,234]. Liu et al. [232] have used the NiFe LDH nanosheet array as the precursor to prepare nano-scale $NiFeO_x$ and $NiFeN_x$ catalysts on 3D NF, as schematically illustrated in Fig. 16a. The two catalysts show outstanding activity and selectivity in GOR-coupled HER. The two-electrode cell assembled with these two catalysts shows a current density of 100 mA cm^{-2} at a voltage of 1.39 V (Fig. 16b) with a Faraday efficiency of 87 % and a GRA yield of 83 %. *In situ* infrared spectroscopy confirms that GRA is produced by glucose electrolysis. The cost of producing GRA by electrochemical reduction of glucose is 54 % lower than that of current chemical methods, indicating that GOR/HER is an energy-saving and cost-effective method for hydrogen production and biomass conversion.

Thakur et al. [184] have demonstrated nickel vanadium phosphide/phosphate-Vulcan carbon (NiVP/Pi-VC) microspheres as

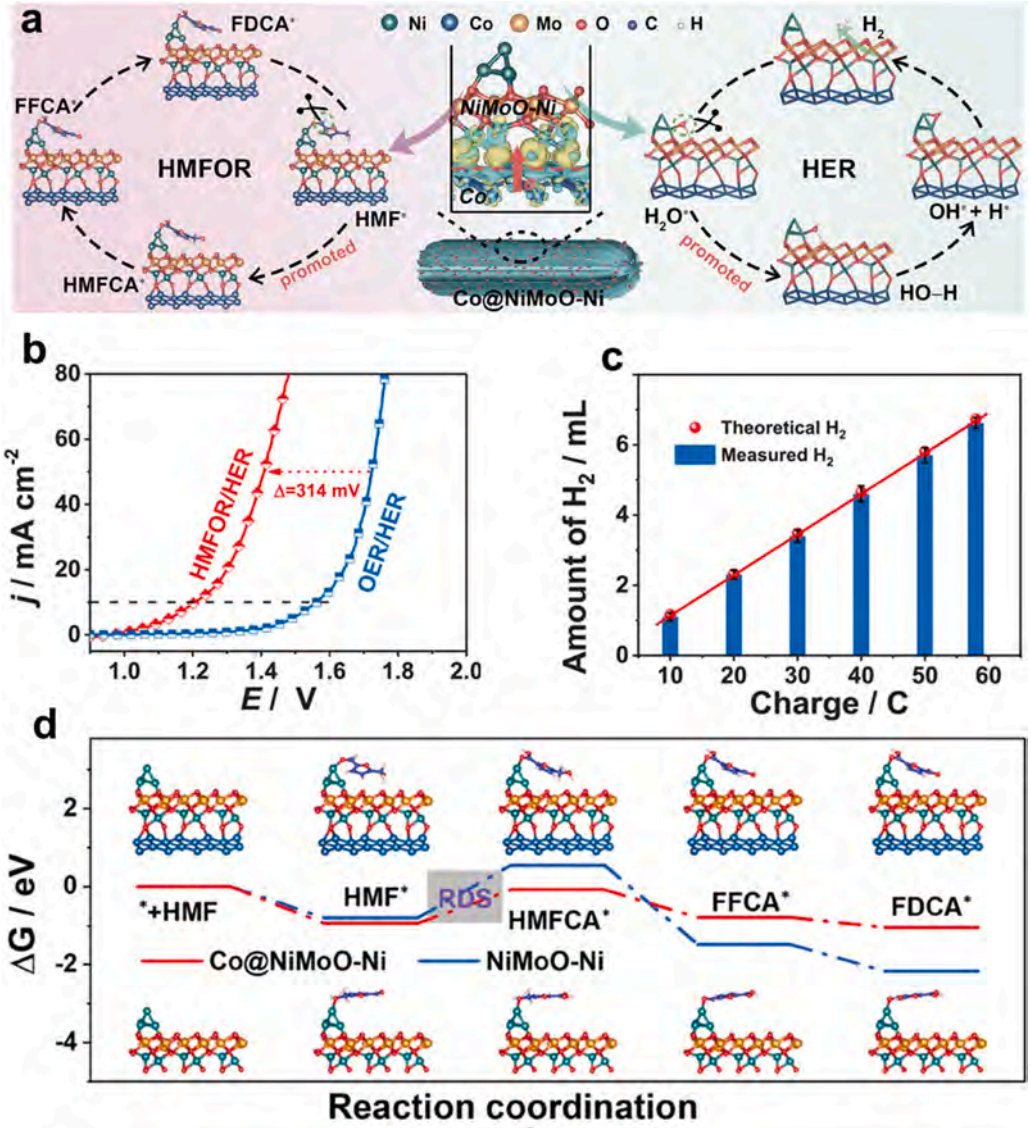

Fig. 15. (a) Schematic diagram of HMFOR/HER and the mechanism. (b) LSV curves of HMFOR/HER and OER/HER couples in a two-electrode electrolyzer. (c) Theoretical calculated and experimental measured amount of H_2. (d) Free energy diagram of HMFOR on Co@NiMoO-Ni and NiMoO-Ni surfaces. Reproduced with permission from reference [182]. Copyright 2024, Wiley-VCH.

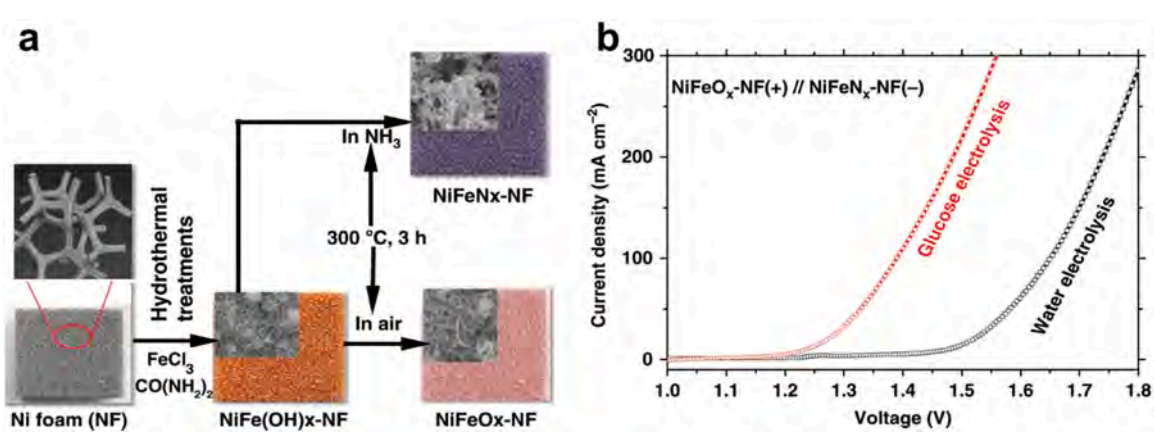

Fig. 16. (a) Schematic illustration for the synthesis of $NiFeN_x$ and $NiFeO_x$ catalysts. (b) LSV curves of electrolysis and water electrolysis with the same anodic $NiFeO_x$ and cathodic $NiFeN_x$ catalysts. Reproduced with permission from reference [232]. Copyright 2020, Springer Nature.

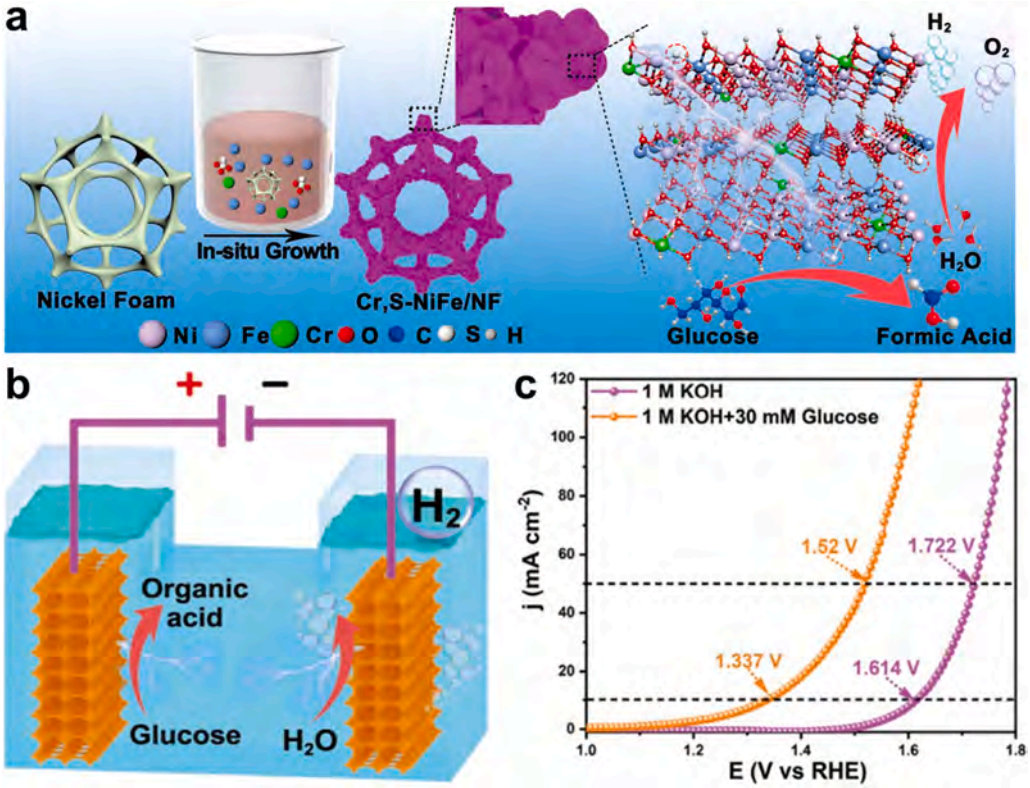

Fig. 17. (a) Scheme of the one-step synthesis of Cr, S-NiFe/NF. (b) Scheme of the electrolyzer for organic acid and hydrogen co-production. (c) LSV curves of the Cr, S-NiFe/NF catalyst for water splitting in 1 M KOH with and without glucose. Reproduced with permission from reference [188]. Copyright 2023, Springer Nature.

GOR/HER bifunctional electrocatalysts, which show good electrocatalytic activity in the alkaline medium for the production of both value-adding products and H_2, in addition to being energy saving and economy. The GOR/HER only requires a voltage of 1.3 V, which is superior to the typical OWS. Wei et al. [188] have developed a cationic and anionic co-doping strategy to synergistically modulate the electronic structure of NiFe layered double hydroxides, which significantly facilitates the exposure of catalytically active centers and improves the electrocatalytic conversion of glucose with hydrogen production (Fig. 17a). The heteroatoms Cr and S promote the reversible redox of Ni $(OH)_2(Ni^{2+})$/NiOOH (Ni^{3+}) as well as the charge transfer and adsorption capacity of glucose. The potential required to afford a current density of 10 mA cm^{-2} in GOR is only 1.219 V *vs*. RHE, which is 226 mV lower than the OER. The two-electrode electrolyzer of GOR/HER with Cr, S-NiFe/NF (Fig. 17b) shows significant glucose oxidation and hydrogen production. The voltage needed to reach a current density of 10 mA cm^{-2} is only 1.337 V, as shown in Fig. 17c. At the same time, value-adding organic acid is generated on the anode, and the hydrogen production rate increases by 9 times compared to the HER/OER couple.

Notably, the integration of metals with semiconductors to form Mott-Schottky heterojunctions is currently one of the most promising strategies to promote catalytic activity [127,235,236]. Electrons at the heterojunction flow spontaneously to constantly regulate the work function of the Schottky barrier and modify the electronic structure and energy band of the interface. Zhang et al. [187] have designed a series of multistage Mott-Schottky beaded CNTs@Co/CoP materials with controllable compositions with high intrinsic activity and multiple active sites. The Schottky heterointerface of Co/CoP reduces the dissociation energy barrier of the initial H_2O, thermal neutral ΔG_{H^*}, and energy barrier of GOR. Therefore, the catalyst shows excellent HER (η_{10} = 151 mV) and GOR characteristics. To produce a current density of 10 mA cm^{-2}, the voltage required by the GOR/HER couple is 0.52 V smaller than that of the HER/OER couple.

Wu et al. [237] have prepared Co@CoO heterojunctions with different structural characteristics. Spontaneous electron transfer from Co to CoO causes the up-shift of the *d*-band center in Co@CoO toward the Volmer-Heyrovsky path. Coupling GOR with HER delivers excellent performance in hydrogen production and value-adding chemical synthesis. The technique can be potentially applied to regulate the Mott-Schottky heterojunction through defective MOF precursors for hydrogen production as low-voltage inputs and biomass upgrading simultaneously.

Coupling a metal electrode with low initial potential with HER reduces the power consumption significantly [238]. It has been reported that Cu(II) can be reduced to Cu(I) by glucose, accompanied by the formation of GRA [239]. Zhang et al. [186] have established a Cu(I)/Cu(II) redox-coupled hydrogen production system by introducing glucose as a reducing sacrificial agent, as shown in Fig. 18a. In this redox cycle, Cu_2O is oxidized to $Cu(OH)_2$ at a low initial potential (0.7 V *vs*. RHE). The $Cu(OH)_2$ is instantly reduced back to Cu_2O by glucose to complete the Cu(I)/Cu(II) redox cycle. With the help of the $Cu(OH)_2$ electrode, glucose adsorbs on the surface with the adsorption-free energy of −1.58 eV (Fig. 18b), indicating the strong interaction between glucose and $Cu(OH)_2$ electrode. The current density of 100 mA·cm^{-2} can be achieved at a voltage input of a mere 0.92 V, as shown in Fig. 18c. Notably, the electricity consumption of the assembled overall reaction is only 2.2 kWh Nm^{-3} (H_2) for the operation at a current density of 100 mA cm^{-2}, which is half of the typical HER/OER hydrogen production (4.5 kWh Nm^{-3} (H_2)), as illustrated in Fig. 18d. This study provides a new method for low cost, high efficiency, and safety of hydrogen production and suggests a new opportunity for the development of organic oxidation coupling electrolytic systems.

3.4. Amine oxidation reaction

Amines (R-NH_2) can be electrocatalytically oxidized into nitriles (R-

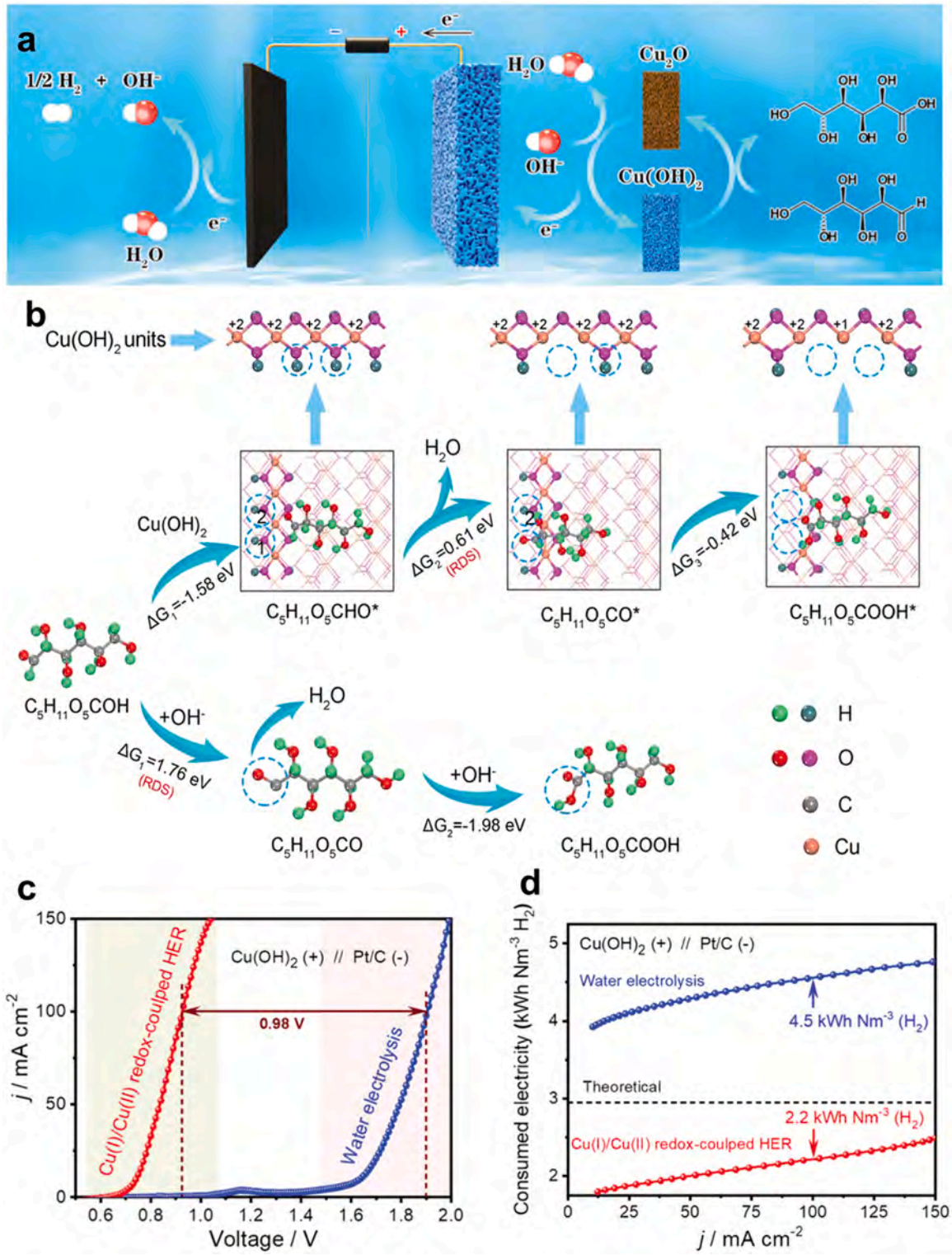

Fig. 18. (a) Mechanism scheme for a glucose-assisted Cu(I)/Cu(II) redox-coupled hydrogen production system. (b) The reaction pathway for glucose to form gluconic acid with/without $Cu(OH)_2$ electrode. The change in valence of Cu^{2+} is shown at the top of the picture. (c) LSV curves in a flow cell electrolyzer using $Cu(OH)_2$ as the anode and Pt/C as the cathode. (d) The calculated electricity consumption for hydrogen production in different configurations. Reproduced with permission from reference [186]. Copyright 2021, Wiley-VCH.

C≡N) at a theoretical potential of 0.5–0.8 V *vs*. RHE and is important to the industrial, pharmaceutical, and coatings sectors [240–243]. Benzonitrile (BN) is a representative aromatic nitrile conventionally synthesized by the benzoic acid amination method, but it suffers from high pollution and low yield. Selective electrooxidation of benzylamine (BA) for the production of BN is operated at a theoretical potential of 0.76 V *vs*. RHE, enabling a mild nitrile evolution reaction (NER) [244,245]. The potential for NER is lower than OER and therefore, coupling NER with HER is possible to reduce the energy consumption of electrocatalytic hydrogen production. However, despite remarkable progress in this

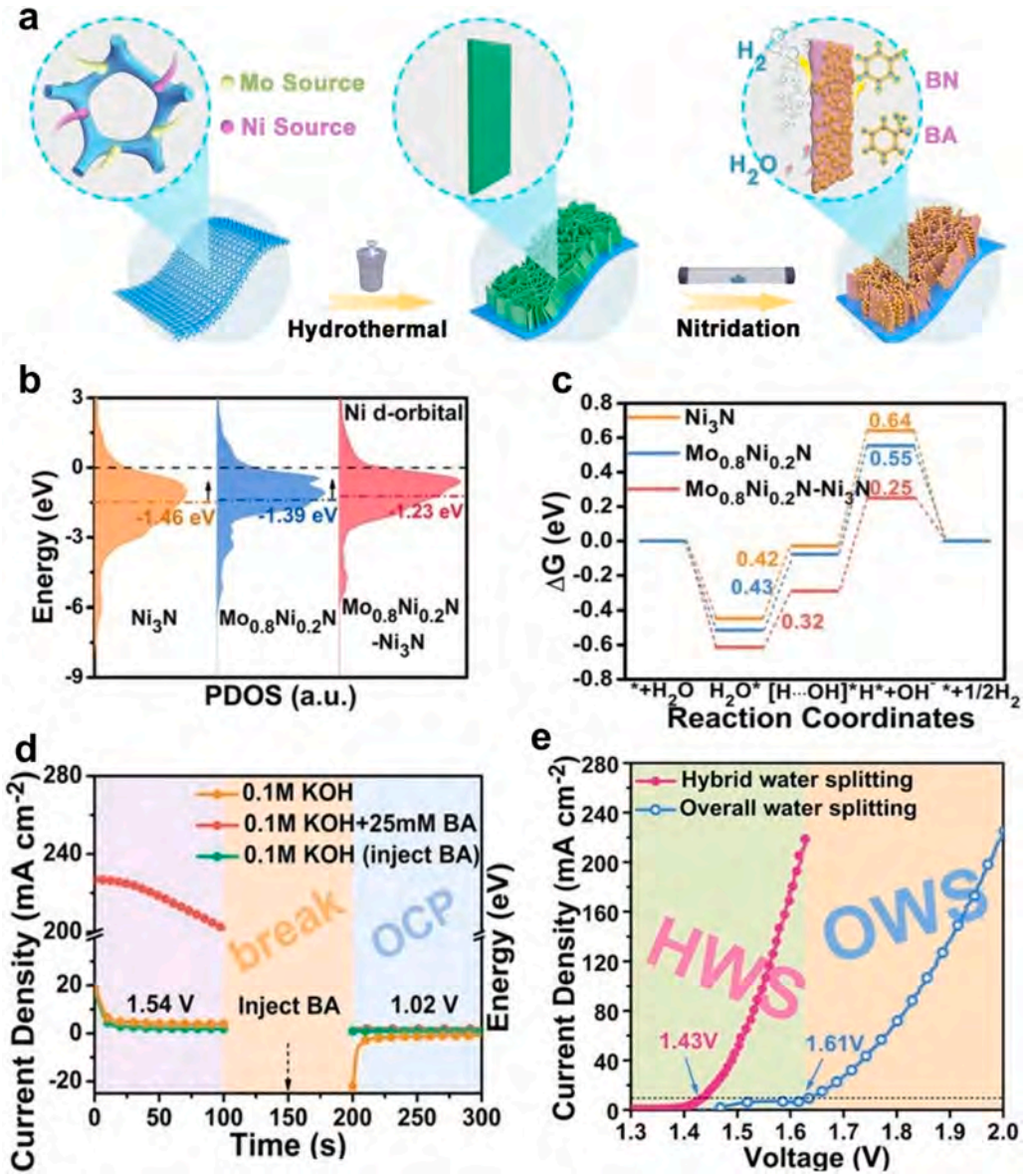

Fig. 19. (a) Schematic diagram for the formation of $Mo_{0.8}Ni_{0.2}N$-Ni_3N and application as bifunctional electrocatalysts for HER and NER. (b) PDOS plots and *d*-band center. (c) Free energy diagram of HER. (d) LSV curves of the two-electrode configurations. (d) The intermittent BAOR electrochemical measurements for $Mo_{0.8}Ni_{0.2}N$-Ni_3N/NF at 1.54 V, circuit break state, and 1.02 V. (e) LSV curves of the two-electrode configurations. Reproduced with permission from reference [194]. Copyright 2023, Wiley-VCH.

field, there remains ample room for thorough exploration in terms of catalytic conversion processes and optimization of conversion efficiency.

Direct electrooxidation of amines in alkaline avoids serious energy consumption and environmental pollution, providing a sustainable opportunity for large-scale industrial production of cyanide [246]. Sun et al. [247] have demonstrated a simple, green and safe electrocatalytic route to selectively oxidize amine into nitrile by anodic oxidation on a metal-doped α-$Ni(OH)_2$ catalyst. Mn doping significantly promotes the oxidation process by modifying the co-adsorption balance of amine molecules and hydroxyl groups on the catalyst surface. The Faraday efficiency of nitrile reaches 96 %.

NER can be further combined with HER to assemble an overall reaction for green hydrogen production. Huang et al. [191] have used a thermodynamically favorable electrooxidation reaction of primary amine (-CH_2-NH_2) to replace OER and couple with HER. Enhanced H_2 yields can be obtained on the cathode, while a variety of aromatic and aliphatic primary amines can be selectively electro-oxidized into nitrile on the anode, catalyzed by NiSe nanorod arrays, showing high yield and good substrate tolerance. Hydrophobic nitrile products float easily to the electrolyte surface to avoid catalyst deactivation and facilitate continuous large-scale synthesis. In addition, Ni^{II}/Ni^{III} formed *in situ* on the NiSe nanorod electrode is a redox-active substance, which effectively accelerates the conversion of primary amine into nitrile [249].

Zeng et al. [193] have designed a $CoSe_2$ sub-nanometer belt with Se vacancy and Ni substitution ($CoSe_2$/Ni-SVs SBs) as an efficient electrocatalyst for NER, which greatly promotes electrooxidation of butylamine to high value-adding nitrile while producing hydrogen. The $CoSe_2$/-Ni-SVs SBs show an ultra-low onset potential of 1.3 V *vs.* RHE and Faraday efficiency of up to 98.5 %, exceeding those of a large number of reported Co- and Ni-based catalysts. The significantly improved electrocatalytic performance can be attributed to the optimized adsorption behavior and accelerated dehydrogenation kinetics, confirmed by *in situ* Fourier transform infrared spectroscopy (FTIR) and electrochemical impedance spectroscopy (EIS) during the electrocatalytic reaction. Theoretical studies further reveal that the Se vacancy is a strong Lewis

Table 3
Typical waste degradation/upcycling coupled hydrogen production systems.

Catalyst	Electrolyte	Cell voltage at 10 mA cm^{-2}	ΔE[a]	ref
Ni_3N/W_5N_4	Seawater + plastics	1.4 V	230 mV @ 50 mA cm^{-2}	[262]
Co-Ni_3N/CC	PET hydrolysate	1.46 V @ 50 mA cm^{-2}	370 mV @ 50 mA cm^{-2}	[263]
Pd-NiTe/NF	PET hydrolysate	1.6 V	200 mV	[264]
Pt-$Ni(OH)_2$/NF	PET hydrolysate	0.68 V @ 50 mA cm^{-2}	–	[265]
N-Ni_3P-$NiMoO_4$/NF	PET hydrolysate	1.53 V @ 100 mA cm^{-2}	194 mV @ 100 mA cm^{-2}	[266]
OMS-Ni_1-CoP	PET hydrolysate	1.57 V	–	[267]
Ni_3N-$Ni_{0.2}Mo_{0.8}N$ NWs/CC	1.0 M KOH+0.1 M Gly	1.4 V	220 mV	[268]
WS_2 NSs	1.0 M NaOH+1.0 M Na_2S	1.17 V	990 mV	[269]
Co-Ni_3S_2	1.0 M NaOH + 1.0 M Na_2S	0.3 V	1.0 V	[270]
a/c S-Pd NSA/NF	1.0 M KOH + 2.0 M Na_2S	0.436 V	1.165 V	[271]
CoS_2@C/MXene/NF	alkaline seawater + 1.0 M Na_2S	0.68 V @ 200 mA cm^{-2}	1.17 V @ 200 mA cm^{-2}	[113]
Cu_2S/NF	1.0 M NaOH + 1.0 M Na_2S	0.64 V @ 100 mA cm^{-2}	–	[272]
V_{Pd}-Pd_4S MNRs	1.0 M KOH +4.0 M Na_2S	0.776 V @ 100 mA cm^{-2}	1.727 V @ 100 mA cm^{-2}	[273]
Ni-MoS_2/SM	1.0 M NaOH + 1.0 M Na_2S	0.49 V	1.13 V	[274]
S-NiP_2Mo_5	1.0 M KOH+phenol	1.47 V @ 25 mA cm^{-2}	400 mV @ 25 mA cm^{-2}	[275]
MP-MO_x	1.0 M KOH+0.05 M CH_4N_2O	1.37 V	120 mV	[276]
	1.0 M KOH+0.05 M CH_4N_2S	1.39 V	100 mV	
	1.0 M KOH+0.05 M NaSCN	1.39 V	100 mV	
Cr-NiO||Cr-Ni_3N	1.0 M KOH+0.1 M 1a	1.46 V @ 5000 mA cm^{-2}	310 mV @ 5000 mA cm^{-2}	[277]
MIL-(IrNiFe)@NF)	1.0 M KOH + Seawater + 0.5 M N_2H_4	0.15 V @ 100 mA cm^{-2}	1520 mV @ 100 mA cm^{-2}	[278]
CoS@NiCu	1.0 M KOH+2000 ppm $NH_3{\cdot}H_2O$	–	120 mV	[279]

[a] ΔE: The voltage decrease of the coupled reactions compared to the HER/OER couple at 10 mA cm^{-2}.

acid site to enhance the adsorption of N atoms, while Ni substitution improves the dehydrogenation thermodynamics by optimizing the sequence of dehydrogenation steps. This work unravels the electrocatalytic mechanism of the NER from the perspectives of both experiments and theoretical calculations.

Li et al. [194] have constructed a $Mo_{0.8}Ni_{0.2}N$-Ni_3N heterostructure on NF as bifunctional electrocatalysts for HER and NER, as illustrated in Fig. 19a. Charge transfer at the heterostructure leads to the up-shift of the *d*-band center to optimize the adsorption of H* and promote HER (Fig. 19b-c). Modification of the *d*-band structure facilitates the generation and adsorption of OH* species from water thus promoting the formation of NiOOH on Ni_3N to catalyze the benzylamine oxidation reaction (BAOR). A multipotential test is performed to verify the function of Ni-OOH species (Fig. 19d). The reduction current response disappears after the injection of BA into the electrolyte before the open circuit potential (OCP) change, indicating that BA reduces high-valent Ni-OOH to Ni-$(OH)_2$ species. It is presumed that Ni^+ on the $Mo_{0.8}Ni_{0.2}N$-Ni_3N surface is first oxidized by OH* generated by water decomposition, and more Ni-OOH species are generated on $Mo_{0.8}Ni_{0.2}N$-Ni_3N. BA can be rapidly oxidized by Ni-OOH and accompanied by spontaneous reductive conversion of Ni-OOH to Ni-$(OH)_2$. As a result, the $Mo_{0.8}Ni_{0.2}N$-Ni_3N catalyzed HER shows an overpotential of only 251 mV in 0.1 M KOH/0.5 M Na_2SO_4 electrolyte to achieve an industrial current density of 500 mA cm^{-2}, surpassing the commercial Pt/C catalyst. Notably, the two-electrode electrolyzer composed of HER and BAOR exhibits a current density of 220 mA cm^{-2} at a voltage of 1.59 V (Fig. 19e), with a Faraday efficiency exceeding 99 % for both H_2 production and BA conversion to BN. This work discloses a *d*-band structure modification strategy to optimize the adsorption of the intermediates and achieve advanced value-adding and energy-efficient hydrogen production in mild alkaline media.

Mondal et al. [248] have designed a colloidal method to control the diffusion of Si atoms into Ni crystals to prepare intermetallic nickel silicide (Ni_2Si). Under basic conditions, the intermetallic Ni_2Si transforms into the active phase of $Ni^{III}O_xH_y$. The organic amine is used as a sacrificial proton donor to selectively oxidize into value-added cyanides. The activated Ni_2Si has high selectivity and a wide range of substrates for the electro-oxidative dehydrogenation of primary amine to nitrile. Electrooxidation of organic amines is carried out in 1.0 M KOH with BA as the model substrate. The reaction mixture of oxidation products analyzed by NMR reveals that BA is completely converted to BN with a Faraday efficiency of 99 %. Notably, H_2 precipitation rate is 10 times higher compared to the OER conditions. This study helps understand the relationship between the electrochemical transformation and catalytic activity of various intermetallic compounds in electrocatalytic water splitting coupled with electrosynthesis of value-added chemicals.

3.5. Other value-adding reactions

Electrosynthesis of high-value-adding chemicals combined with electrocatalytic hydrogen production is an effective strategy to achieve carbon neutralization [250,251]. Electrocatalytic oxidation of methanol, glycerol, and benzyl alcohol has been used to replace OER, and some lower alcohols and aromatic alcohols, such as ethanol [30,166] and cyclohexanol [252], as well as biomass such as chitin [253], aloe extract [254], and lignin [255], are widely studied as substitutes for the anodic oxidation reaction.

Qin et al. [252] have synthesized $CO_2(OH)_3Cl$/FeOOH nanosheets on NF to serve as both cathode and anode catalysts for the simultaneous production of hydrogen and high-value-added cyclohexanone in an alkaline medium. Due to the strong synergistic effect between $CO_2(OH)_3Cl$ and FeOOH, $CO_2(OH)_3Cl$ acts as the optimal active center for the cyclohexanol oxidation reaction (COR), while FeOOH accelerates the reaction kinetics by reducing the charge transfer resistance for both reactions. The two-electrode COR/HER configuration requires a voltage of only 1.46 V to generate a current density of 10 mA cm^{-2}. Furthermore, a cyclohexanone yield of 3.44 g h^{-1} and energy savings of approximately 0.24 kWh m^{-3} (H_2) are achieved by amplifying the configuration into an anionic membrane electrode assembly reactor. The reaction pathway is studied in detail and the work suggests a highly selective and industrially practical approach to organic conversion driven by renewable energy under environmental conditions. Huang et al. [256] have demonstrated that semi-dehydrogenation of tetrahydroisoquinoline can be applied to replace OER in an aqueous solution on a Ni_2P nanosheet catalyst. The value-adding semi-dehydrogenation product, dihydroisoquinoline (DHIQ), can be selectively generated at high yields at the anode, leading to the *in situ* formation of Ni^{II}/Ni^{III} redox-active species. This strategy can produce various DHIQs with electron-attracting/electron-feeding groups with high yields and selectivity, and can even be applied to g-level synthesis. The coupled overall reaction based on Ni_2P can produce both hydrogen and DHIQs at a much lower cell voltage than the HER/OER couple in addition to excellent stability and high Faraday efficiency.

Organosulfur compounds play an important role in many biological

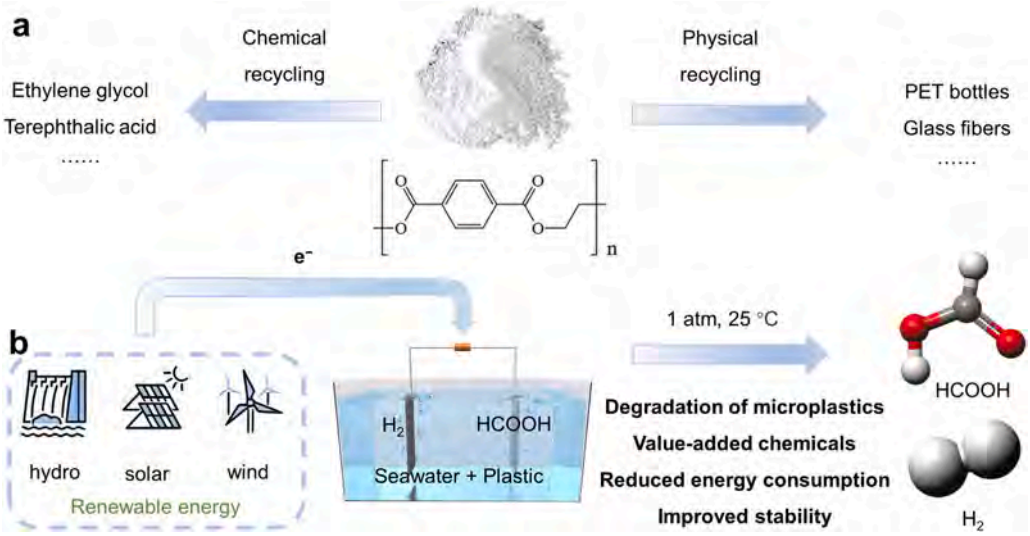

Fig. 20. (a) Chemical and physical recycling pathways of PET. (b) Electrocatalytic reforming of PET coupled hydrogen production.

processes related to the treatment of human diseases. However, the homogeneous catalysts (Mn- and Fe-based catalysts) and strong oxidizers (H_2O_2) for sulfide oxidation have some defects [257]. Recently, Ma et al. [258] have reported an electrochemical protocol for the selective oxidation of sulfides to sulfoxides on a CoFe LDH anode in an aqueous-methyl cyanide (MeCN) electrolyte. Coupling the sulfide oxidation reaction with HER, the cathodic hydrogen productivity is promoted by 2 folds. Under ambient conditions, various aryl, heteroaryl, and alkyl sulfides on the CoFe-LDH/CC anode can be selectively converted to sulfoxides with high yields of 85–96 %. Further studies suggest that the reaction pathway is a free radical process. The *in situ* formed CoFe-hydroxyl oxide can be used as active species for sulfide oxidation. This electrocatalytic reaction system can pave the way for the electrosynthesis of valuable organic molecules under environmental conditions using heterogeneous catalysts without external oxidants.

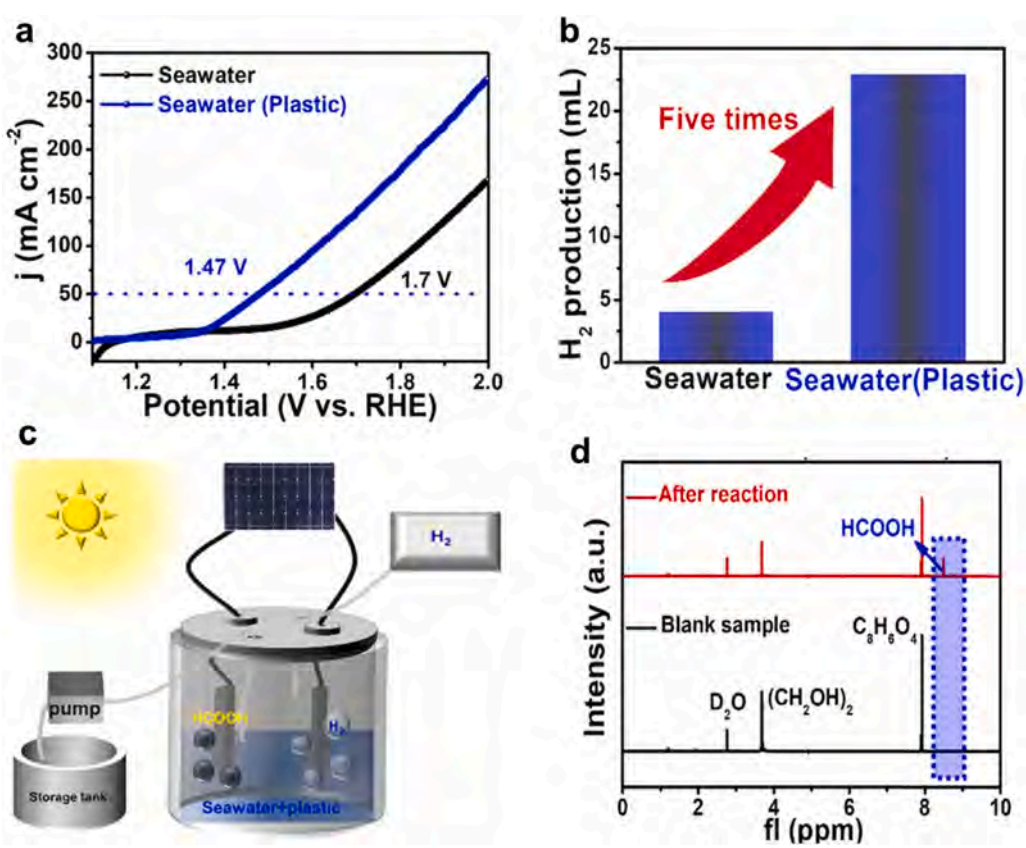

Fig. 21. (a) LSV curves of bifunctional Ni_3N/W_5N_4 catalyst performed in seawater (with and without plastics). (b) The amount of H_2 production. (c) Schematic illustration of a small factory powered by solar energy for HER and plastic waste upcycling. (d) ^1H NMR spectra collected after operating at 1.47 V for 2 h. Reproduced with permission from reference [262]. Copyright 2022, Elsevier.

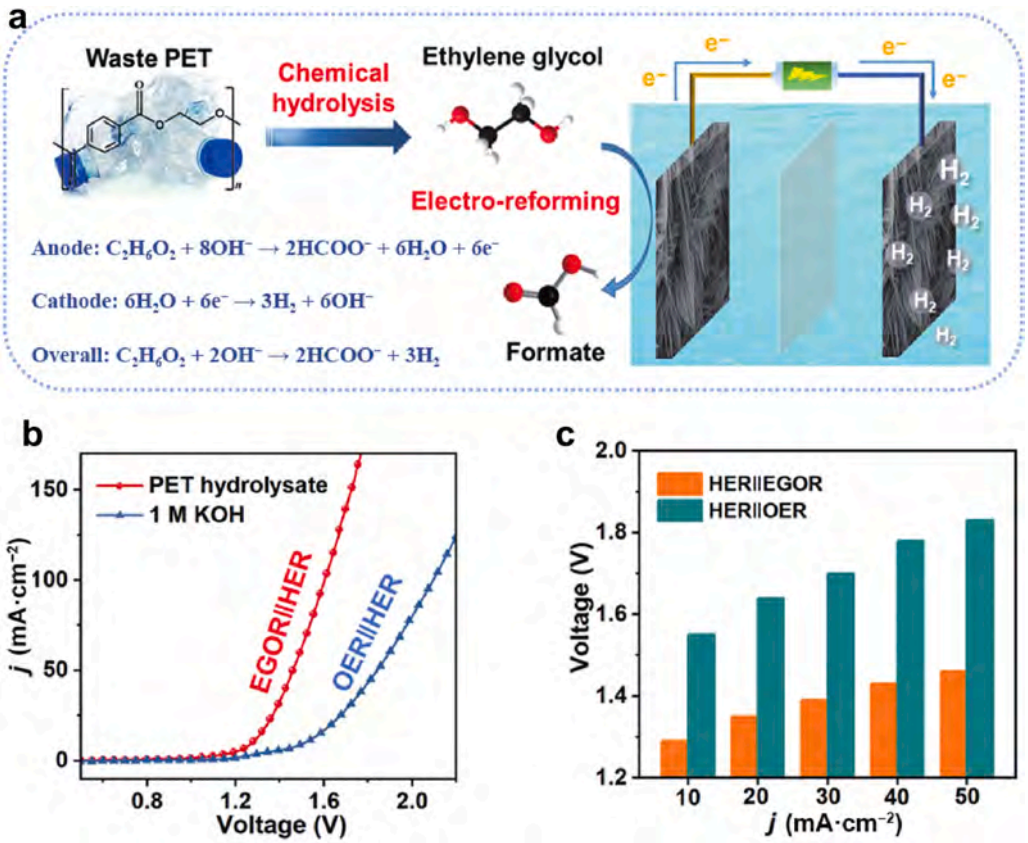

Fig. 22. (a) Schematic illustration for concurrent electrolytic hydrogen production and PET upcycling. (b) LSV curves and (c) voltages required to achieve different current densities for the HER||EGOR and HER||OER couples. Reproduced with permission from reference [263]. Copyright 2022, Springer Nature.

4. Waste degradation/upcycling coupled with hydrogen production

Wastes and pollutants are serious threats to the ecological environment and biological security [259,260]. Degradation of pollutants, such as phenols, sulfides, and waste plastics, usually involves oxidative reactions. Plastic wastes, which normally are high molecular weight polymers, can be hydrolyzed into monomers under extreme conditions. The hydrolyzed monomers can be electrocatalytic oxidized into high-value chemicals to realize the upcycling of waste polymers [261]. Coupling these electrocatalytic oxidation reactions with HER enables green hydrogen production, pollutant recovery, and production of value-added chemicals, as listed in Table 3. However, pollutants and wastes usually have complex compositions. The electrocatalytic efficiency and product selectivity for high-value-adding chemicals depend on the electrocatalysts, and therefore, the design and construction of high-performance catalysts are crucial to the development of the waste degradation/upcycling coupled hydrogen production systems.

4.1. Microplastic upcycling coupled with hydrogen production

In 2004, Thompson first proposed the concept of microplastics (MPs) as plastics with particle sizes smaller than 5 mm [280]. Plastic waste in the environment is decomposed into smaller particles through solar radiation, oxidation, biodegradation process, and mechanical pressure, thus producing MPs waste in various species (PE, PP, PVC, PS, PUR, etc.) [281–283] and forms (fibers, fragments, films, particles, beads, etc.) [284–287]. Polyethylene terephthalate (PET) is one of the common disposable plastics, which are likely to invade natural organisms and even human bodies through biological circulation [288,289]. Therefore, the degradation and recycling of these plastic wastes have become a hot topic at present. Compared with the traditional physical and chemical recovery (Fig. 20a) [290], the electrochemical reforming of plastics provides a green and efficient recovery route (Fig. 20b) [291,292]. More importantly, green hydrogen and value-adding chemicals can be co-produced.

The efficient coupling of plastic waste upcycling with HER holds paramount significance in environment recovery and sustainable energy [115]. Ma et al. [262] have synthesized a 3D sponge-like Ni_3N/W_5N_4 Janus catalyst. Due to the synergistic effects of the hierarchical sponge-like structure and the heterointerface, it demonstrates Pt-like HER activity in seawater. Interestingly, the Ni_3N/W_5N_4 Janus catalyst is also efficient in the electrochemical reforming of waste plastics and an ultra-low potential of about 1.33 V *vs.* RHE is essential to generate a current density of 10 mA cm^{-2}, as shown in Fig. 21a. The amount of H_2 produced by seawater (with plastics) is about five times that of pure seawater at the same potential of 1.47 V, suggesting that plastics upgrading is a powerful pathway for energy-efficient hydrogen production (Fig. 21b). Furthermore, at a high current of 120 mA cm^{-2}, the Faraday efficiency for HCOOH generation reaches 85 %, indicating its high selectivity for plastic upcycling. The solar-driven small-scale "chemical factory" based on the bifunctional electrocatalyst Ni_3N/W_5N_4 achieves efficient H_2 production through HER in seawater and value-adding HCOOH production through plastic upcycling (Fig. 21c-d).

Liu et al. [263] have utilized a bifunctional nickel-cobalt nitride nanosheet electrocatalyst (Co-Ni_3N/CC) for electrocatalytic PET waste upcycling while generating hydrogen concurrently, as schematically illustrated in Fig. 22a. The introduction of Co enhances the Ni^{2+}/Ni^{3+} redox and facilitates the ethylene glycol (EG, chemical hydrolyzed product of PET waste) oxidation reaction (EGOR) at an ultralow potential of 1.15 V *vs.* RHE. The EGOR-integrated HER configuration achieves a current density of 50 mA·cm^{-2} at a cell voltage of 1.46 V, demonstrating a 370 mV reduction compared to the OER/HER couple for water electrolysis (Fig. 22b-c). This work uncovers the significance of

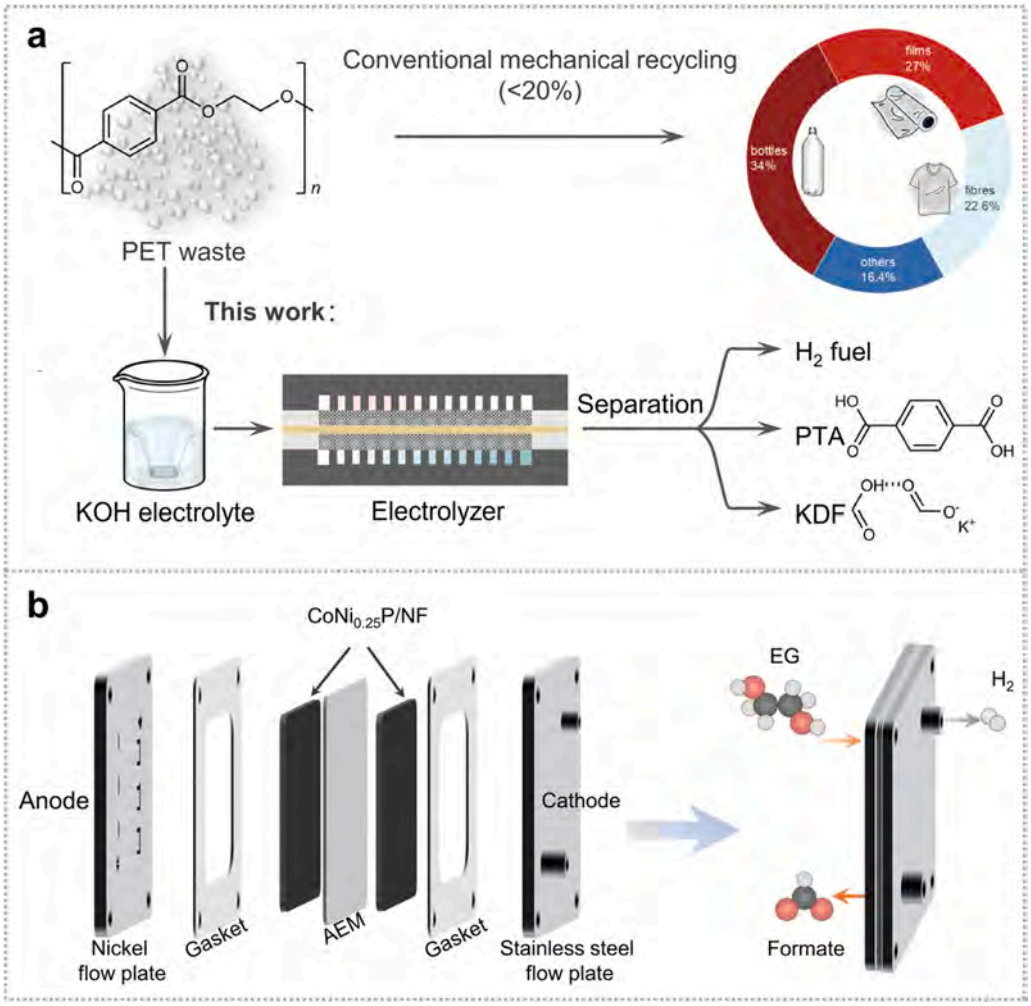

Fig. 23. (a) Route for PET waste recycling. (b) Membrane electrode assembly setup. Reproduced with permission from reference [292]. Copyright 2021, Springer Nature.

heterostructure engineering in optimizing the adsorption energy of the intermediates to promote electrocatalytic PET waste upcycling coupled hydrogen production.

Currently, only a small fraction (<20 %) of PET waste is recycled by mechanical methods [293]. Thermal recovery methods such as hydrogenolysis and glycolysis require high temperatures for the recovery of monomers (terephthalic acid (PTA) and bis(2-hydroxyethyl) terephthalate) [294,295]. Therefore, electrochemical reforming of PET wastes at room temperature with high-value-adding chemicals produced is promising. Zhou et al. [292] have utilized a bifunctional $CoNi_{0.25}P$ electrocatalyst in a KOH electrolyte to convert PET waste into commercially valuable chemicals, potassium dimethyl terephthalate (KDF), and PTA while generating hydrogen gas, as illustrated in Fig. 23a. The process becomes profitable when the EG is selectively electro-oxidized into formic acid with a selectivity of more than 80 % at a high current density (>100 mA cm^{-2}). The net income for recycling PET waste is approximately \$350 t^{-1}. A membrane electrode assembly reactor using $CoNi_{0.25}P$ catalyst as both cathode and anode (Fig. 23b) achieves a current density of 500 mA cm^{-2} at a voltage of 1.8 V, with Faraday efficiency and formic acid selectivity of more than 80 %. This work paves the way for the continuous electrosynthesis of value-adding chemicals from plastic waste and hydrogen fuel production. Behera et al. [296] have demonstrated the complete recyclability of electrocatalytic PET using cobalt-containing one-dimensional coordination polymers as electrocatalysts at a low starting potential of 1.27 V *vs.* RHE. The isolation product, TPA, is obtained with 100 % yield and KDF with ~ 80 % selectivity, while synergistic production of hydrogen is also accomplished.

4.2. *Wastes degradation coupled with hydrogen production*

A large amount of H_2S waste is discharged from refineries, the coal chemical industry, and other industries, and it is corrosive and toxic. The Claus process ($H_2S + 1/2O_2 \rightarrow S + H_2O$) is the main method to remove H_2S [297]. Generally, H_2S is a hydrogen-rich source, while the sulfur ion (S^{2-}), as an electron donor, is prone to be oxidized. Specifically, the sulfide oxidation reaction (SOR, $S^{2-} + 2e^- = S$, −0.48 V *vs.* RHE) saves 86 % electricity consumption compared to the theoretical OER [113, 298]. Therefore, coupling the SOR with HER for hydrogen production would be energy efficient. However, S^{2-} is more likely to corrode bare metals, thereby decreasing the activity and stability of the electrocatalyst [299]. Therefore, the development of advanced and economical electrocatalysts for SOR is the key to achieving efficient pollutant degradation and simultaneous hydrogen production [36,299,300].

Pei et al. [272] have synthesized Cu_2S/NF catalysts using NF with strong corrosion resistance as a brass substrate. According to the theory of hard and soft acids and bases (HSAB), the lattice Cu(I) in the Cu_2S catalyst makes it easy to combine the soft Lewis acid site with the soft base HS^- in the electrolyte, rather than with hard acids or critical acids [301,302]. This provides an opportunity for the Cu^+ catalyst to strengthen the adsorption of sulfide ions to promote the reaction kinetics of SOR. As a result, an anode potential of 0.44 V *vs.* RHE can drive a

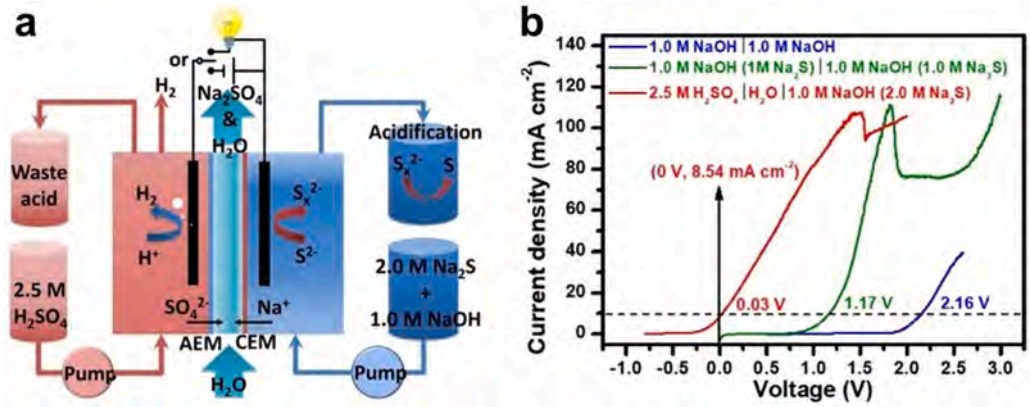

Fig. 24. (a) Diagram of the flow cell system for HER in acid and SOR in alkali. (b) LSV curves for alkali-alkali OER/HER, alkali-alkali SOR/HER, and alkali-acid SOR/HER cells. Reproduced with permission from reference [269]. Copyright 2021, Wiley-VCH.

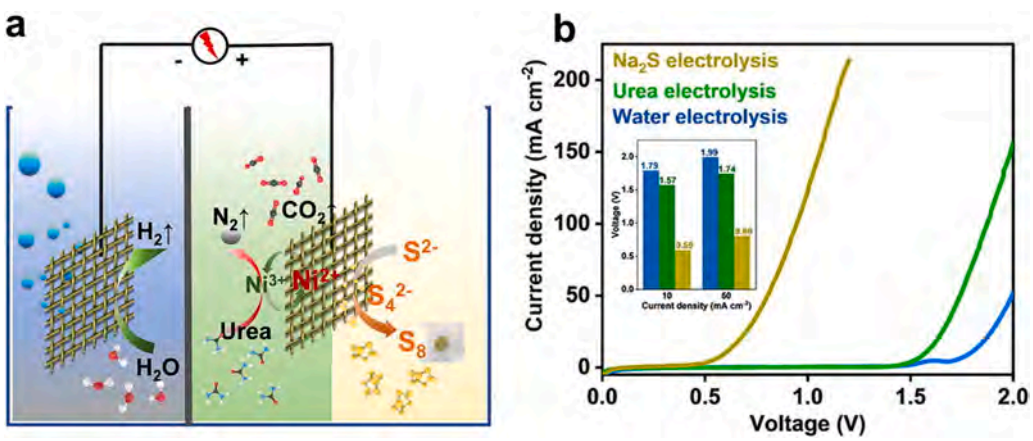

Fig. 25. (a) Schematic diagram of the two-electrode electrolytic cell. (b) LSV curves of the two-electrode configurations in various electrolytes. Reproduced with permission from reference [270]. Copyright 2022, Elsevier.

current density of 100 mA cm^{-2} in SOR in addition to the Faraday efficiency of more than 97 %. In the two-electrode SOR/HER configuration, a current density of 100 mA cm^{-2} can be achieved at a voltage of 0.64 V. The SOR/HER couple saves 74 % of energy consumption compared to the OER/HER couple for hydrogen production. This work indicates that the sulfide waste can be degraded *via* the electrocatalytic route while achieving energy efficient hydrogen production.

It is worth noting that the acid electrolyte is beneficial to the HER kinetics only, while the SOR kinetics is inferior. Therefore, the acid-alkali mixed electrochemical cell should be designed to compromise this incompatibility, where S^{2-} undergoes SOR in an alkaline solution and HER in an acidic solution. The asymmetric electrolyzer optimizes the catalytic efficiency in its advantageous electrolyte and provides an environmentally friendly and energy-saving way for pollutant degradation and hydrogen production [303]. Yi et al. [269] have prepared WS_2 nanosheets (WS_2 NSs) for an asymmetric electrolyzer to perform SOR and HER concurrently, as illustrated in Fig. 24a. Owing to the large number of active sites and the asymmetric electrolyzer system, excellent catalytic performance and significant stability in both HER and SOR have been achieved. The two-electrode SOR/HER configuration requires a mere 0.03 V to afford a current density of 10 mA cm^{-2}, as shown in Fig. 24b. The research reveals self-power or low voltage electrolysis to produce hydrogen and degrades toxic sulfides by the alkali-acid electrochemical cell.

Li et al. [270] have prepared the foliated cobalt combined nickel sulfide (Co-Ni_3S_2/Ni) catalyst by electrodeposition and hydrothermal vulcanization on a nickel network. *In situ* Raman characterization shows that the formation of NiOOH species at the surface accelerates the oxidation of urea *via* UOR. In addition, the direct electron transfer to surface active sites facilitates the oxidation of sulfide *via* SOR, during which the sulfide (S^{2-}) is oxidized from short-chain polysulfides such as S_2^{2-} and S_4^{2-} into elemental sulfur (S_8). The Co-Ni_3S_2/Ni catalyst has excellent catalytic properties in HER, UOR, and SOR in alkaline electrolytes, thus presenting multifunctional capability in the UOR/HER, SOR/HER, and OER/HER couples (Fig. 25a). Specifically, to drive a current density of 50 mA cm^{-2} in the sulfide-containing electrolyte, the SOR/HER couple requires a voltage of 0.80 V, which is 0.94 and 1.20 V lower than the UOR/HER and OER/HER couples, respectively, as shown in Fig. 25b. The effective coupling of SOR and HER can improve the electron utilization efficiency to produce hydrogen and achieve sulfide waste degradation [304,305].

Pd-based materials have been applied extensively in various electrocatalytic fields [306]. However, the bare metal Pd is prone to passivation during the SOR process [307]. Doping the S atoms with strong electronegativity can produce an amorphous layer with improved activity to enhance the electrocatalytic capability. Additionally, doping the S into Pd facilitates sulfur absorption during the SOR process and prevents passivation [308]. Wang et al. [271] have prepared an amorphous/crystalline sulfur-doped palladium nanosheet array on NF (a/c S-Pd NSA/NF) by S doping into Pd NSA/NF. The two-electrode SOR/HER configuration requires 0.642 V to generate a current density of 100 mA cm^{-2}, which is 1.257 V lower than the OER/HER couple, thus significantly reducing the energy consumption for hydrogen production. This finding demonstrates that the a/c S-Pd NSA/NF catalyst is

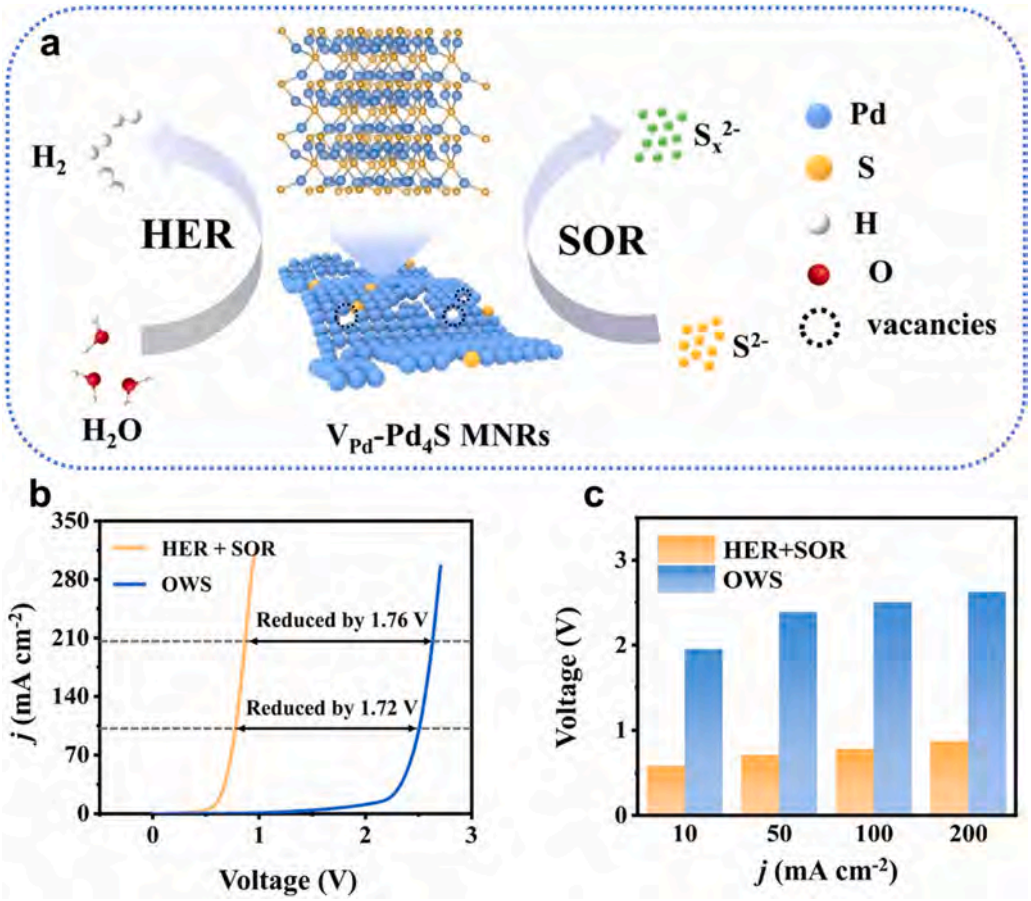

Fig. 26. (a) Schematic diagram of the HER/SOR mechanism. (b) LSV curves of HER/SOR and HER/OER couples. (c) Voltages required to produce different current densities for HER/SOR and HER/OER couples. Reproduced with permission from reference [273]. Copyright 2024, Elsevier.

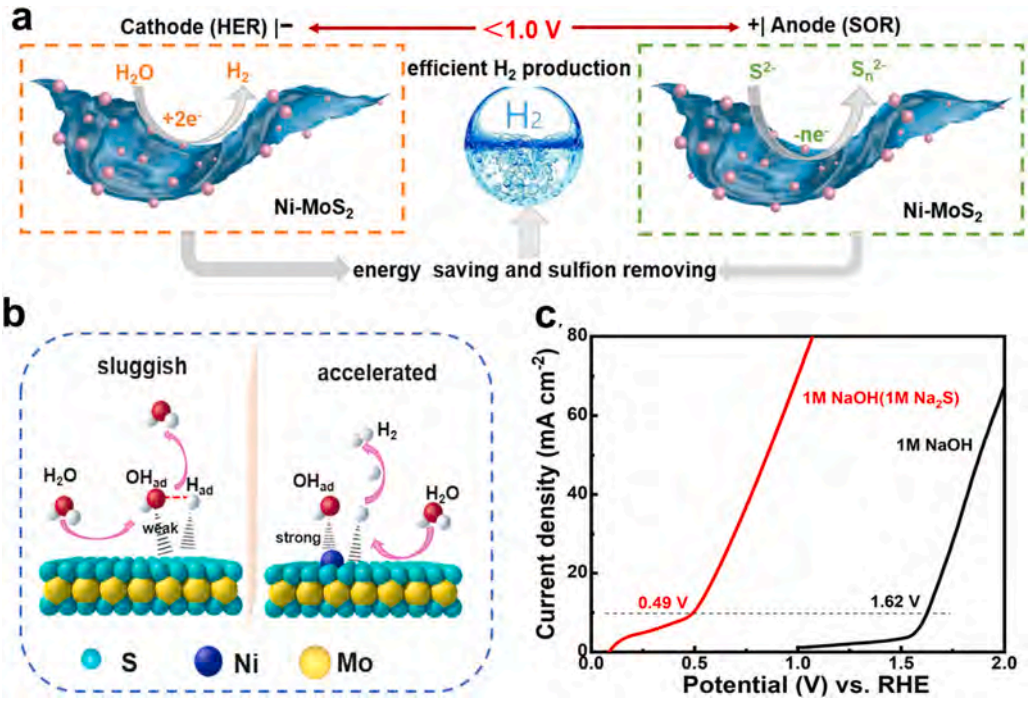

Fig. 27. (a) Schematic illustration of simultaneous SOR and HER. (b) The schematic illustration of the catalytic role of Ni and MoS_2 during the alkaline HER process. (c) LSV curves for SOR/HER and OER/HER systems. Reproduced with permission from reference [274]. Copyright 2024, Wiley-VCH.

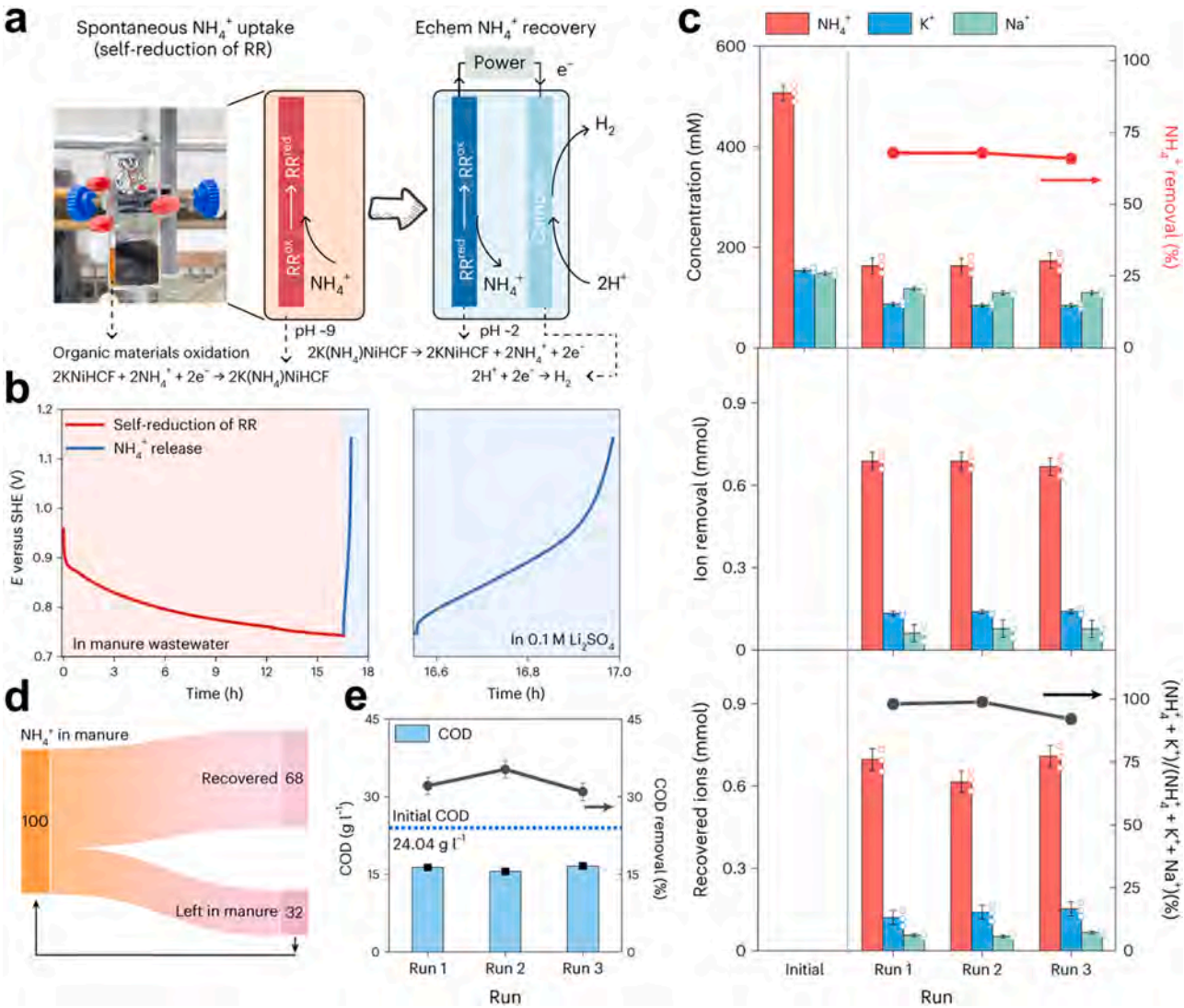

Fig. 28. (a) Schematic illustration of the NH_4^+ recovery process using the KNiHCF RR electrode from manure wastewater. (b) The potential of the KNiHCF RR electrode in the NH_4^+ uptake and release steps. (c) Concentration changes and ion balance of NH_4^+, Na^+, and K^+ over the three recovery runs from manure wastewater. (d) NH_4^+ balance over the three runs. (e) Change of COD over the three NH_4^+ recovery runs. Reproduced with permission from reference [309]. Copyright 2024, Springer Nature.

capable of energy-efficient hydrogen production while converting S^{2-} in wastewater into high-value sulfur powder simultaneously.

Wang et al. [273] have utilized a hydrothermal sulfurization method to construct ultra-thin Pd_4S nanoribbons with rich palladium vacancies (V_{Pd}-Pd_4S MNRs). Due to the synergistic effects of the metallopolymer form and palladium vacancies, the V_{Pd}-Pd_4S MNRs exhibit outstanding intrinsic activity for both HER and SOR. The two-electrode SOR/HER system (Fig. 26a) requires voltages of 0.776 and 0.865 V to achieve current densities of 100 and 200 mA cm^{-2}, respectively, surpassing OER/HER systems significantly, as shown in Fig. 26b-c. DFT calculations indicate that the Pd vacancies and electron transfer between Pd and S atoms modulate the electronic structure and charge distribution of the Pd sites. This study provides a forward-looking approach for the rational design and preparation of metallopolymer with vacancies and different crystal phases, applicable for developing energy-efficient hydrogen production systems.

Generally, electrocatalysts are susceptible to poisoning by sulfur ions during the SOR process, thus posing a significant challenge to their long-term application. MoS_2, which has excellent sulfur tolerance and HER capability, emerges as a promising candidate for a bifunctional catalyst in the SOR/HER couple. Liu et al. [274] have employed an electrodeposition method to assemble nanoscale Ni onto MoS_2 nanosheets, achieving Ni-functionalized MoS_2. The anchor structure not only optimizes the adsorption of polysulfides but also accelerates the HER kinetics by optimizing the adsorption of OH_{ad} to enhance both the SOR and HER capability (Fig. 27a-b). The catalyst in a two-electrode SOR/HER system achieves cost-effective hydrogen production in which a low voltage of 0.49 V drives a current density of 10 mA cm^{-2} (Fig. 27c) in addition to nearly 100 % hydrogen production efficiency. Furthermore, the electricity consumption decreases by 61 % compared to the OER/HER system.

Ammonia is an important nitrogen fertilizer, and the effective recovery of ammonia from fecal wastewater would provide multiple sustainability benefits from both pollution control and resource recovery perspectives. Wang et al. [309] have investigated the recovery of NH_4^+ from wastewater using an integrated electrochemical system. To gain insight into the recovery of NH_4^+ from real fecal water, they use a two-step recovery process (Fig. 28a) consisting of spontaneous uptake of NH_4^+ from fecal water and electrochemical recovery of NH_4^+ from 0.1 M Li_2SO_4 solution (pH≈2). When NH_4^+ is inserted into the KNiHCF redox reservoir (RR) electrode, the electrode is spontaneously reduced by the oxidation of organic matter in the organic fertilizer wastewater

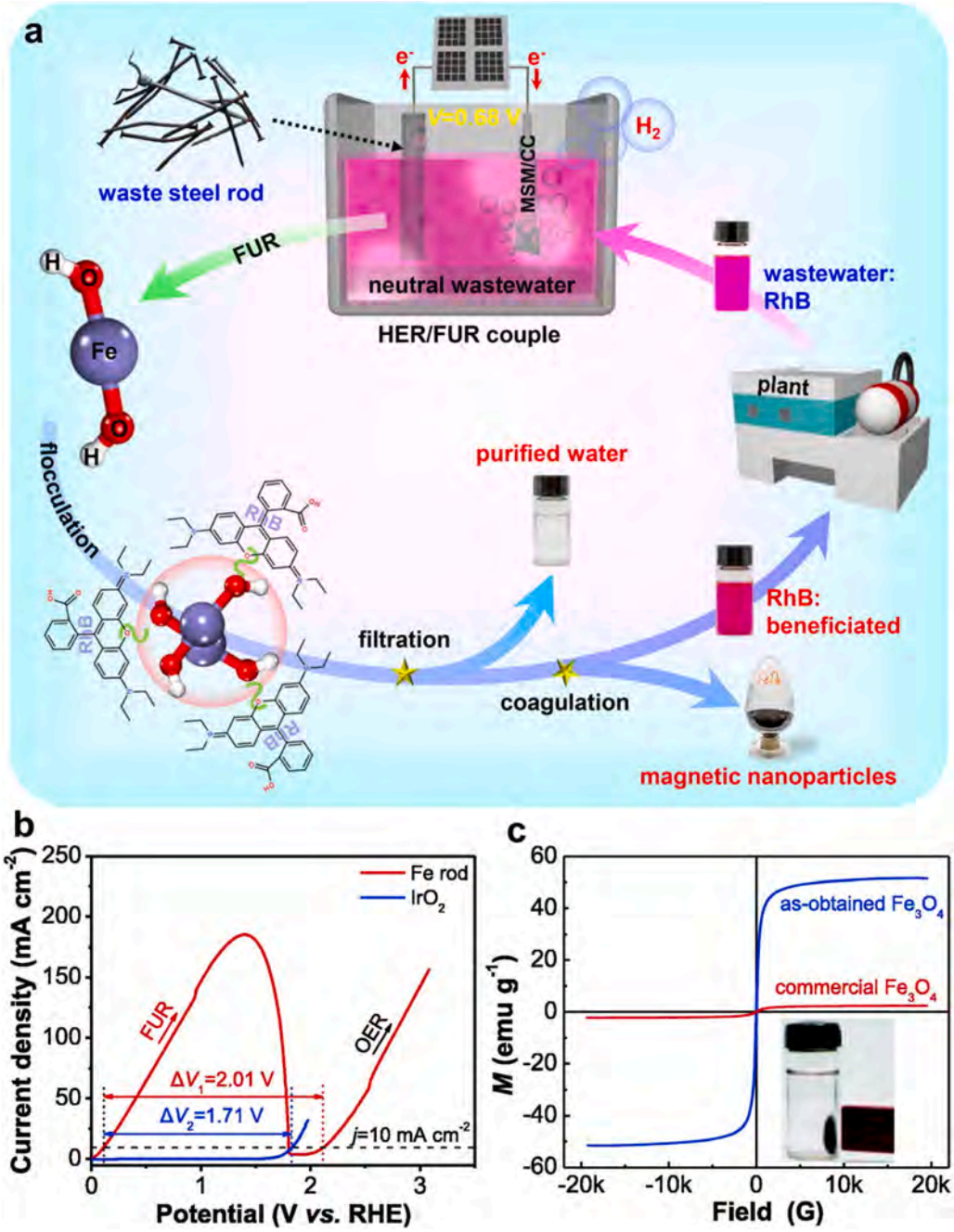

Fig. 29. (a) Schematically illustration of the concept of HER/FUR couple for ultralow-voltage hydrogen production and simultaneous magnetic Fe_3O_4 nanoparticles production, wastewater purification as well as RhB beneficiation in neutral media. (b) LSV curves of FUR and OER. (c) Magnetic properties of the as-obtained Fe_3O_4. Reproduced with permission from reference [20]. Copyright 2023, Elsevier.

(Fig. 28b). NH_4^+ is then released during RR oxidation and paired with HER at the Pt electrode to complete a recovery cycle. In the recovery run experiments, [NH_4^+], [K^+], and [Na^+] in fecal water are reduced by ~344, 69, and 35 mM, respectively (Fig. 28c). The removal of NH_4^+ from the fecal water is ~66–68 % per operation and the nutrient selectivity is approximately 93–98 % in the recovered solution (Fig. 28d). The chemical oxygen demand (COD) decreases from 24.04 ± 0.4 g l^{-1} to approximately 15.5–16.6 ± 0.4 g l^{-1} (a COD removal of approximately 31–35 %) during each run (Fig. 28e). The results confirm the spontaneous oxidation of organic matter in manure wastewater by the RR.

Ammonia is a typical pollutant in wastewater but also a valuable carbon-free hydrogen carrier [310]. Low-temperature ammonia electrolysis provides an cost-effective way to degrade ammonia in wastewater while producing hydrogen by minimizing the release of nitrous oxide from wastewater aeration basins [311]. In the electrolyzer, the ammonia oxidation reaction in alkaline media can be coupled with HER. Compared to typical water electrolysis (1.23 V), the overall ammonia electrolysis process theoretically reduces the power consumption by 95 % [312]. For instance, Yoon et al. [313] have prepared a heterostructured bilayer electrode using the Pt-Ir catalyst for ammonia oxidation. The catalyst contains a dense layer and a porous structure for enhanced ammonia mass transfer. It shows better durability for 10 h than the single-layer catalyst electrode. The single cell is expanded to an 8-cell stack with a total area of 200 cm^{-2} to develop a large alkaline ammonia electrolysis system. The stack produces 25 L h^{-1} of hydrogen from ammonia at a current density of 175 mA cm^{-2}. Notably, the

alkaline ammonia electrolysis tower consumes 45 % less electrical energy than the water electrolysis tower for hydrogen production.

Peng et al. [20] have proposed a strategy to couple HER with Fe upgrading reaction (FUR) for efficient hydrogen production in neutral media, as shown in Fig. 29a. The heterostructured $MoSe_2/MoO_2$ grown on carbon cloth (MSM/CC) shows superior HER properties compared to the commercial Pt/C catalyst at large current densities. By replacing OER with FUR, the potential required to reach a current density of 10 mA cm^{-2} diminishes by 95 % (Fig. 29b). The FUR/HER overall reaction requires an ultralow voltage of 0.68 V to generate a current density of 10 mA cm^{-2} with a power equivalent of 2.69 kWh per m^3 of H_2. In addition, iron species formed at the anode are able to extract Rhodamine B contaminants by flocculation and produce nanoscale magnetic powder for value-adding applications (Fig. 29c). This work demonstrates the ability of a single system to both produce hydrogen in an energy-efficient manner and recover pollutants without carbon emissions while revealing new directions for combining hydrogen production with environmental recycling to achieve carbon neutrality.

5. Conclusion and outlook

In this review, coupled electrocatalytic hydrogen production is discussed by focusing on various aspects such as assisted hydrogen production, value-adding electrosynthesis coupled with hydrogen production, and waste degradation/upcycling coupled with hydrogen production. The hydrazine oxidation reaction and urea oxidation reaction offer promising avenues for efficient and sustainable hydrogen production. Furthermore, value-adding electrosynthesis coupled with hydrogen production, including reactions such as alcohol oxidation, aldehyde oxidation, glucose oxidation, amine oxidation, and other value-adding reactions, not only produces hydrogen but also generates valuable chemical products, consequently opening up new possibilities for integrated and sustainable processes. The role of coupled electrocatalytic hydrogen production in waste degradation and upcycling is also described. Microplastic upcycling and waste degradation coupled with HER have the potential to address environmental concerns by simultaneously producing hydrogen and mitigating waste-related issues. By means of in-depth analysis of different reactions and processes, valuable insights into the potential of coupling electrocatalytic hydrogen production with diverse applications have been gained.

The field of coupled electrocatalytic hydrogen production presents exciting prospects for future research and industrial applications. By harnessing the power of electrocatalysis, we can revolutionize the way to produce hydrogen and address key challenges in energy and environmental sustainability. To further enhance this field, several key areas of future research and development can be identified.

Firstly, the application of small molecule oxidation is to minimize the energy consumption required for water splitting. Highly active and selective catalysts are crucial to the conversion efficiency in order to facilitate the production of high-value-adding products. Novel catalysts and materials with improved activity, productivity selectivity, and stability are crucial. Advancements in catalyst design, including the use of highly efficient and abundant materials, as well as the development of environmentally friendly synthesis processes, will contribute to more cost-effective and sustainable hydrogen production.

Second, plastic wastes are normally high molecular-weight polymers that should be hydrolyzed to monomers before electrocatalytic oxidation. For example, PET can be chemically hydrolyzed under alkaline conditions to produce terephthalic acid (PTA) and ethylene glycol (EG). Driven by renewable energy sources (solar, wind, and hydro), the upgrading of PET derived EG into high-value chemicals using electrocatalytic means under mild conditions is promising. By utilizing intermittent energy sources to drive electrocatalysis, we can optimize the overall efficiency and environmental impact of hydrogen generation to further promote the transition toward clean and renewable energy.

Thirdly, electrocatalytic hydrogen production coupled with other oxidation reactions involves a complex reaction mechanism, which requires an in-depth understanding of the interactions among catalysts, electrolytes, and reactants. In addition, the reaction condition is crucial to the efficiency of electrocatalytic hydrogen production. The combination of the electrocatalytic reaction process with emerging technologies, such as artificial intelligence and machine learning, can help to optimize reaction conditions, catalyst performance, and system operation, leading to improved efficiency and reliability in hydrogen production.

Fourthly, the selectivity and efficiency at high current densities is challenging for industrial and commercial applications pertaining to coupled electrocatalytic hydrogen production. However, the development of scalable and economically viable processes for coupled electrocatalytic hydrogen production is essential. The assembly of flow electrolyzers facilitates the transport of reactants, allows rapid separation of value-adding products, maximizes the contact between the reactants and the active sites, and provides large current densities. Upscaling the production and integration of these systems into existing infrastructure will be critical to the widespread adoption and commercialization.

CRediT authorship contribution statement

Donglian Li: Writing – original draft, Visualization, Methodology, Investigation, Formal analysis, Data curation, Writing – review & editing. **Xuerong Xu:** Writing – original draft, Methodology, Investigation, Formal analysis, Data curation, Writing – review & editing. **Junzheng Jiang:** Visualization, Investigation. **Hao Dong:** Visualization, Methodology, Writing – review & editing. **Hao Li:** Writing – review & editing. **Xiang Peng:** Writing – review & editing, Supervision, Project administration, Funding acquisition, Conceptualization. **Paul K. Chu:** Writing – review & editing, Validation, Supervision, Funding acquisition, Conceptualization.

Declaration of Competing Interest

The authors declare that they have no known competing financial interests or personal relationships that could have appeared to influence the work reported in this paper.

Data availability

Data will be made available on request.

Acknowledgments

This work was financially supported by the National Natural Science Foundation of China (52002294), the Key Research and Development Program of Hubei Province (2021BAA208), the Knowledge Innovation Program of Wuhan-Shuguang Project (2022010801020364), Graduate Innovative Fund of Wuhan Institute of Technology (No. CX2023083), City University of Hong Kong Donation Research Grants (DON-RMG 9229021 and 9220061), and City University of Hong Kong Strategic Research Grant (SRG) (7005505).

References

[1] Z.W. Seh, J. Kibsgaard, C.F. Dickens, I. Chorkendorff, J.K. Nørskov, T. F. Jaramillo, Combining theory and experiment in electrocatalysis: insights into materials design, Science 355 (2017) eaad4998.
[2] J. Zhu, L. Hu, P. Zhao, L.Y.S. Lee, K.-Y. Wong, Recent advances in electrocatalytic hydrogen evolution using nanoparticles, Chem. Rev. 120 (2019) 851–918.
[3] Z. Zhao, H. Liu, W. Gao, W. Xue, Z. Liu, J. Huang, X. Pan, Y. Huang, Surface-engineered PtNi-O nanostructure with record-high performance for electrocatalytic hydrogen evolution reaction, J. Am. Chem. Soc. 140 (2018) 9046–9050.
[4] Y. Liu, Q. Wang, J. Zhang, J. Ding, Y. Cheng, T. Wang, J. Li, F. Hu, H.B. Yang, B. Liu, Recent advances in carbon-supported noble-metal electrocatalysts for

hydrogen evolution reaction: syntheses, structures, and properties, Adv. Energy Mater. 12 (2022) 2200928.
[5] L. Xiong, Y. Qiu, X. Peng, Z. Liu, P.K. Chu, Electronic structural engineering of transition metal-based electrocatalysts for the hydrogen evolution reaction, Nano Energy 104 (2022) 107882.
[6] Z. Wang, Z. Lin, Y. Wang, S. Shen, Q. Zhang, J. Wang, W. Zhong, Nontrivial topological surface states in Ru_3Sn_7 toward wide pH-range hydrogen evolution reaction, Adv. Mater. 35 (2023) 2302007.
[7] G. Wu, X. Han, J. Cai, P. Yin, P. Cui, X. Zheng, H. Li, C. Chen, G. Wang, X. Hong, In-plane strain engineering in ultrathin noble metal nanosheets boosts the intrinsic electrocatalytic hydrogen evolution activity, Nat. Commun. 13 (2022) 4200.
[8] J.G. Zhang, Q. Hu, S.M. Zhang, S. Li, F. Ma, F.C. Chen, Y.L. Wang, L.M. Wang, Electrocatalytic characterization of Ni-Fe-TiO_2 overlayers for hydrogen evolution reaction in alkaline solution, Rare Met 42 (2023) 1858–1864.
[9] Z. Huang, A.R. Woldu, X. Peng, P. Chu, Remarkably boosted water oxidation activity and dynamic stability at large-current-density of $Ni(OH)_2$ nanosheet arrays by Fe ion association and underlying mechanism, Chem. Eng. J. 477 (2023) 147155.
[10] X. Peng, X. Jin, N. Liu, P. Wang, Z. Liu, Gao, A high-performance electrocatalyst composed of nickel clusters encapsulated with a carbon network on TiN nanaowire arrays for the oxygen evolution reaction, Appl. Surf. Sci. 567 (2021) 150779.
[11] X. Peng, S. Feng, S. Lai, Z. Liu, J. Gao, M. Javanbakht, B. Gao, Structural engineering of rare-earth-based perovskite electrocatalysts for advanced oxygen evolution reaction, Int. J. Hydrog. Energ. 47 (2022) 39470–39485.
[12] M. Qiang, X. Zhang, H. Song, C. Pi, X. Wang, B. Gao, Y. Zheng, X. Peng, P.K. Chu, K. Huo, General synthesis of nanostructured Mo_2C electrocatalysts using a carbon template for electrocatalytic applications, Carbon 197 (2022) 238–245.
[13] C. Huang, X. Miao, C. Pi, B. Gao, X. Zhang, P. Qin, K. Huo, X. Peng, P.K. Chu, Mo_2C/VC heterojunction embedded in graphitic carbon network: an advanced electrocatalyst for hydrogen evolution, Nano Energy 60 (2019) 520–526.
[14] X. Peng, L. Hu, L. Wang, X. Zhang, J. Fu, K. Huo, L.Y.S. Lee, K.-Y. Wong, P.K. Chu, Vanadium carbide nanoparticles encapsulated in graphitic carbon network nanosheets: a high-efficiency electrocatalyst for hydrogen evolution reaction, Nano Energy 26 (2016) 603–609.
[15] L. Xiong, Y. Qiu, H. Dong, B. Gao, X. Zhang, P.K. Chu, X. Peng, Metallic Ni_3N/Ni heterostructure for efficient hydrogen evolution reaction, Int. J. Hydrog. Energ. 59 (2024) 400–407.
[16] X. Wang, X. Zhang, Y. Xu, H. Song, X. Min, Z. Tang, C. Pi, J. Li, B. Gao, Y. Zheng, Heterojunction Mo-based binary and ternary nitride catalysts with Pt-like activity for the hydrogen evolution reaction, Chem. Eng. J. 470 (2023) 144370.
[17] S. Feng, D. Li, H. Dong, S. Xie, Y. Miao, X. Zhang, B. Gao, P.K. Chu, X. Peng, Tailoring the Mo-N/Mo-O configuration in MoO_2/Mo_2N heterostructure for ampere-level current density hydrogen production, Appl. Catal. B Environ. 342 (2024) 123451.
[18] X. Peng, Y. Yan, S. Xiong, Y. Miao, J. Wen, Z. Liu, B. Gao, L. Hu, Se-$NiSe_2$ hybrid nanosheet arrays with self-regulated elemental Se for efficient alkaline water splitting, J. Mater. Sci. Technol. 118 (2022) 136–143.
[19] R. Li, S. Xie, Y. Zeng, Q. Zhao, M. Mao, Z. Liu, P.K. Chu, X. Peng, Synergistic dual-regulating the electronic structure of NiMo selenides composite for highly efficient hydrogen evolution reaction, Fuel 358 (2024) 130203.
[20] X. Peng, S. Xie, S. Xiong, R. Li, P. Wang, X. Zhang, Z. Liu, L. Hu, Ultralow-voltage hydrogen production and simultaneous Rhodamine B beneficiation in neutral wastewater, J. Energy Chem. 81 (2023) 574–582.
[21] X. Peng, S. Xie, X. Wang, C. Pi, Z. Liu, B. Gao, L. Hu, W. Xiao, P.K. Chu, Energy-saving hydrogen production by the methanol oxidation reaction coupled with the hydrogen evolution reaction co-catalyzed by a phase separation induced heterostructure, J. Mater. Chem. A 10 (2022) 20761–20769.
[22] B.-C. Xu, Y.-P. Miao, M.-Q. Mao, D.-L. Li, S. Xie, W.-H. Jin, S. Xiao, J. Wen, Z. Abd-Allah, Z.-T. Liu, X. Peng, P.K. Chu, Heterophase junction engineering-induced Co spin-state modulation of $CoSe_2$ for large-current hydrogen evolution reaction, Rare Met. 43 (2024) 2660–2670.
[23] M. Li, X. Wang, K. Liu, Z. Zhu, H. Guo, M. Li, H. Du, D. Sun, H. Li, K. Huang, Y. Tang, G. Fu, Ce-induced differentiated regulation of Co sites via gradient orbital coupling for bifunctional water-splitting reactions, Adv. Energy Mater. 13 (2023) 2301162.
[24] X. Peng, A.M. Qasim, W. Jin, L. Wang, L. Hu, Y. Miao, W. Li, Y. Li, Z. Liu, K. Huo, K.-Y. Wong, P.K. Chu, Ni-doped amorphous iron phosphide nanoparticles on TiN nanowire arrays: an advanced alkaline hydrogen evolution electrocatalyst, Nano Energy 53 (2018) 66–73.
[25] S. Xie, H. Dong, X. Peng, Paul K. Chu, Non-precious electrocatalysts for the hydrogen evolution reaction, Innov. Discov. 1 (2024) 11.
[26] X. Peng, X. Jin, B. Gao, Z. Liu, P.K. Chu, Strategies to improve cobalt-based electrocatalysts for electrochemical water splitting, J. Catal. 398 (2021) 54–66.
[27] X. Ding, M. Li, J. Jin, X. Huang, X. Wu, L. Feng, Graphene aerogel supported Pt-Ni alloy as efficient electrocatalysts for alcohol fuel oxidation, Chin. Chem. Lett. 33 (2022) 2687–2691.
[28] A. Qayum, X. Peng, J. Yuan, Y. Qu, J. Zhou, Z. Huang, H. Xia, Z. Liu, D.Q. Tan, P. K. Chu, F. Lu, L. Hu, Highly durable and efficient Ni-FeO_x/$FeNi_3$ electrocatalysts synthesized by a facile in situ combustion-based method for overall water splitting with large current densities, ACS Appl. Mater. Interfaces 14 (2022) 27842–27853.
[29] J. Du, D. Xiang, K. Zhou, L. Wang, J. Yu, H. Xia, L. Zhao, H. Liu, W. Zhou, Electrochemical hydrogen production coupled with oxygen evolution, organic synthesis, and waste reforming, Nano Energy 104 (2022) 107875.
[30] L. Dai, Q. Qin, X. Zhao, C. Xu, C. Hu, S. Mo, Y.O. Wang, S. Lin, Z. Tang, N. Zheng, Electrochemical partial reforming of ethanol into ethyl acetate using ultrathin Co_3O_4 nanosheets as a highly selective anode catalyst, ACS Cent. Sci. 2 (2016) 538–544.
[31] J. Zheng, X. Chen, X. Zhong, S. Li, T. Liu, G. Zhuang, X. Li, S. Deng, D. Mei, J. G. Wang, Hierarchical porous NC@CuCo nitride nanosheet networks: Highly efficient bifunctional electrocatalyst for overall water splitting and selective electrooxidation of benzyl alcohol, Adv. Funct. Mater. 27 (2017) 1704169.
[32] W.-J. Liu, L. Dang, Z. Xu, H.-Q. Yu, S. Jin, G.W. Huber, Electrochemical oxidation of 5-hydroxymethylfurfural with NiFe layered double hydroxide (LDH) nanosheet catalysts, ACS Catal. 8 (2018) 5533–5541.
[33] Z.-Y. Yu, C.-C. Lang, M.-R. Gao, Y. Chen, Q.-Q. Fu, Y. Duan, S.-H. Yu, Ni-Mo-O nanorod-derived composite catalysts for efficient alkaline water-to-hydrogen conversion via urea electrolysis, Energy Environ. Sci. 11 (2018) 1890–1897.
[34] H. Jiang, M. Sun, S. Wu, B. Huang, C.-S. Lee, W. Zhang, Oxygen-incorporated NiMoP nanotube arrays as efficient bifunctional electrocatalysts for urea-assisted energy-saving hydrogen production in alkaline electrolyte, Adv. Funct. Mater. 31 (2021) 2104951.
[35] G. Ma, X. Zhang, G. Zhou, X. Wang, Hydrogen production from methanol reforming electrolysis at NiO nanosheets supported Pt nanoparticles, Chem. Eng. J. 411 (2021) 128292.
[36] Q. Zhou, Z. Shen, C. Zhu, J. Li, Z. Ding, P. Wang, F. Pan, Z. Zhang, H. Ma, S. Wang, Nitrogen-doped CoP electrocatalysts for coupled hydrogen evolution and sulfur generation with low energy consumption, Adv. Mater. 30 (2018) 1800140.
[37] Z. Li, L.M. Sun, Y. Zhang, Y.L. Han, W.C. Zhuang, L. Tian, W.Y. Tan, Coupled and decoupled electrochemical water splitting for boosting hydrogen evolution: a review and perspective, Coord. Chem. Rev. 510 (2024) 215837.
[38] S. Paygozar, A.S.R. Aghdam, E. Hassanizadeh, R. Andaveh, G.B. Darband, Recent progress in non-noble metal-based electrocatalysts for urea-assisted electrochemical hydrogen production, Int. J. Hydrog. Energ. 48 (2023) 7219–7259.
[39] T. Kahlstorf, J.N. Hausmann, T. Sontheimer, P.W. Menezes, Challenges for hybrid water electrolysis to replace the oxygen evolution reaction on an industrial scale, Glob. Chall. 7 (2023) 2200242.
[40] T. Wang, X. Cao, L. Jiao, Progress in hydrogen production coupled with electrochemical oxidation of small molecules, Angew. Chem. Int. Ed. 61 (2022) e202213328.
[41] K. Veeramani, G. Janani, J. Kim, S. Surendran, J. Lim, S.C. Jesudass, S. Mahadik, H. lee, T.-H. Kim, J.K. Kim, U. Sim, Hydrogen and value-added products yield from hybrid water electrolysis: a critical review on recent developments, Renew. Sustain. Energy Rev. 177 (2023) 113227.
[42] J.Y. Zhang, H. Wang, Y. Tian, Y. Yan, Q. Xue, T. He, H. Liu, C. Wang, Y. Chen, B. Y. Xia, Anodic hydrazine oxidation assists energy-efficient hydrogen evolution over a bifunctional cobalt perselenide nanosheet electrode, Angew. Chem. Int. Ed. 57 (2018) 7649–7653.
[43] J. Si, Q. Zheng, H. Chen, C. Lei, Y. Suo, B. Yang, Z. Zhang, Z. Li, L. Lei, Y. Hou, Scalable production of few-layer niobium disulfide nanosheets via electrochemical exfoliation for energy-efficient hydrogen evolution reaction, ACS Appl. Mater. Interfaces 11 (2019) 13205–13213.
[44] Y. Li, J. Yin, L. An, M. Lu, K. Sun, Y.-Q. Zhao, D. Gao, F. Cheng, P. Xi, FeS_2/CoS_2 Interface nanosheets as efficient bifunctional electrocatalyst for overall water splitting, Small 14 (2018) 1801070.
[45] C. Feng, M. Lv, J. Shao, H. Wu, W. Zhou, S. Qi, C. Deng, X. Chai, H. Yang, Q. Hu, C. He, Lattice strain engineering of Ni_2P enables efficient catalytic hydrazine oxidation-assisted hydrogen production, Adv. Mater. 35 (2023) e2305598.
[46] J. Zhao, H. Guo, Q. Zhang, Y. Li, L. Gu, R. Song, Trace Ru atoms implanted into a Ni/Fe-based oxalate solid-solution-like with high-indexed facets for energy-saving overall seawater electrolysis assisted by hydrazine, Appl. Catal. B Environ. 325 (2022) 122354.
[47] Z. Wang, L. Xu, F. Huang, L. Qu, J. Li, K.A. Owusu, Z. Liu, Z. Lin, B. Xiang, X. Liu, K. Zhao, X. Liao, W. Yang, Y.-B. Cheng, L. Mai, Copper-nickel nitride nanosheets as efficient bifunctional catalysts for hydrazine-assisted electrolytic hydrogen production, Adv. Energy Mater. 9 (2019) 1900390.
[48] Y. Zhao, N. Jia, X.-R. Wu, F.-M. Li, P. Chen, P.-J. Jin, S. Yin, Y. Chen, Rhodium phosphide ultrathin nanosheets for hydrazine oxidation boosted electrochemical water splitting, Appl. Catal. B Environ. 270 (2020) 118880.
[49] Y. Xie, Y. Zhu, J. Zhang, Q. Qian, L. Yapeng, Z. Li, Y. Liu, C. Xiao, G. Zhang, Dual Nanoislands on Ni/C hybrid nanosheet activate superior hydrazine oxidation-assisted high-efficiency H_2 production, Angew. Chem. Int. Ed. 61 (2022) e202113082.
[50] P. Shen, B. Zhou, Z. Chen, W. Xiao, Y. Fu, J. Wan, Z. Wu, L. Wang, Ruthenium-doped 3D Cu_2O nanochains as efficient electrocatalyst towards hydrogen evolution and hydrazine oxidation, Appl. Catal. B Environ. 325 (2022) 122305.
[51] X. Zhai, Q. Yu, J. Chi, X. Wang, B. Li, B. Yang, Z. Li, J. Lai, L. Wang, Accelerated dehydrogenation kinetics through Ru, Fe dual-doped Ni_2P as bifunctional electrocatalyst for hydrazine-assisted self-powered hydrogen generation, Nano Energy 105 (2023) 108008.
[52] M. Zhang, Z. Wang, Z. Duan, S. Wang, Y. Xu, X. Li, L. Wang, H. Wang, Anodic hydrazine oxidation assisted hydrogen evolution over bimetallic RhIr mesoporous nanospheres, J. Mater. Chem. A 9 (2021) 18323–18328.
[53] Q. Qian, J. Zhang, J. Li, Y. Li, X. Jin, Y. Zhu, Y. Liu, Z. Li, A. El-Harairy, C. Xiao, G. Zhang, Y. Xie, Artificial heterointerfaces achieve delicate reaction kinetics towards hydrogen evolution and hydrazine oxidation catalysis, Angew. Chem. Int. Ed. 60 (2021) 5984–5993.

[54] Y. Liu, J. Zhang, Y. Li, Q. Qian, Z. Li, G. Zhang, Realizing the synergy of interface engineering and chemical substitution for Ni_3N enables its bifunctionality toward hydrazine oxidation assisted energy-saving hydrogen production, Adv. Funct. Mater. 31 (2021) 2103673.

[55] G. Chen, X. Li, X. Feng, Upgrading organic compounds through the coupling of electrooxidation with hydrogen evolution, Angew. Chem. Int. Ed. 61 (2022) e202209014.

[56] Z. Li, X. He, Q. Qian, Y. Zhu, Y. Feng, W. Wan, G. Zhang, Active site implantation for $Ni(OH)_2$ nanowire network achieves superior hybrid seawater electrolysis at 1 A cm^{-2} with record-low cell voltage, Adv. Funct. Mater. 33 (2023) 2304079.

[57] G. Meng, Z. Chang, L. Zhu, C. Chen, Y. Chen, H. Tian, W. Luo, W. Sun, X. Cui, J. Shi, Adsorption site regulations of [W-O]-doped CoP boosting the hydrazine oxidation-coupled hydrogen evolution at elevated current density, Nano Micro Lett. 15 (2023) 212.

[58] C. Tang, R. Zhang, W. Lu, Z. Wang, D. Liu, S. Hao, G. Du, A.M. Asiri, X. Sun, Energy-saving electrolytic hydrogen generation: Ni_2P nanoarray as a high-performance non-noble-metal electrocatalyst, Angew. Chem. Int. Ed. 56 (2017) 842–846.

[59] S. Zhang, C. Zhang, X. Zheng, G. Su, H. Wang, M. Huang, Integrating electrophilic and nucleophilic dual sites on heterogeneous bimetallic phosphide via enhancing interfacial electronic field to boost hydrazine oxidation and hydrogen evolution, Appl. Catal. B-Environ. 324 (2023) 122207.

[60] X. Fu, D. Cheng, C. Wan, S. Kumari, H. Zhang, A. Zhang, H. Huyan, J. Zhou, H. Ren, S. Wang, Z. Zhao, X. Zhao, J. Chen, X. Pan, P. Sautet, Y. Huang, X. Duan, Bifunctional ultrathin $RhRu_{0.5}$-Alloy nanowire electrocatalysts for hydrazine-assisted water splitting, Adv. Mater. 35 (2023) 2301533.

[61] Y. Hu, T. Chao, L. Yapeng, P. Liu, T. Zhao, G. Yu, C. Chen, X. Liang, H. Jin, S. Niu, W. Chen, D. Wang, Y. Li, Cooperative Ni(Co)-Ru-P sites activate dehydrogenation for hydrazine oxidation assisting self-powered H_2 production, Angew. Chem. Int. Ed. 62 (2023) e202308800.

[62] X. Ma, J. Wang, D. Liu, R. Kong, S. Hao, G. Du, A.M. Asiri, X. Sun, Hydrazine-assisted electrolytic hydrogen production: CoS_2 nanoarray as a superior bifunctional electrocatalyst, N. J. Chem. 41 (2017) 4754–4757.

[63] G. Liu, Z. Sun, X. Zhang, H. Wang, G. Wang, X. Wu, H. Zhang, H. Zhao, Vapor-phase hydrothermal transformation of a nanosheet array structure $Ni(OH)_2$ into ultrathin Ni_3S_2 nanosheets on nickel foam for high-efficiency overall water splitting, J. Mater. Chem. A 6 (2018) 19201–19209.

[64] J. Yang, L. Xu, W. Zhu, M. Xie, F. Liao, T. Cheng, Z. Kang, M. Shao, Rh/RhO_x nanosheets as pH-universal bifunctional catalysts for hydrazine oxidation and hydrogen evolution reactions, J. Mater. Chem. A 10 (2022) 1891–1898.

[65] Y. Li, J. Zhang, Y. Liu, Q. Qian, Z. Li, Y. Zhu, G. Zhang, Partially exposed RuP_2 surface in hybrid structure endows its bifunctionality for hydrazine oxidation and hydrogen evolution catalysis, Sci. Adv. 6 (2020) eabb4197.

[66] L. Zhu, J. Huang, G. Meng, T. Wu, C. Chen, H. Tian, Y. Chen, F. Kong, Z. Chang, X. Cui, J. Shi, Active site recovery and N-N bond breakage during hydrazine oxidation boosting the electrochemical hydrogen production, Nat. Commun. 14 (2023) 1997.

[67] K. Li, J. He, X. Guan, Y. Tong, Y. Ye, L. Chen, P. Chen, Phosphorus-modified amorphous high-entropy CoFeNiCrMn compound as high-performance electrocatalyst for hydrazine-assisted water electrolysis, Small 19 (2023) e2302130.

[68] K. Li, G. Zhou, Y. Tong, Y. Ye, P. Chen, Interface engineering of a hierarchical P-modified Co/Ni_3P heterostructure for highly efficient water electrolysis coupled with hydrazine degradation, ACS Sustain. Chem. Eng. 11 (2023) 14186–14196.

[69] Y. Hao, D. Yu, S. Zhu, C.H. Kuo, Y.M. Chang, L. Wang, H.Y. Chen, M. Shao, S. Peng, Methanol upgrading coupled with hydrogen product at large current density promoted by strong interfacial interactions, Energy Environ. Sci. 16 (2023) 1100–1110.

[70] Y. Liu, J. Zhang, Y. Li, Q. Qian, Z. Li, Y. Zhu, G. Zhang, Manipulating dehydrogenation kinetics through dual-doping Co_3N electrode enables highly efficient hydrazine oxidation assisting self-powered H_2 production, Nat. Commun. 11 (2020) 1853.

[71] Y. Yang, X. Li, G. Liu, H. Liu, Y. Shi, C. Ye, Z. Fang, M. Ye, J. Shen, Hierarchical ohmic contact interface engineering for efficient hydrazine-assisted hydrogen evolution reaction, Adv. Mater. 36 (2023) 2307979.

[72] S. Chen, C. Wang, S. Liu, M. Huang, J. Lu, P. Xu, H. Tong, L. Hu, Q. Chen, Boosting hydrazine oxidation reaction on CoP/Co Mott-Schottky electrocatalyst through engineering active Sites, J. Phys. Chem. Lett. 12 (2021) 4849–4856.

[73] S. Zhao, Y. Zhang, H. Li, S. Zeng, R. Li, Q. Yao, H. Chen, Y. Zheng, K. Qu, Regulating Ru active sites by Pd alloying to significantly enhance hydrazine oxidation for energy-saving hydrogen production, J. Mater. Chem. A 11 (2023) 13783–13792.

[74] G. Qian, J. Chen, W. Jiang, T. Yu, K. Tan, S. Yin, Strong electronic coupling of CoNi and N-doped-carbon for efficient urea-assisted H_2 production at a large current density, Carbon Energy 5 (2023) e368.

[75] J. Xie, L. Gao, S. Cao, W. Liu, F. Lei, P. Hao, X. Xia, B. Tang, Copper-incorporated hierarchical wire-on-sheet α-$Ni(OH)_2$ nanoarrays as robust trifunctional catalysts for synergistic hydrogen generation and urea oxidation, J. Mater. Chem. A 7 (2019) 13577–13584.

[76] L. Sha, J. Yin, K. Ye, G. Wang, K. Zhu, K. Cheng, J. Yan, G. Wang, D. Cao, The construction of self-supported thorny leaf-like nickel-cobalt bimetal phosphides as efficient bifunctional electrocatalysts for urea electrolysis, J. Mater. Chem. A 7 (2019) 9078–9085.

[77] R.-Q. Li, X.-Y. Wan, B.-L. Chen, R.-Y. Cao, Q.-H. Ji, J. Deng, K. Qu, X.-B. Wang, Y. Zhu, Hierarchical $Ni_3N/Ni_{0.2}Mo_{0.8}N$ heterostructure nanorods arrays as efficient electrocatalysts for overall water and urea electrolysis, Chem. Eng. J. 409 (2021) 1385–8947.

[78] M. Qin, L. Chen, H. Zhang, M. Humayun, Y. Fu, X. Xu, X. Xue, C. Wang, Achieving highly efficient pH-universal hydrogen evolution by Mott-Schottky heterojunction of Co_2P/Co_4N, Chem. Eng. J. 454 (2023) 140230.

[79] J. Zheng, K. Wu, C. Lyu, X.-Y. Pan, X. Zhang, Y. Zhu, Wang Anting, W.-M. Lau, N. Wang, Electrocatalyst of two-dimensional CoP nanosheets embedded by carbon nanoparticles for hydrogen generation and urea oxidation in alkaline solution, Appl. Surf. Sci. 506 (2020) 144977.

[80] L. Wang, L. Ren, X. Wang, X. Feng, J. Zhou, B. Wang, Multivariate MOF-templated pomegranate-like Ni/C as efficient bifunctional electrocatalyst for hydrogen evolution and urea oxidation, ACS Appl. Mater. Interfaces 10 (2018) 4750–4756.

[81] Y. Zhou, Y. Wang, D. Kong, Q. Zhao, L. Zhao, J. Zhang, X. Chen, Y. Li, X. Yan, C. Meng, Revealing the reactant mediation role of low-valence Mo for accelerated urea-assisted water splitting, Adv. Funct. Mater. 33 (2023) 2210656.

[82] H. Yu, S. Zhu, Y. Hao, Y.-M. Chang, L. Li, J. Ma, H.-Y. Chen, M. Shao, S. Peng, Modulating local interfacial bonding environment of heterostructures for energy-saving hydrogen production at high current densities, Adv. Funct. Mater. 33 (2023) 2212811.

[83] Q. Xu, G. Qian, S. Yin, C. Yu, W. Chen, T. Yu, L. Luo, Y. Xia, P. Tsiakaras, Design and synthesis of highly performing bifunctional Ni-NiO-MoNi hybrid catalysts for enhanced urea oxidation and hydrogen evolution reactions, ACS Sustain. Chem. Eng. 8 (2020) 7174–7181.

[84] N. Chen, Y.-X. Du, G. Zhang, W.-T. Lu, F.-F. Cao, Amorphous nickel sulfoselenide for efficient electrochemical urea-assisted hydrogen production in alkaline media, Nano Energy 81 (2021) 105605.

[85] F. Shen, W. Jiang, G. Qian, W. Chen, H. Zhang, L. Luo, S. Yin, Strongly coupled carbon encapsulated $Ni-WO_2$ hybrids as efficient catalysts for water-to-hydrogen conversion via urea electro-oxidation, J. Power Sources 458 (2020) 228014.

[86] X. Xu, H. Liao, L. Huang, S. Chen, R. Wang, S. Wu, Y. Wu, Z. Sun, H. Huang, Surface reconstruction and directed electron transport in $NiSe_2/MoSe_2$ Mott-Schottky heterojunction catalysts promote urea-assisted water splitting, Appl. Catal. B Environ. 341 (2024) 123312.

[87] K. Wang, W. Huang, Q. Cao, Y. Zhao, X. Sun, R. Ding, W. Lin, E. Liu, P. Gao, Engineering NiF_3/Ni_2P heterojunction as efficient electrocatalysts for urea oxidation and splitting, Chem. Eng. J. 427 (2021) 130865.

[88] Z. Chen, W. Wang, S. Huang, P. Ning, Y. Wu, C. Gao, T.-T. Le, J. Zai, Y. Jiang, Z. Hu, Well-defined $CoSe_2@MoSe_2$ hollow heterostructured nanocubes with enhanced dissociation kinetics for overall water splitting, Nanoscale 12 (2020) 326–335.

[89] R. Li, Y. Li, P. Yang, P. Ren, D. Wang, X. Lu, H. Zhang, Z. Zhang, P. Yan, J. Zhang, M. An, B. Wang, H. Liu, S. Dou, Key Roles of interfacial OH^- ion distribution on proton coupled electron transfer kinetics toward urea oxidation reaction, Small 19 (2023) e2302151.

[90] C. Xu, X. Yang, K. Feng, M. Zhang, L. Yang, S. Yin, Carbon-encapsulated multimetallic hybrid electrocatalyst for overall water splitting and urea oxidation, ACS Appl. Energy Mater. 6 (2023) 1404–1412.

[91] X. Ding, L. Pei, Y. Huang, D. Chen, Z. Xie, Hollow NiCoP nanoprisms derived from prussian blue analogues as bifunctional electrocatalysts for urea-ssisted hydrogen production in alkaline media, Small 18 (2022) 2205547.

[92] X. Xu, H. Ullah, M. Humayun, L. Li, X. Zhang, M. Bououdina, D.P. Debecker, K. Huo, D. Wang, C. Wang, Fluorinated Ni-O-C heterogeneous catalyst for efficient urea-assisted hydrogen production, Adv. Funct. Mater. 33 (2023) 2303986.

[93] G. Feng, L. An, B. Li, Y. Zuo, J. Song, F. Ning, N. Jiang, X. Cheng, Y. Zhang, D. Xia, Atomically ordered non-precious Co_3Ta intermetallic nanoparticles as high-performance catalysts for hydrazine electrooxidation, Nat. Commun. 10 (2019) 4514.

[94] T.Y. Burshtein, Y. Yasman, L. Muñoz-Moene, J.H. Zagal, D. Eisenberg, Hydrazine oxidation electrocatalysis, ACS Catal. 14 (2024) 2264–2283.

[95] Q. Liu, X. Liao, Y. Tang, J. Wang, X. Lv, X. Pan, R. Lu, Y. Zhao, X.-Y. Yu, H.B. Wu, Low-coordinated cobalt arrays for efficient hydrazine electrooxidation, Energy Environ. Sci. 15 (2022) 3246–3256.

[96] Y. Jeong, S. Shankar Naik, Y. Yu, J. Theerthagiri, S.J. Lee, P.L. Show, H.C. Choi, M.Y. Choi, Ligand-free monophasic CuPd alloys endow boosted reaction kinetics toward energy-efficient hydrogen fuel production paired with hydrazine oxidation, J. Mater. Sci. Technol. 143 (2023) 20–29.

[97] Z. Liu, Y. Li, H. Guo, J. Zhao, H. Zhang, R. Song, Interface engineering of amorphous/crystalline heterojunctions with synergistic Ru doping for efficient hydrazine oxidation assisted overall water splitting, J. Mater. Chem. A 11 (2023) 24667–24677.

[98] H. Li, S. Chen, H. Lin, X. Xu, H. Yang, L. Song, X. Wang, Nickel diselenide ultrathin nanowires decorated with amorphous nickel oxide nanoparticles for enhanced water splitting electrocatalysis, Small 13 (2017) 1701487.

[99] B.J. Taitt, D.-H. Nam, K.-S. Choi, A comparative study of nickel, cobalt, and iron oxyhydroxide anodes for the electrochemical oxidation of 5-hydroxymethylfurfural to 2, 5-furandicarboxylic acid, ACS Catal. 9 (2018) 660–670.

[100] G. Hu, J. Xiang, J. Li, P. Liu, R.N. Ali, B. Xiang, Urchin-like ternary cobalt phosphosulfide as high-efficiency and stable bifunctional electrocatalyst for overall water splitting, J. Catal. 371 (2019) 126–134.

[101] S. Yang, Y. Wang, H. Zhang, Y. Zhang, L. Liu, L. Fang, X. Yang, X. Gu, Y. Wang, Unique three-dimensional $Mo_2C@MoS_2$ heterojunction nanostructure with S vacancies as outstanding all-pH range electrocatalyst for hydrogen evolution, J. Catal. 371 (2019) 20–26.

[102] R.A. Senthil, S. Jung, A. Min, A. Kumar, C.J. Moon, M. Singh, M.Y. Choi, Revealing the impact of pulsed laser-produced single-Pd nanoparticles on a bimetallic $NiCo_2O_4$ electrocatalyst for energy-saving hydrogen production via hybrid water electrolysis, ACS Catal. 14 (2024) 3320–3335.
[103] Z. Jiang, S. Song, X. Zheng, X. Liang, Z. Li, H. Gu, Z. Li, Y. Wang, S. Liu, W. Chen, D. Wang, Y. Li, Lattice strain and schottky junction dual regulation boosts ultrafine ruthenium nanoparticles anchored on a N-modified carbon catalyst for H_2 production, J. Am. Chem. Soc. 144 (2022) 19619–19626.
[104] J. Mahmood, F. Li, S.-M. Jung, M.S. Okyay, I. Ahmad, S.-J. Kim, N. Park, H. Y. Jeong, J.-B. Baek, An efficient and pH-universal ruthenium-based catalyst for the hydrogen evolution reaction, Nat. Nanotechnol. 12 (2017) 441–446.
[105] J. Li, Y. Li, J. Wang, C. Zhang, H. Ma, C. Zhu, D. Fan, Z. Guo, M. Xu, Y. Wang, H. Ma, Elucidating the critical role of ruthenium single atom sites in water dissociation and dehydrogenation behaviors for robust hydrazine oxidation-boosted alkaline hydrogen evolution, Adv. Funct. Mater. 32 (2022) 2109439.
[106] Y. Hu, T. Chao, Y. Li, P. Liu, T. Zhao, G. Yu, C. Chen, X. Liang, H. Jin, S. Niu, W. Chen, D. Wang, Y. Li, Cooperative Ni(Co)-Ru-P sites activate dehydrogenation for hydrazine oxidation assisting self-powered H_2 production, Angew. Chem. Int. Ed. 62 (2023) e202308800.
[107] J.T. Ren, G.G. Yuan, C.C. Weng, L. Chen, Z.Y. Yuan, Uniquely integrated Fe-doped $Ni(OH)_2$ nanosheets for highly efficient oxygen and hydrogen evolution reactions, Nanoscale 10 (2018) 10620–10628.
[108] P. Zhang, L. Li, D. Nordlund, H. Chen, L. Fan, B. Zhang, X. Sheng, Q. Daniel, L. Sun, Dendritic core-shell nickel-iron-copper metal/metal oxide electrode for efficient electrocatalytic water oxidation, Nat. Commun. 9 (2018) 381.
[109] K.N. Dinh, P. Zheng, Z. Dai, Y. Zhang, R. Dangol, Y. Zheng, B. Li, Y. Zong, Q. Yan, Ultrathin porous NiFeV ternary layer hydroxide nanosheets as a highly efficient bifunctional electrocatalyst for overall water splitting, Small 14 (2018) 1703257.
[110] Q. Sun, M. Zhou, Y. Shen, L. Wang, Y. Ma, Y. Li, X. Bo, Z. Wang, C. Zhao, Hierarchical nanoporous Ni(Cu) alloy anchored on amorphous NiFeP as efficient bifunctional electrocatalysts for hydrogen evolution and hydrazine oxidation, J. Catal. 373 (2019) 180–189.
[111] Q. Qian, J. Zhang, J. Li, Y. Li, X. Jin, Y. Zhu, Y. Liu, Z. Li, A. El-Harairy, C. Xiao, Artificial heterointerfaces achieve delicate reaction kinetics towards hydrogen evolution and hydrazine oxidation catalysis, Angew. Chem. Int. Ed. 60 (2021) 5984–5993.
[112] W. Tong, M. Forster, F. Dionigi, S. Dresp, R. Sadeghi Erami, P. Strasser, A. J. Cowan, P. Farràs, Electrolysis of low-grade and saline surface water, Nat. Energy 5 (2020) 367–377.
[113] L. Zhang, Z. Wang, J. Qiu, Energy-saving hydrogen production by seawater electrolysis coupling sulfion degradation, Adv. Mater. 34 (2022) 2109321.
[114] Y. Xin, K. Shen, T. Guo, L. Chen, Y. Li, Coupling hydrazine oxidation with seawater electrolysis for energy-saving hydrogen production over bifunctional CoNC nanoarray electrocatalysts, Small 19 (2023) 2300019.
[115] H. Jin, X. Wang, C. Tang, A. Vasileff, L. Li, A. Slattery, S.Z. Qiao, Stable and highly efficient hydrogen evolution from seawater enabled by an unsaturated nickel surface nitride, Adv. Mater. 33 (2021) 2007508.
[116] F. Sun, J. Qin, Z. Wang, M. Yu, X. Wu, X. Sun, J. Qiu, Energy-saving hydrogen production by chlorine-free hybrid seawater splitting coupling hydrazine degradation, Nat. Commun. 12 (2021) 4182.
[117] Q. Yu, J. Chi, G. Liu, X. Wang, X. Liu, Z. Li, Y. Deng, X. Wang, L. Wang, Dual-strategy of hetero-engineering and cation doping to boost energy-saving hydrogen production via hydrazine-assisted seawater electrolysis, Sci. China Mater. 65 (2022) 1539–1549.
[118] B.K. Boggs, R.L. King, G.G. Botte, Urea electrolysis: direct hydrogen production from urine, Chem. Commun. (2009) 4859–4861.
[119] D. Liu, T. Liu, L. Zhang, F. Qu, G. Du, A.M. Asiri, X. Sun, High-performance urea electrolysis towards less energy-intensive electrochemical hydrogen production using a bifunctional catalyst electrode, J. Mater. Chem. A 5 (2017) 3208–3213.
[120] D. Khalafallah, A.A. Farghaly, C. Ouyang, W. Huang, Z. Hong, Atomically dispersed Pt single sites and nanoengineered structural defects enable a high electrocatalytic activity and durability for hydrogen evolution reaction and overall urea electrolysis, J. Power Sources 558 (2023) 232563.
[121] C. Xiao, S. Li, X. Zhang, D.R. MacFarlane, $MnO_2/MnCo_2O_4$/Ni heterostructure with quadruple hierarchy: a bifunctional electrode architecture for overall urea oxidation, J. Mater. Chem. A 5 (2017) 7825–7832.
[122] J.-Y. Zhang, T. He, M. Wang, R. Qi, Y. Yan, Z. Dong, H. Liu, H. Wang, B.Y. Xia, Energy-saving hydrogen production coupling urea oxidation over a bifunctional nickel-molybdenum nanotube array, Nano Energy 60 (2019) 894–902.
[123] N.K. Shrestha, S.A. Patil, A.S. Salunke, A.I. Inamdar, H. Im, Unprecedented urea oxidation on Zn@Ni-MOF with an ultra-high current density: understanding the competition between UOR and OER, catalytic activity limitation and reaction selectivity, J. Mater. Chem. A 11 (2023) 14870–14877.
[124] Q.X. Huang, F. Wang, Y. Liu, B.Y. Zhang, F.Y. Guo, Z.Q. Jia, H. Wang, T.X. Yang, H.T. Wu, F.Z. Ren, T.F. Yi, Recent progress of two-dimensional metal-base catalysts in urea oxidation reaction, Rare Met. 43 (2024) 3607–3633.
[125] L. Sha, T. Liu, K. Ye, K. Zhu, J. Yan, J. Yin, G. Wang, D. Cao, A heterogeneous interface on NiS@Ni_3S_2/$NiMoO_4$ heterostructures for efficient urea electrolysis, J. Mater. Chem. A 8 (2020) 18055–18063.
[126] T. Wang, L. Miao, S. Zheng, H. Qin, X. Cao, L. Yang, L. Jiao, Interfacial engineering of Ni_3N/Mo_2N heterojunctions for urea-assisted hydrogen evolution reaction, ACS Catal. 13 (2023) 4091–4100.
[127] C. Wang, H. Lu, Z. Mao, C. Yan, G. Shen, X. Wang, Bimetal schottky heterojunction boosting energy-saving hydrogen production from alkaline water via urea electrocatalysis, Adv. Funct. Mater. 30 (2020) 2000556.
[128] Z. Cao, T. Zhou, X. Ma, Y. Shen, Q. Deng, W. Zhang, Y. Zhao, Hydrogen production from urea sewage on NiFe-based porous electrocatalysts, ACS Sustain. Chem. Eng. 8 (2020) 11007–11015.
[129] Z. Dong, F. Lin, Y. Yao, L. Jiao, Crystalline $Ni(OH)_2$/amorphous $NiMoO_x$ mixed-catalyst with Pt-like performance for hydrogen production, Adv. Energy Mater. 9 (2019) 1902703.
[130] X. Xu, X. Hou, P. Du, C. Zhang, S. Zhang, H. Wang, A. Toghan, M. Huang, Controllable Ni/NiO interface engineering on N-doped carbon spheres for boosted alkaline water-to-hydrogen conversion by urea electrolysis, Nano Res. 15 (2022) 7124–7133.
[131] C. Zhang, R. Du, J.J. Biendicho, M. Yi, K. Xiao, D. Yang, T. Zhang, X. Wang, J. Arbiol, J. Llorca, Y. Zhou, J.R. Morante, A. Cabot, Tubular CoFeP@CN as a mott-schottky catalyst with multiple adsorption sites for robust lithium-sulfur batteries, Adv. Energy Mater. 11 (2021) 2100432.
[132] X. Luo, P. Ji, P. Wang, R. Cheng, D. Chen, C. Lin, J. Zhang, J. He, Z. Shi, N. Li, S. Xiao, S. Mu, Interface engineering of hierarchical branched Mo-doped Ni_3S_2/Ni_xP_y hollow heterostructure nanorods for efficient overall water splitting, Adv. Energy Mater. 10 (2020) 1903891.
[133] J. Liu, Y. Wang, Y. Liao, C. Wu, Y. Yan, H. Xie, Y. Chen, Heterostructured Ni_3S_2-Ni_3P/NF as a bifunctional catalyst for overall urea-water electrolysis for hydrogen generation, ACS Appl. Mater. Interfaces 13 (2021) 26948–26959.
[134] C. Li, Y. Liu, Z. Zhuo, H. Ju, D. Li, Y. Guo, X. Wu, H. Li, T. Zhai, Local charge distribution engineered by schottky heterojunctions toward urea electrolysis, Adv. Energy Mater. 8 (2018) 1801775.
[135] C. Gu, G. Zhou, J. Yang, H. Pang, M. Zhang, Q. Zhao, X. Gu, S. Tian, J. Zhang, L. Xu, Y. Tang, NiS/MoS_2 Mott-Schottky heterojunction-induced local charge redistribution for high-efficiency urea-assisted energy-saving hydrogen production, Chem. Eng. J. 443 (2022) 136321.
[136] K. Ji, J. Wang, P. Yang, NiCo nanolayered double hydroxides on Fe/Ni metal-organic frameworks for oxygen evolution, ACS Appl. Nano Mater. 6 (2023) 7931–7941.
[137] H.N. Dhandapani, A. Karmakar, S.S. Selvasundarasekar, S. Kumaravel, S. Nagappan, R. Madhu, B. Ramesh Babu, S. Kundu, Modulating the surface electronic structure of active Ni sites by engineering hierarchical NiFe-LDH/CuS over Cu Foam as an efficient electrocatalyst for water splitting, Inorg. Chem. 61 (2022) 21055–21066.
[138] M. Gu, L. Jiang, S. Zhao, H. Wang, M. Lin, X. Deng, X. Huang, A. Gao, X. Liu, P. Sun, X. Zhang, Deciphering the space charge effect of the p-n Junction between copper sulfides and molybdenum selenides for efficient water electrolysis in a wide pH range, ACS Nano 16 (2022) 15425–15439.
[139] D. Xu, S.-N. Zhang, J.-S. Chen, X.-H. Li, Design of the synergistic rectifying interfaces in mott-schottky catalysts, Chem. Rev. 123 (2023) 1–30.
[140] Y. Zhou, B. Chu, Z. Sun, L. Dong, F. Wang, B. Li, M. Fan, Z. Chen, Surface reconstruction and charge distribution enabling Ni/W_5N_4 mott-schottky heterojunction bifunctional electrocatalyst for efficient urea-assisted water electrolysis at a large current density, Appl. Catal. B Environ. 323 (2023) 122168.
[141] Q. Zhang, B. Liu, L. Li, Y. Ji, C. Wang, L. Zhang, Z. Su, Maximized schottky effect: The ultrafine V_2O_3/Ni heterojunctions repeatedly arranging on monolayer nanosheets for efficient and stable water-to-hydrogen conversion, Small 17 (2021) 2005769.
[142] Y. Sun, T. Liu, Z. Li, A. Meng, G. Li, L. Wang, S. Li, Morphology and interfacial charge regulation strategies constructing 3D flower-like Co@CoP_2 heterostructure electrocatalyst for efficient overall water splitting, Chem. Eng. J. 433 (2022) 133684.
[143] X.-L. Zhang, X. Su, Y.-R. Zheng, S.-J. Hu, L. Shi, F.-Y. Gao, P.-P. Yang, Z.-Z. Niu, Z.-Z. Wu, S. Qin, R. Wu, Y. Duan, C. Gu, X.-S. Zheng, J.-F. Zhu, M.-R. Gao, Strongly coupled cobalt diselenide monolayers for selective electrocatalytic oxygen reduction to H_2O_2 under acidic conditions, Angew. Chem. Int. Ed. 60 (2021) 26922–26931.
[144] Y. Yang, F.-Y. Gao, X.-L. Zhang, S. Qin, L.-R. Zheng, Y.-H. Wang, J. Liao, Q. Yang, M.-R. Gao, Suppressing electron back-donation for a highly CO-tolerant fuel cell anode catalyst via cobalt modulation, Angew. Chem. Int. Ed. 61 (2022) e202208040.
[145] X. Xu, Q. Deng, H.-C. Chen, M. Humayun, D. Duan, X. Zhang, H. Sun, X. Ao, X. Xue, A. Nikiforov, Metal-organic frameworks offering tunable binary active sites toward highly efficient urea oxidation electrolysis, Research 2022 (2022) 9837109.
[146] J. Li, J. Li, T. Liu, L. Chen, Y. Li, H. Wang, X. Chen, M. Gong, Z.P. Liu, X. Yang, Deciphering and suppressing over-oxidized nitrogen in nickel-catalyzed urea electrolysis, Angew. Chem. Int. Ed. 60 (2021) 26656–26662.
[147] W.K. Han, J.X. Wei, K. Xiao, T. Ouyang, X. Peng, S. Zhao, Z.Q. Liu, Activating lattice oxygen in layered lithium oxides through cation vacancies for enhanced urea electrolysis, Angew. Chem. Int. Ed. 61 (2022) e202206050.
[148] M.L. Guo, Z.Y. Wu, M.M. Zhang, Z.J. Huang, K.X. Zhang, B.R. Wang, J.C. Tu, Coupling interface constructions of FeOOH/$NiCo_2S_4$ by microwave-assisted method for efficient oxygen evolution reaction, Rare Met. 42 (2023) 1847–1857.
[149] R.P. Forslund, C.T. Alexander, A.M. Abakumov, K.P. Johnston, K.J. Stevenson, Enhanced electrocatalytic activities by substitutional tuning of nickel-based ruddlesden-popper catalysts for the oxidation of urea and small alcohols, ACS Catal. 9 (2019) 2664–2673.
[150] Z. Xiao, Y. Qian, T. Tan, H. Lu, C. Liu, B. Wang, Q. Zhang, M.T. Sarwar, R. Gao, A. Tang, H. Yang, Energy-saving hydrogen production by water splitting coupling urea decomposition and oxidation reactions, J. Mater. Chem. A 11 (2023) 259–267.
[151] R.R. Rao, S. Corby, A. Bucci, M. García-Tecedor, C.A. Mesa, J. Rossmeisl, S. Giménez, J. Lloret-Fillol, I.E.L. Stephens, J.R. Durrant, Spectroelectrochemical

analysis of the water oxidation mechanism on doped nickel oxides, J. Am. Chem. Soc. 144 (2022) 7622–7633.
[152] W. Chen, L. Xu, X. Zhu, Y.-C. Huang, W. Zhou, D. Wang, Y. Zhou, S. Du, Q. Li, C. Xie, L. Tao, C.-L. Dong, J. Liu, Y. Wang, R. Chen, H. Su, C. Chen, Y. Zou, Y. Li, Q. Liu, S. Wang, Unveiling the electrooxidation of urea: intramolecular coupling of the N-N bond, Angew. Chem. Int. Ed. 60 (2021) 7297–7307.
[153] R.P. Forslund, J.T. Mefford, W.G. Hardin, C.T. Alexander, K.P. Johnston, K. J. Stevenson, Nanostructured $LaNiO_3$ perovskite electrocatalyst for enhanced urea oxidation, ACS Catal. 6 (2016) 5044–5051.
[154] Y. Zhu, C. Liu, S. Cui, Z. Lu, J. Ye, Y. Wen, W. Shi, X. Huang, L. Xue, J. Bian, Y. Li, Y. Xu, B. Zhang, multistep dissolution of lamellar crystals generates superthin amorphous $Ni(OH)_2$ catalyst for UOR, Adv. Mater. 35 (2023) 2301549.
[155] Y. Li, H. Jiang, Z. Cui, S. Zhu, Z. Li, S. Wu, L. Ma, X. Han, Y. Liang, Spin state tuning of the octahedral sites in Ni-Co-based spinel toward highly efficient urea oxidation reaction, J. Phys. Chem. C. 125 (2021) 9190–9199.
[156] J. Deng, P. Ren, D. Deng, X. Bao, Enhanced electron penetration through an ultrathin graphene layer for highly efficient catalysis of the hydrogen evolution reaction, Angew. Chem. Int. Ed. 54 (2015) 2100–2104.
[157] J. Lu, S. Yin, P.K. Shen, Carbon-encapsulated electrocatalysts for the hydrogen evolution reaction, Electrochem. Energy R 2 (2019) 105–127.
[158] J. Wang, Z. Zhao, C. Shen, H. Liu, X. Pang, M. Gao, J. Mu, F. Cao, G. Li, Ni/NiO heterostructures encapsulated in oxygen-doped graphene as multifunctional electrocatalysts for the HER, UOR and HMF oxidation reaction, Catal. Sci. Technol. 11 (2021) 2480–2490.
[159] Y. Xu, M. Liu, M. Wang, T. Ren, K. Ren, Z. Wang, X. Li, L. Wang, H. Wang, Methanol electroreforming coupled to green hydrogen production over bifunctional NiIr-based metal-organic framework nanosheet arrays, Appl. Catal. B Environ. 300 (2022) 120753.
[160] K. Xiang, D. Wu, X. Deng, M. Li, S. Chen, P. Hao, X. Guo, J.-L. Luo, X.-Z. Fu, Boosting H_2 generation coupled with selective oxidation of methanol into value-added chemical over cobalt hydroxide@hydroxysulfide nanosheets electrocatalysts, Adv. Funct. Mater. 30 (2020) 1909610.
[161] Y.C. Jiang, H.Y. Sun, Y.N. Li, J.W. He, Q. Xue, X. Tian, F.M. Li, S.B. Yin, D.S. Li, Y. Chen, Bifunctional Pd@RhPd core-shell nanodendrites for methanol electrolysis, ACS Appl. Mater. Interfaces 13 (2021) 35767–35776.
[162] Z. Lu, J. Xie, J. Hu, K. Wang, Y. Cao, In situ replacement synthesis of Co@NCNT encapsulated $CoPt_3$@Co_2P heterojunction boosting methanol oxidation and hydrogen evolution, Small 17 (2021) e2104656.
[163] Z. Pi, H. Zhong, Integrating hydrogen production with selective methanol oxidation to value-added formate over a NiS bifunctional electrocatalyst, IOP Conf. Ser. Earth Environ. Sci. 651 (2021) 042062.
[164] W. Ao, C. Cheng, H. Ren, Z. Fan, P. Yin, Q. Qin, Z.N. Chen, L. Dai, Heterostructured Ru/$Ni(OH)_2$ nanomaterials as multifunctional electrocatalysts for selective reforming of ethanol, ACS Appl. Mater. Interfaces 14 (2022) 45042–45050.
[165] H. Chen, X. Wu, D. Liu, C. Ye, L. Huang, X. Long, L. Wang, J. Zhang, J.-L. Luo, X.-Z. Fu, Highly efficient C@Ni-Pd bifunctional electrocatalyst for energy-saving hydrogen evolution and value-added chemicals co-production from ethanol aqueous solution, Chem. Eng. J. 474 (2023) 145639.
[166] Y. Zhu, X. Zhu, L. Bu, Q. Shao, Y. Li, Z. Hu, C.-T. Chen, C.-W. Pao, S. Yang, X. Huang, Single-atom in-doped subnanometer Pt nanowires for simultaneous hydrogen generation and biomass upgrading, Adv. Funct. Mater. 30 (2020) 2004310.
[167] X. Yu, E.C. dos Santos, J. White, G. Salazar-Alvarez, L.G.M. Pettersson, A. Cornell, M. Johnsson, Electrocatalytic glycerol oxidation with concurrent hydrogen evolution utilizing an efficient MoO_x/Pt Catalyst, Small 17 (2021) 2104288.
[168] Y. Li, X. Wei, L. Chen, J. Shi, M. He, Nickel-molybdenum nitride nanoplate electrocatalysts for concurrent electrolytic hydrogen and formate productions, Nat. Commun. 10 (2019) 5335.
[169] H. Liu, R. Zhang, L. Chen, L. Wang, Y. Guo, Y. Yang, Synergistic coupling of nickel boride with Ru cluster as a highly active multifunctional electrocatalyst for overall water splitting and glucose electrolysis, Adv. Sustain. Syst. 5 (2021) 2000184.
[170] Y. Xu, T. Liu, K. Shi, H. Yu, K. Deng, X. Wang, Z. Wang, L. Wang, H. Wang, Ru-doping induced lattice strain in hetero-phase Ni_2P-$Ni_{12}P_5$ arrays enables simultaneous efficient energy-saving hydrogen generation and formate electrosynthesis, J. Mater. Chem. A 10 (2022) 20365–20374.
[171] J. Wu, X. Liu, Y. Hao, S. Wang, R. Wang, W. Du, S. Cha, X.-Y. Ma, X. Yang, M. Gong, Ligand hybridization for electro-reforming waste glycerol into isolable oxalate and hydrogen, Angew. Chem. Int. Ed. 62 (2023) e202216083.
[172] Y. Zhu, Q. Qian, Y. Chen, X. He, X. Shi, W. Wang, Z. Li, Y. Feng, G. Zhang, F. Cheng, Biphasic transition metal nitride electrode promotes nucleophile oxidation reaction for practicable hybrid water electrocatalysis, Adv. Funct. Mater. 33 (2023) 2300547.
[173] B. Liu, G. Wang, X. Feng, L. Dai, Z. Wen, S. Ci, Energy-saving H_2 production from a hybrid acid/alkali electrolyzer assisted by anodic glycerol oxidation, Nanoscale 14 (2022) 12841–12848.
[174] Z. Li, Y. Yan, S.M. Xu, H. Zhou, M. Xu, L. Ma, M. Shao, X. Kong, B. Wang, L. Zheng, H. Duan, Alcohols electrooxidation coupled with H_2 production at high current densities promoted by a cooperative catalyst, Nat. Commun. 13 (2022) 147.
[175] C. Chen, Z. Zhou, J. Liu, B. Zhu, H. Hu, Y. Yang, G. Chen, M. Gao, J. Zhang, Sustainable biomass upgrading coupled with H_2 generation over in-situ oxidized Co_3O_4 electrocatalysts, Appl. Catal. B-Environ. 307 (2022) 121209.
[176] N. Zhang, Y. Zou, L. Tao, W. Chen, L. Zhou, Z. Liu, B. Zhou, G. Huang, H. Lin, S. Wang, Electrochemical oxidation of 5-hydroxymethylfurfural on nickel nitride/carbon nanosheets: reaction pathway determined by in situ sum frequency generation vibrational spectroscopy, Angew. Chem. Int. Ed. 58 (2019) 15895–15903.
[177] N. Jiang, B. You, R. Boonstra, I.M. Terrero Rodriguez, Y. Sun, Integrating electrocatalytic 5-hydroxymethylfurfural oxidation and hydrogen production via Co–P-derived electrocatalysts, ACS Energy Lett. 1 (2016) 386–390.
[178] G. Yang, Y. Jiao, H. Yan, Y. Xie, A. Wu, X. Dong, D. Guo, C. Tian, H. Fu, Interfacial engineering of MoO_2-FeP heterojunction for highly efficient hydrogen evolution coupled with biomass electrooxidation, Adv. Mater. 32 (2020) 2000455.
[179] X. Deng, X. Kang, M. Li, K. Xiang, C. Wang, Z. Guo, J. Zhang, X.-Z. Fu, J.-L. Luo, Coupling efficient biomass upgrading with H_2 production via bifunctional Cu_xS@NiCo-LDH core-shell nanoarray electrocatalysts, J. Mater. Chem. A 8 (2020) 1138–1146.
[180] P. Zhou, G. Hai, G. Zhao, R. Li, X. Huang, Y. Lu, G. Wang, CeO_2 as an "electron pump" to boost the performance of Co_4N in electrocatalytic hydrogen evolution, oxygen evolution and biomass oxidation valorization, Appl. Catal. B Environ. 325 (2023) 122364.
[181] J. Wu, J. Chen, T. Yu, Z. Zhai, Y. Zhu, X. Wu, S. Yin, Boosting electrochemical kinetics of $NiCo_2$ via MoO_2 modification for biomass upgrading assisted hydrogen evolution, ACS Catal. 13 (2023) 13257–13266.
[182] J. Wu, Z. Zhai, S. Yin, S. Wang, General formation of interfacial assembled hierarchical micro-nano arrays for biomass upgrading-coupled hydrogen production, Adv. Funct. Mater. 34 (2024) 2308198.
[183] P. Xu, Z. Bao, Y. Zhao, L. Zheng, Z. Lv, X. Shi, H.E. Wang, X. Fang, H. Zheng, Anionic regulation and heteroatom doping of Ni-based electrocatalysts to boost biomass valorization coupled with hydrogen production, Adv. Energy Mater. 14 (2024) 2303557.
[184] N. Thakur, D. Mehta, A. Chaturvedi, D. Mandal, T.C. Nagaiah, Glucose oxidation assisted hydrogen and gluconic/glucaric acid production using NiVP/Pi bifunctional electrocatalyst, J. Mater. Chem. A 11 (2023) 15868–15877.
[185] X. Liu, P. Cai, G. Wang, Z. Wen, Nickel doped MoS_2 nanoparticles as precious-metal free bifunctional electrocatalysts for glucose assisted electrolytic H_2 generation, Int. J. Hydrog. Energ. 45 (2020) 32940–32948.
[186] Y. Zhang, B. Zhou, Z. Wei, W. Zhou, D. Wang, J. Tian, T. Wang, S. Zhao, J. Liu, L. Tao, S. Wang, Coupling glucose-assisted Cu(I)/Cu(II) redox with electrochemical hydrogen production, Adv. Mater. 33 (2021) e2104791.
[187] Y. Zhang, Y. Qiu, Z. Ma, Y. Wang, Y. Zhang, Y. Ying, Y. Jiang, Y. Zhu, S. Liu, Core-corona Co/CoP clusters strung on carbon nanotubes as a Schottky catalyst for glucose oxidation assisted H_2 production, J. Mater. Chem. A 9 (2021) 10893–10908.
[188] N. Wei, S. Zhang, X. Yao, J. Yang, V. Nica, Q. Zhou, Cation and anion-codoped Cr, S-NiFe nanosheet arrays as efficient electrocatalysts for boosting electrocatalytic glucose conversion coupled with H_2 generation, Sci. China Mater. 66 (2023) 4650–4662.
[189] X. Lin, H. Zhong, W. Hu, J. Du, Nickel-cobalt selenide electrocatalytic electrode toward glucose oxidation coupling with alkaline hydrogen production, Inorg. Chem. 62 (2023) 10513–10521.
[190] K. Chen, W. Zhang, Y. Bai, W. Gong, N. Zhang, R. Long, Y. Xiong, Boosting electrochemical hydrogen evolution by coupling anodically oxidative dehydrogenation of benzylamine to benzonitrile, Chin. Chem. Lett. 34 (2023) 107319.
[191] Y. Huang, X. Chong, C. Liu, Y. Liang, B. Zhang, Boosting hydrogen production by anodic oxidation of primary amines over a NiSe nanorod electrode, Angew. Chem. Int. Ed. 57 (2018) 13163–13166.
[192] M. Xiang, Z. Xu, Q. Wu, Y. Wang, Z. Yan, Selective electrooxidation of primary amines over a Ni/Co metal-organic framework derived electrode enabling effective hydrogen production in the membrane-free electrolyzer, J. Power Sources 535 (2022) 231461.
[193] L. Zeng, W. Chen, Q. Zhang, S. Xu, W. Zhang, F. Lv, Q. Huang, S. Wang, K. Yin, M. Li, Y. Yang, L. Gu, S. Guo, $CoSe_2$ subnanometer belts with Se vacancies and Ni substitutions for the efficient electrosynthesis of high-value-added nitriles coupled with hydrogen generation, ACS Catal. 12 (2022) 11391–11401.
[194] Y. Li, Y. Jiao, H. Yan, G. Yang, Y. Liu, C. Tian, A. Wu, H. Fu, Mo-Ni-based heterojunction with fine-customized *d*-band centers for hydrogen production coupled with benzylamine electrooxidation in low alkaline medium, Angew. Chem. Int. Ed. 62 (2023) e202306640.
[195] Y. Ding, B.-Q. Miao, S.-N. Li, Y.-C. Jiang, Y.-Y. Liu, H.-C. Yao, Y. Chen, Benzylamine oxidation boosted electrochemical water-splitting: hydrogen and benzonitrile co-production at ultra-thin Ni_2P nanomeshes grown on nickel foam, Appl. Catal. B Environ. 268 (2020) 118393.
[196] X. Wei, Y. Li, L. Chen, J. Shi, Formic acid electro-synthesis by concurrent cathodic CO_2 reduction and anodic CH_3OH oxidation, Angew. Chem. Int. Ed. 60 (2021) 3148–3155.
[197] M.I. Abdullah, A. Hameed, N. Zhang, M.H. Islam, M. Ma, B.G. Pollet, Ultrasonically surface-activated Nickel foam as a highly efficient monolith electrode for the catalytic oxidation of methanol to formate, ACS Appl. Mater. Interfaces 13 (2021) 30603–30613.
[198] J. Li, R. Wei, X. Wang, Y. Zuo, X. Han, J. Arbiol, J. Llorca, Y. Yang, A. Cabot, C. Cui, Selective methanol-to-formate electrocatalytic conversion on branched nickel carbide, Angew. Chem. Int. Ed. 59 (2020) 20826–20830.
[199] M. Li, X. Deng, Y. Liang, K. Xiang, D. Wu, B. Zhao, H. Yang, J.-L. Luo, X.-Z. Fu, CoP@NiCo-LDH heteronanosheet arrays as efficient bifunctional electrocatalysts for co-generation of value-added formate and hydrogen with less-energy consumption, J. Energy Chem. 50 (2020) 314–323.
[200] B. Zhao, J. Liu, C. Xu, R. Feng, P. Sui, L. Wang, J. Zhang, J.L. Luo, X.Z. Fu, Hollow NiSe nanocrystals heterogenized with carbon nanotubes for efficient

electrocatalytic methanol upgrading to boost hydrogen co-production, Adv. Funct. Mater. 31 (2020) 2008812.
[201] B. Zhao, J.-W. Liu, Y.-R. Yin, D. Wu, J.-L. Luo, X.-Z. Fu, Carbon nanofibers@NiSe core/sheath nanostructures as efficient electrocatalysts for integrating highly selective methanol conversion and less-energy intensive hydrogen production, J. Mater. Chem. A 7 (2019) 25878–25886.
[202] W. Luo, H. Tian, Q. Li, G. Meng, Z. Chang, C. Chen, R. Shen, X. Yu, L. Zhu, F. Kong, X. Cui, J. Shi, Controllable electron distribution reconstruction of spinel $NiCo_2O_4$ boosting glycerol oxidation at elevated current density, Adv. Funct. Mater. 34 (2023) 2306995.
[203] D.M. Morales, D. Jambrec, M.A. Kazakova, M. Braun, N. Sikdar, A. Koul, A. C. Brix, S. Seisel, C. Andronescu, W. Schuhmann, Electrocatalytic conversion of glycerol to oxalate on Ni oxide nanoparticles-modified oxidized multiwalled carbon nanotubes, ACS Catal. 12 (2022) 982–992.
[204] C. Liu, M. Hirohara, T. Maekawa, R. Chang, T. Hayashi, C.-Y. Chiang, Selective electro-oxidation of glycerol to dihydroxyacetone by a non-precious electrocatalyst-CuO, Appl. Catal. B-Environ. 265 (2020) 118543.
[205] H. Yu, M. Hu, C. Chen, C. Hu, Q. Li, F. Hu, S. Peng, J. Ma, Ambient γ-rays-mediated noble-metal deposition on defect-rich manganese oxide for glycerol-assisted H_2 evolution at industrial-level current density, Angew. Chem. Int. Ed. 62 (2023) e202314569.
[206] N. Yao, G. Wang, H. Jia, J. Yin, H. Cong, S. Chen, W. Luo, Intermolecular energy gap-induced formation of high-valent cobalt species in CoOOH surface layer on cobalt sulfides for efficient water oxidation, Angew. Chem. Int. Ed. 61 (2022) e202117178.
[207] D. Si, M. Wang, X. Yang, C. Wang, K. Shi, B. Huang, L. Chen, J. Shi, Hydrogen anode/cathode co-productions-coupled anode alcohol selective oxidation and distinctive H/e transfer pathways, Appl. Catal. B-Environ. 331 (2023) 122664.
[208] Q. Mao, K. Deng, H. Yu, Y. Xu, Z. Wang, X. Li, L. Wang, H. Wang, In situ reconstruction of partially hydroxylated porous Rh metallene for ethylene glycol-assisted seawater splitting, Adv. Funct. Mater. 32 (2022) 2201081.
[209] H. Huang, C. Yu, X. Han, H. Huang, Q. Wei, W. Guo, Z. Wang, J. Qiu, Ni, Co hydroxide triggers electrocatalytic production of high-purity benzoic acid over 400 mA cm^{-2}, Energy Environ. Sci. 13 (2020) 4990–4999.
[210] Z. Li, Y. Yan, S.-M. Xu, H. Zhou, M. Xu, L. Ma, M. Shao, X. Kong, B. Wang, L. Zheng, H. Duan, Alcohols electrooxidation coupled with H_2 production at high current densities promoted by a cooperative catalyst, Nat. Commun. 13 (2022) 147.
[211] Y. Xie, Z. Zhou, N. Yang, G. Zhao, An overall reaction integrated with highly selective oxidation of 5-hydroxymethylfurfural and efficient hydrogen evolution, Adv. Funct. Mater. 31 (2021) 2102886.
[212] N. Heidary, N. Kornienko, Electrochemical biomass valorization on gold-metal oxide nanoscale heterojunctions enables investigation of both catalyst and reaction dynamics with surface-enhanced Raman spectroscopy, Chem. Sci. 11 (2020) 1798–1806.
[213] S. Xie, H. Fu, L. Chen, Y. Li, K. Shen, Carbon-based nanoarrays embedded with Ce-doped ultrasmall Co_2P nanoparticles enable efficient electrooxidation of 5-hydroxymethylfurfural coupled with hydrogen production, Sci. China Chem. 66 (2023) 2141–2152.
[214] Y. Sun, J. Wang, Y. Qi, W. Li, C. Wang, Efficient electrooxidation of 5-hydroxymethylfurfural using Co-doped Ni_3S_2 catalyst: Promising for H_2 production under industrial-level current density, Adv. Sci. 9 (2022) 2200957.
[215] S. Barwe, J. Weidner, S. Cychy, D.M. Morales, S. Dieckhöfer, D. Hiltrop, J. Masa, M. Muhler, W. Schuhmann, Electrocatalytic oxidation of 5-(hydroxymethyl) furfural using high-surface-area nickel boride, Angew. Chem. Int. Ed. 57 (2018) 11460–11464.
[216] Z. Zhou, C. Chen, M. Gao, B. Xia, J. Zhang, In situ anchoring of a Co_3O_4 nanowire on nickel foam: an outstanding bifunctional catalyst for energy-saving simultaneous reactions, Green. Chem. 21 (2019) 6699–6706.
[217] M. Park, M. Gu, B.-S. Kim, Tailorable electrocatalytic 5-hydroxymethylfurfural oxidation and H_2 production: architecture-performance relationship in bifunctional multilayer electrodes, ACS Nano 14 (2020) 6812–6822.
[218] B. Mondal, N. Karjule, C. Singh, R. Shimoni, M. Volokh, I. Hod, M. Shalom, Unraveling the mechanisms of electrocatalytic oxygenation and dehydrogenation of organic molecules to value-added chemicals over a Ni-Fe oxide catalyst, Adv. Energy Mater. 11 (2021) 2101858.
[219] M.T. Bender, Y.C. Lam, S. Hammes-Schiffer, K.-S. Choi, Unraveling two pathways for electrochemical alcohol and aldehyde oxidation on NiOOH, J. Am. Chem. Soc. 142 (2020) 21538–21547.
[220] T. Wang, X. Cao, L. Jiao, Progress in hydrogen production coupled with electrochemical oxidation of small molecules, Angew. Chem. Int. Ed. 61 (2022) e202213328.
[221] M. Zhang, Y. Liu, B. Liu, Z. Chen, H. Xu, K. Yan, Trimetallic NiCoFe-layered double hydroxides nanosheets efficient for oxygen evolution and highly selective oxidation of biomass-derived 5-hydroxymethylfurfural, ACS Catal. 10 (2020) 5179–5189.
[222] Y. Zhong, R.-Q. Ren, L. Qin, J.-B. Wang, Y.-Y. Peng, Q. Li, Y.-M. Fan, Electrodeposition of hybrid nanosheet-structured $NiCo_2O_4$ on carbon fiber paper as a non-noble electrocatalyst for efficient electrooxidation of 5-hydroxymethylfurfural to 2, 5-furandicarboxylic acid, N. J. Chem. 45 (2021) 11213–11221.
[223] S. Yang, Y. Guo, Y. Zhao, L. Zhang, H. Shen, J. Wang, J. Li, C. Wu, W. Wang, Y. Cao, Construction of synergistic Ni_3S_2-MoS_2 nanoheterojunctions on Ni foam as bifunctional electrocatalyst for hydrogen evolution integrated with biomass valorization, Small 18 (2022) 2201306.
[224] T. Wang, L. Tao, X. Zhu, C. Chen, W. Chen, S. Du, Y. Zhou, B. Zhou, D. Wang, C. Xie, Combined anodic and cathodic hydrogen production from aldehyde oxidation and hydrogen evolution reaction, Nat. Catal. 5 (2022) 66–73.
[225] J. Zeng, W. Chen, G. Zhang, L. Yu, L. Zhong, Y. Liu, S. Zhao, Y. Qiu, Heterostructured Ni_3N-NiMoN nanowires as bifunctional electrocatalysts for hydrogen evolution and 5-hydroxymethylfurfural oxidation, ACS Appl. Nano Mater. 5 (2022) 7321–7330.
[226] A. Wu, Y. Xie, H. Ma, C. Tian, Y. Gu, H. Yan, X. Zhang, G. Yang, H. Fu, Integrating the active OER and HER components as the heterostructures for the efficient overall water splitting, Nano Energy 44 (2018) 353–363.
[227] Z. Zhuang, Y. Li, Z. Li, F. Lv, Z. Lang, K. Zhao, L. Zhou, L. Moskaleva, S. Guo, L. Mai, MoB/g-C_3N_4 interface materials as a schottky catalyst to boost hydrogen evolution, Angew. Chem. Int. Ed. 57 (2018) 496–500.
[228] L. Thapa, A. Bhaumik, S. Mondal, C.R. Raj, A heterostructured electrocatalyst for the electrochemical valorization of 5-hydroxymethylfurfural coupled with the hydrogen evolution reaction, J. Mater. Chem. A 11 (2023) 26242–26251.
[229] Y. Du, D. Liu, T. Li, Y. Yan, Y. Liang, S. Yan, Z. Zou, A phase transformation-free redox couple mediated electrocatalytic oxygen evolution reaction, Appl. Catal. B Environ. 306 (2022) 121146.
[230] X. Huang, K. Zhang, B. Peng, G. Wang, M. Muhler, F. Wang, Ceria-based materials for thermocatalytic and photocatalytic organic synthesis, ACS Catal. 11 (2021) 9618–9678.
[231] Y. Xie, L. Sun, X. Pan, Z. Zhou, G. Zhao, Selective two-electron electrocatalytic conversion of 5-Hydroxymethylfurfural boosting hydrogen production under neutral condition over $Co(OH)_2$-CeO_2 catalyst, Appl. Catal. B Environ. 338 (2023) 123068.
[232] W.-J. Liu, Z. Xu, D. Zhao, X.-Q. Pan, H.-C. Li, X. Hu, Z.-Y. Fan, W.-K. Wang, G.-H. Zhao, S. Jin, Efficient electrochemical production of glucaric acid and H_2 via glucose electrolysis, Nat. Commun. 11 (2020) 265.
[233] L.T. Mika, E. Cséfalvay, Á. Németh, Catalytic conversion of carbohydrates to initial platform chemicals: Chemistry and sustainability, Chem. Rev. 118 (2018) 505–613.
[234] S. Vogt, M. Schneider, H. Schäfer-Eberwein, G. Nöll, Determination of the pH dependent redox potential of glucose oxidase by spectroelectrochemistry, Anal. Chem. 86 (2014) 7530–7535.
[235] J.-Y. Wang, T. Ouyang, N. Li, T. Ma, Z.-Q. Liu, S, N co-doped carbon nanotube-encapsulated core-shelled CoS_2@Co nanoparticles: efficient and stable bifunctional catalysts for overall water splitting, Sci. Bull. 63 (2018) 1130–1140.
[236] Z.H. Xue, H. Su, Q.Y. Yu, B. Zhang, H.H. Wang, X.H. Li, J.S. Chen, Janus Co/CoP nanoparticles as efficient Mott-Schottky electrocatalysts for overall water splitting in wide pH range, Adv. Energy Mater. 7 (2017) 1602355.
[237] M. Wu, J. Zhao, C. Li, R. Liu, Heterogeneity in a metal-organic framework in situ guides engineering Co@CoO heterojunction for electrocatalytic H_2 production in tandem with glucose oxidation, J. Mater. Chem. A 10 (2022) 4791–4799.
[238] X. Liu, S. Cui, Z. Sun, Y. Ren, X. Zhang, P. Du, Self-supported copper oxide electrocatalyst for water oxidation at low overpotential and confirmation of its robustness by Cu K-Edge X-ray absorption spectroscopy, J. Phys. Chem. C 120 (2016) 831–840.
[239] H.H. Fan, W.L. Weng, C.Y. Lee, C.N. Liao, Electrochemical cycling-induced spiky Cu_xO/Cu nanowire array for glucose sensing, ACS Omega 4 (2019) 12222–12229.
[240] Y. Mu, T.T. Nguyen, M.J. Koh, R.R. Schrock, A.H. Hoveyda, E- and Z-, di- and tri-substituted alkenyl nitriles through catalytic cross-metathesis, Nat. Chem. 11 (2019) 478–487.
[241] X.-Q. Chu, D. Ge, Z.-L. Shen, T.-P. Loh, Recent advances in radical-initiated C (sp^3)-H bond oxidative functionalization of alkyl nitriles, ACS Catal. 8 (2018) 258–271.
[242] F.-D. Lu, L.-Q. Lu, G.-F. He, J.-C. Bai, W.-J. Xiao, Enantioselective radical carbocyanation of 1,3-dienes via photocatalytic generation of allylcopper complexes, J. Am. Chem. Soc. 143 (2021) 4168–4173.
[243] L.R. Mills, J.M. Graham, P. Patel, S.A.L. Rousseaux, Ni-catalyzed reductive cyanation of aryl halides and phenol derivatives via transnitrilation, J. Am. Chem. Soc. 141 (2019) 19257–19262.
[244] T. Schareina, A. Zapf, W. Mägerlein, N. Müller, M. Beller, A state-of-the-art cyanation of aryl bromides: a novel and versatile copper catalyst system inspired by nature, Chem. Eur. J. 13 (2007) 6249–6254.
[245] P. Anbarasan, T. Schareina, M. Beller, Recent developments and perspectives in palladium-catalyzed cyanation of aryl halides: synthesis of benzonitriles, Chem. Soc. Rev. 40 (2011) 5049–5067.
[246] M. Yu, E. Budiyanto, H. Tuysuz, Principles of water electrolysis and recent progress in cobalt-, nickel-, and iron-based oxides for the oxygen evolution reaction, Angew. Chem. Int. Ed. 61 (2022) e202103824.
[247] Y. Sun, H. Shin, F. Wang, B. Tian, C.-W. Chiang, S. Liu, X. Li, Y. Wang, L. Tang, W. A. Goddard, III, M. Ding, Highly selective electrocatalytic oxidation of amines to nitriles assisted by water oxidation on metal-doped α-$Ni(OH)_2$, J. Am. Chem. Soc. 144 (2022) 15185–15192.
[248] I. Mondal, J.N. Hausmann, G. Vijaykumar, S. Mebs, H. Dau, M. Driess, P. W. Menezes, Nanostructured intermetallic nickel silicide (pre) catalyst for anodic oxygen evolution reaction and selective dehydrogenation of primary amines, Adv. Energy Mater. 12 (2022) 2200269.
[249] Y. Liang, S.-H. Shi, R. Jin, X. Qiu, J. Wei, H. Tan, X. Jiang, X. Shi, S. Song, N. Jiao, Electrochemically induced nickel catalysis for oxygenation reactions with water, Nat. Catal. 4 (2021) 116–123.
[250] K. Yin, Y. Chao, F. Lv, L. Tao, W. Zhang, S. Lu, M. Li, Q. Zhang, L. Gu, H. Li, S. Guo, One nanometer PtIr nanowires as high-efficiency bifunctional catalysts for electrosynthesis of ethanol into high value-added multicarbon compound coupled with hydrogen production, J. Am. Chem. Soc. 143 (2021) 10822–10827.

[251] B. Mondal, N. Karjule, C. Singh, R. Shimoni, M. Volokh, I. Hod, M. Shalom, Unraveling the mechanisms of electrocatalytic oxygenation and dehydrogenation of organic molecules to value-added chemicals over a Ni-Fe oxide catalyst, Adv. Energy Mater. 11 (2021) 2101858.
[252] M. Qin, R. Fan, J. Chen, H. Wang, X. Zheng, S. Mao, R. Du, Y. Wang, Elucidating electrocatalytic mechanism for large-scale cycloalkanol oxidation integrated with hydrogen evolution, Chem. Eng. J. 442 (2022) 136264.
[253] H. Zhao, D. Lu, J. Wang, W. Tu, D. Wu, S.W. Koh, P. Gao, Z.J. Xu, S. Deng, Y. Zhou, B. You, H. Li, Raw biomass electroreforming coupled to green hydrogen generation, Nat. Commun. 12 (2021) 2008.
[254] S. Hao, L. Yang, D. Liu, R. Kong, G. Du, A.M. Asiri, Y. Yang, X. Sun, Integrating natural biomass electro-oxidation and hydrogen evolution: using a porous Fe-doped CoP nanosheet array as a bifunctional catalyst, Chem. Commun. 53 (2017) 5710–5713.
[255] H. Zhou, Z. Li, S.M. Xu, L. Lu, M. Xu, K. Ji, R. Ge, Y. Yan, L. Ma, X. Kong, L. Zheng, H. Duan, Selectively upgrading lignin derivatives to carboxylates through electrochemical oxidative C(OH)-C bond cleavage by a Mn-doped cobalt oxyhydroxide catalyst, Angew. Chem. Int. Ed. 60 (2021) 8976–8982.
[256] C. Huang, Y. Huang, C. Liu, Y. Yu, B. Zhang, Integrating hydrogen production with aqueous selective semi-dehydrogenation of tetrahydroisoquinolines over a Ni_2P bifunctional electrode, Angew. Chem. Int. Ed. 58 (2019) 12014–12017.
[257] F. Hosseinpoor, H. Golchoubian, Mn(III)-catalyzed oxidation of sulfides to sulfoxides with hydrogen peroxide, Tetrahedron Lett. 47 (2006) 5195–5197.
[258] L. Ma, H. Zhou, M. Xu, P. Hao, X. Kong, H. Duan, Integrating hydrogen production with anodic selective oxidation of sulfides over a CoFe layered double hydroxide electrode, Chem. Sci. 12 (2020) 938–945.
[259] C.-Y. Lin, S.-C. Huang, Y.-G. Lin, L.-C. Hsu, C.-T. Yi, Electrosynthesized Ni-P nanospheres with high activity and selectivity towards photoelectrochemical plastics reforming, Appl. Catal. B-Environ. 296 (2021) 120351.
[260] V. Tournier, C. Topham, A. Gilles, B. David, C. Folgoas, E. Moya-Leclair, E. Kamionka, M.-L. Desrousseaux, H. Texier, S. Gavalda, An engineered PET depolymerase to break down and recycle plastic bottles, Nature 580 (2020) 216–219.
[261] J. Liu, X. Peng, Interface-engineering of the catalysts for efficient electrocatalytic upcycling of polyethylene terephthalate Waste, Innov. Discov. 1 (2024) 1.
[262] F. Ma, S. Wang, X. Gong, X. Liu, Z. Wang, P. Wang, Y. Liu, H. Cheng, Y. Dai, Z. Zheng, B. Huang, Highly efficient electrocatalytic hydrogen evolution coupled with upcycling of microplastics in seawater enabled via Ni_3N/W_5N_4 janus nanostructures, Appl. Catal. B Environ. 307 (2022) 121198.
[263] X. Liu, Z. Fang, D. Xiong, S. Gong, Y. Niu, W. Chen, Z. Chen, Upcycling PET in parallel with energy-saving H_2 production via bifunctional nickel-cobalt nitride nanosheets, Nano Res. 16 (2023) 4625–4633.
[264] H. Zhang, Y. Wang, X. Li, K. Deng, H. Yu, Y. Xu, H. Wang, Z. Wang, L. Wang, Electrocatalytic upcycling of polyethylene terephthalate plastic to formic acid coupled with energy-saving hydrogen production over hierarchical Pd-doped NiTe nanoarrays, Appl. Catal. B Environ. 340 (2024) 123236.
[265] X. Liu, X. He, D. Xiong, G. Wang, Z. Tu, D. Wu, J. Wang, J. Gu, Z. Chen, Electro-reforming of PET plastic to C_2 chemicals with concurrent generation of hydrogen and electric energy, ACS Catal. 14 (2024) 5366–5376.
[266] H. Wang, W. Zhan, H. Yu, S. Jiang, B. Wang, K. Deng, Z. Wang, Y. Xu, L. Wang, Nitrogen-doped Ni_3P-$NiMoO_4$ heterostructure arrays for coupling hydrogen production with polyethylene terephthalate plastic electro-recycling, Mater. Today Phys. 37 (2023) 101192.
[267] N. Wang, X. Li, M.-K. Hu, W. Wei, S.-H. Zhou, X.-T. Wu, Q.-L. Zhu, Ordered macroporous superstructure of bifunctional cobalt phosphide with heteroatomic modification for paired hydrogen production and polyethylene terephthalate plastic recycling, Appl. Catal. B Environ. 316 (2022) 121667.
[268] X. Liu, Z. Fang, X. Teng, Y. Niu, S. Gong, W. Chen, T.J. Meyer, Z. Chen, Paired formate and H_2 productions via efficient bifunctional Ni-Mo nitride nanowire electrocatalysts, J. Energy Chem. 72 (2022) 432–441.
[269] L. Yi, Y. Ji, P. Shao, J. Chen, J. Li, H. Li, K. Chen, X. Peng, Z. Wen, Scalable synthesis of tungsten disulfide nanosheets for alkali-acid electrocatalytic sulfion recycling and H_2 generation, Angew. Chem. Int. Ed. 60 (2021) 21550–21557.
[270] Y. Li, Y. Duan, K. Zhang, W. Yu, Efficient anodic chemical conversion to boost hydrogen evolution with low energy consumption over cobalt-doped nickel sulfide electrocatalyst, Chem. Eng. J. 433 (2022) 134472.
[271] W. Wang, Q. Mao, K. Deng, H. Yu, Z. Wang, Y. Xu, X. Li, L. Wang, H. Wang, Sulfur-induced low crystallization of ultrathin Pd nanosheet arrays for sulfur ion degradation-assisted energy-efficient H_2 production, Small 19 (2023) 2207852.
[272] Y. Pei, J. Cheng, H. Zhong, Z. Pi, Y. Zhao, F. Jin, Sulfide-oxidation-assisted electrochemical water splitting for H_2 production on a bifunctional Cu_2S/nickel foam catalyst, Green. Chem. 23 (2021) 6975–6983.
[273] W. Wang, Q. Mao, S. Jiang, K. Deng, H. Yu, Z. Wang, Y. Xu, L. Wang, H. Wang, Hetero-phase Pd_4S metallene nanoribbons with Pd-rich vacancies for sulfur ion degradation-assisted hydrogen production, Appl. Catal. B Environ. 340 (2024) 123194.
[274] F. Liu, X. Cai, Y. Tang, W. Liu, Q. Chen, P. Dong, M. Xu, Y. Tan, S. Bao, Nano-Ni-induced electronic modulation of MoS_2 nanosheets enables energy-saving H_2 production and sulfide degradation, Energy Environ. Mater. 7 (2024) e12644.
[275] Y. Zheng, X. Xu, Surface atom regulation on polyoxometalate electrocatalyst for simultaneous low-voltage H_2 production and phenol degradation, ACS Appl. Mater. Interfaces 12 (2020) 53739–53748.
[276] J. Deng, S. Chen, N. Yao, Q. Wang, J. Li, Z. Wei, Integrating H_2 generation with sewage disposal by an efficient anti-poisoning bifunctional electrocatalyst, Appl. Catal. B-Environ. 277 (2020) 119175.
[277] S. Li, S. Wang, J. He, K. Li, Y. Xu, M. Wang, S. Zhao, Y. Wang, X. Li, X. Zhong, J. Wang, Chromium-doped nickel oxide and nickel nitride mediate selective electrocatalytic oxidation of sterol intermediates coupled with H_2 evolution, Angew. Chem. Int. Ed. 62 (2023) e202306553.
[278] X. Zhai, Q. Yu, G. Liu, J. Bi, Y. Zhang, J. Chi, J. Lai, B. Yang, L. Wang, Hierarchical microsphere MOF arrays with ultralow Ir doping for efficient hydrogen evolution coupled with hydrazine oxidation in seawater, J. Mater. Chem. A 9 (2021) 27424–27433.
[279] Y. Zhang, D. Ma, Y. Lei, T. Zhu, J. Hu, Y. Tang, Z. Chen, J. Huang, Y. Lai, Z. Lin, Markedly enhanced hydrogen production in wastewater via ammonia-mediated metal oxyhydroxides active sites on bifunctional electrocatalysts, Nano Energy 117 (2023) 108896.
[280] R.C. Thompson, Y. Olsen, R.P. Mitchell, A. Davis, S.J. Rowland, A.W. John, D. McGonigle, A.E. Russell, Lost at sea: where is all the plastic? Science 304 (2004) 838-838.
[281] V. Hidalgo-Ruz, L. Gutow, R.C. Thompson, M. Thiel, Microplastics in the marine environment: a review of the methods used for identification and quantification, Environ. Sci. Technol. 46 (2012) 3060–3075.
[282] D. Yao, H. Yang, H. Chen, P.T. Williams, Investigation of nickel-impregnated zeolite catalysts for hydrogen/syngas production from the catalytic reforming of waste polyethylene, Appl. Catal. B Environ. 227 (2018) 477–487.
[283] K. Hu, W. Tian, Y. Yang, G. Nie, P. Zhou, Y. Wang, X. Duan, S. Wang, Microplastics remediation in aqueous systems: strategies and technologies, Water Res. 198 (2021) 117144.
[284] H. Wu, W.P. Fahy, S. Kim, H. Kim, N. Zhao, L. Pilato, A. Kafi, S. Bateman, J. H. Koo, Recent developments in polymers/polymer nanocomposites for additive manufacturing, Prog. Mater. Sci. 111 (2020) 100638.
[285] X.-X. Wang, G.-F. Yu, J. Zhang, M. Yu, S. Ramakrishna, Y.-Z. Long, Conductive polymer ultrafine fibers via electrospinning: preparation, physical properties and applications, Prog. Mater. Sci. 115 (2021) 100704.
[286] W.F. Yong, H. Zhang, Recent advances in polymer blend membranes for gas separation and pervaporation, Prog. Mater. Sci. 116 (2021) 100713.
[287] W. Tian, P. Song, H. Zhang, X. Duan, Y. Wei, H. Wang, S. Wang, Microplastic materials in the environment: problem and strategical solutions, Prog. Mater. Sci. 132 (2023) 101035.
[288] T. Uekert, H. Kasap, E. Reisner, Photoreforming of nonrecyclable plastic waste over a carbon nitride/nickel phosphide catalyst, J. Am. Chem. Soc. 141 (2019) 15201–15210.
[289] Y. Yang, J. Yang, W.-M. Wu, J. Zhao, Y. Song, L. Gao, R. Yang, L. Jiang, Biodegradation and mineralization of polystyrene by plastic-eating mealworms: part 1. Chemical and physical characterization and isotopic tests, Environ. Sci. Technol. 49 (2015) 12080–12086.
[290] Q. Hou, M. Zhen, H. Qian, Y. Nie, X. Bai, T. Xia, M. Laiq Ur Rehman, Q. Li, M. Ju, Upcycling and catalytic degradation of plastic wastes, Cell Rep. Phys. Sci. 2 (2021) 100514.
[291] C. Tang, Y. Zheng, M. Jaroniec, S.Z. Qiao, Electrocatalytic refinery for sustainable production of fuels and chemicals, Angew. Chem. Int. Ed. 60 (2021) 19572–19590.
[292] H. Zhou, Y. Ren, Z. Li, M. Xu, Y. Wang, R. Ge, X. Kong, L. Zheng, H. Duan, Electrocatalytic upcycling of polyethylene terephthalate to commodity chemicals and H_2 fuel, Nat. Commun. 12 (2021) 4679.
[293] A. Rahimi, J.M. García, Chemical recycling of waste plastics for new materials production, Nat. Rev. Chem. 1 (2017) 0046.
[294] Y. Kratish, J. Li, S. Liu, Y. Gao, T.J. Marks, Polyethylene terephthalate deconstruction catalyzed by a carbon-supported single-site molybdenum-dioxo complex, Angew. Chem. Int. Ed. 59 (2020) 19857–19861.
[295] L. Wang, G.A. Nelson, J. Toland, J.D. Holbrey, Glycolysis of PET using 1,3-dimethylimidazolium-2-carboxylate as an organocatalyst, ACS Sustain. Chem. Eng. 8 (2020) 13362–13368.
[296] S. Behera, S. Dinda, R. Saha, B. Mondal, Quantitative electrocatalytic upcycling of polyethylene terephthalate plastic and its oligomer with a cobalt-based one-dimensional coordination polymer having open metal sites along with coproduction of hydrogen, ACS Catal. 13 (2023) 469–474.
[297] A. Piéplu, O. Saur, J.-C. Lavalley, O. Legendre, C. Nédez, Claus catalysis and H_2S selective oxidation, Catal. Rev. 40 (1998) 409–450.
[298] K. Petrov, S. Srinivasan, Low temperature removal of hydrogen sulfide from sour gas and its utilization for hydrogen and sulfur production, Int. J. Hydrog. Energ. 21 (1996) 163–169.
[299] M. Zhang, J. Guan, Y. Tu, S. Chen, Y. Wang, S. Wang, L. Yu, C. Ma, D. Deng, X. Bao, Highly efficient H_2 production from H_2S via a robust graphene-encapsulated metal catalyst, Energy Environ. Sci. 13 (2020) 119–126.
[300] S. Hao, L. Yang, D. Liu, G. Du, Y. Yang, A.M. Asiri, X. Sun, Replacing oxygen evolution with sodium sulfide electro-oxidation toward energy-efficient electrochemical hydrogen production: using cobalt phosphide nanoarray as a bifunctional catalyst, Int. J. Hydrog. Energ. 42 (2017) 26289–26295.
[301] R.G. Pearson, Hard and soft acids and bases, HSAB, part II: underlying theories, J. Chem. Educ. 45 (1968) 643.
[302] R.G. Pearson, Hard and soft acids and bases, HSAB, part 1: Fundamental principles, J. Chem. Educ. 45 (1968) 581.
[303] M. Zhang, J. Chen, H. Li, P. Cai, Y. Li, Z. Wen, Ru-RuO_2/CNT hybrids as high-activity pH-universal electrocatalysts for water splitting within 0.73 V in an asymmetric-electrolyte electrolyzer, Nano Energy 61 (2019) 576–583.
[304] M. Kumar, T.C. Nagaiah, Efficient production of hydrogen from H_2S via electrolysis using a $CoFeS_2$ catalyst, J. Mater. Chem. A 10 (2022) 7048–7057.

[305] M. Kumar, T.C. Nagaiah, Pure hydrogen and sulfur production from H_2S by an electrochemical approach using a NiCu-MoS_2 catalyst, J. Mater. Chem. A 10 (2022) 13031–13041.
[306] Z. Li, Z. Xie, H. Chen, X. Liang, X. Ai, L. Yuan, X. Li, X. Zou, Realization of interstitial boron ordering and optimal near-surface electronic structure in Pd-B alloy electrocatalysts, Chem. Eng. J. 419 (2021) 129568.
[307] H. Wang, W. Wang, Q. Mao, H. Yu, K. Deng, Y. Xu, X. Li, Z. Wang, L. Wang, Tensile strained PdNi bimetallene for energy-efficient hydrogen production integrated with formate oxidation, Chem. Eng. J. 450 (2022) 137995.
[308] X. Yang, W. Xu, S. Cao, S. Zhu, Y. Liang, Z. Cui, X. Yang, Z. Li, S. Wu, A. Inoue, L. Chen, An amorphous nanoporous PdCuNi-S hybrid electrocatalyst for highly efficient hydrogen production, Appl. Catal. B Environ. 246 (2019) 156–165.
[309] R. Wang, K. Yang, C. Wong, H. Aguirre-Villegas, R. Larson, F. Brushett, M. Qin, S. Jin, Electrochemical ammonia recovery and co-production of chemicals from manure wastewater, Nat. Sustain. 7 (2024) 179–190.
[310] E. Latvtyte, X.H. Zhu, L. Wu, R. Lan, P. Vale, J.E. Graves, A low-temperature ammonia electrolyser for wastewater treatment and hydrogen production, Int. J. Hydrog. Energ. 52 (2024) 265–282.
[311] C. Zamfirescu, I. Dincer, Using ammonia as a sustainable fuel, J. Power Sources 185 (2008) 459–465.
[312] F. Vitse, M. Cooper, G.G. Botte, On the use of ammonia electrolysis for hydrogen production, J. Power Sources 142 (2005) 18–26.
[313] D. Yoon, S. Chung, M. Choi, E. Yang, J. Lee, 100 W-class green hydrogen production from ammonia at a dual-layer electrode containing a Pt-Ir catalyst for an alkaline electrolytic process, J. Energy Chem. 93 (2024) 352–360.

Donglian Li received her BS in Materials Chemistry from Jiujiang University in 2022. She is studying for her master's degree at Wuhan Institute of Technology under the supervision of Prof. Xiang Peng. Her research interest is nanostructured transition metal compounds for energy-efficient hydrogen production.

Xiang Peng received his PhD in physics and materials science from City University of Hong Kong in 2017. He was a postdoctoral fellow at City University of Hong Kong from 2017 to 2018. He is currently a professor of materials science and engineering at Wuhan Institute of Technology. His research focuses on the design of functional nanomaterials and their application in energy storage and conversion. He was honored as one of the World's Top 2 % Scientists in 2023 conferred by Elsevier and Stanford University.

Paul K. Chu received his BS in mathematics from The Ohio State University and MS/PhD in chemistry from Cornell University. He is Chair Professor of Materials Engineering in the Department of Physics, Department of Materials Science & Engineering, and Department of Biomedical Engineering at City University of Hong Kong. His research interests are quite diverse spanning plasma science as well as materials science and engineering. He has received more than 30 research and technical awards and is a highly cited researcher (8 consecutive years since 2026). Besides being a fellow and council member of the Hong Kong Academy of Engineering Sciences, he is a fellow of the American Physical Society (APS), American Vacuum Society (AVS), Institute of Electrical and Electronics Engineers (IEEE), Materials Research Society (MRS), and Hong Kong Institution of Engineers (HKIE).